An investigation of Ultra Low Frequency (ULF) pulsations using radar data and solar wind data.

by

Sibusiso H. Mthembu

Submitted in fulfilment of the academic requirements for the Degree of Master of Science in the School of Physics University of Kwazulu-Natal Durban

Supervisor: Dr. S. B. Malinga

Co-supervisors: Prof. A. D. M. Walker and Mr. L Magnus

December 2006

Abstract

An investigation of Ultra Low Frequency (ULF) pulsations was conducted using data collected from the Super Dual Auroral Radar Network HF radars located at Goose Bay (53.32° N, 60.46° W, geographic) and Syowa East (69.01° S, 39.61° E, geographic) as well as solar wind data collected from the WIND and the Advanced Composition Explorer (ACE) Satellites. The aim for this thesis was to study the physics of the ULF pulsations and to determine how they transmit energy from solar wind to the magnetosphere. The Fourier transform was used to determine the frequency content of the time series. Frequencies of pulsations which fall in a Pc5 band with a period range of 150 to 600 s were observed near 1.3 and 1.9 mHz (Goose Bay) and near 1.3, 1.9, 2.3 and 2.7 mHz. (Syowa East) using a frequency resolution of about 0.1 mHz for both data sets. In each data set the amplitudes of the component were relatively equal and a detailed analysis was done on the 1.9 mHz component. The instantaneous amplitude and phase of the 1.9 mHz component was used to identify FLR features which were characterized by an enhancement in amplitude at a resonance latitude of 71.3° (Goose Bay) and -72.6° (Syowa East) as well as a phase change of ~180° across these latitudes. Sources of these ULF pulsations were investigated using wavelet spectral correlations to find time delays between oscillations in the solar wind and those observed in the ground. The time delays compared well with the solar wind travel time estimates and the results suggest a possible link between solar wind and the observed pulsations. During this process energy from the solar wind is transferred to the magnetosphere and hence deposited in the ionosphere. The instantaneous amplitude was also used to determine the spatial as well as the temporal extent of the 1.9 mHz component. It was found that in both data sets the longitudinal span of this component decreased by ~15° in an hour. The amplitude of this component was also found to decay by ~60 % (Goose Bay) and ~29 % (Syowa East) in an hour.

Preface

The work described in this thesis was carried by the author in the Department of Physics, University of KwaZulu-Natal, under the supervision of Dr. S. B. Malinga and Prof. A. D. M. Walker. These studies represent original work by the author and have not been submitted in any form to another university. Where use is made of the work of others, it has been duly acknowledged in the text.

Sibusiso Hector Mthembu

Signature: 

Date: 29/03/07

Acknowledgements

The author would like to sincerely thank and acknowledge gratefully the following for their generous contribution to the success of this thesis:

- My supervisors Dr S.B. Malinga, Prof. A.D.M. Walker and Mr. L. Magnus for their assistance and guidance provided during the preparation and compilation of the thesis

- Dr Judy Stephenson for her valuable assistance.

- Hermanus Magnetic Observatory (HMO) for financial assistance through graduate Bursary

- K.W. Ogilvie for providing WIND solar wind experiment (SWE) data and D. J. McComas of Southwest Research Institute for providing ACE Solar Wind Electron, Proton Alpha Monitor (SWEPAM) data

- Johns Hopkins University Applied Physics Laboratory HF radar at Goose Bay and National Institute of Polar Research Syowa East HF radar for HF radar data

- My family and friends for their moral support, in particular Philani for his advice.

Dedication

To my late Mother

List of acronyms

GSE	Geocentric Solar Eclipse
GSM	Geocentric Solar Magnetic
SuperDARN	Super Dual Auroral Radar Network
ACE	Advanced Composition Explorer
WIND	Interactive Physics Laboratory
SWE	Solar Wind Experiment
SWEPAM	Solar Wind Electron, Proton and Alpha Monitor
NASA	National Aeronautics and Space Administration
ISTP	International Solar-Terrestrial Physics

Table of contents

Table of figures

Chapter 1 Introduction and background theory

1.1 Introduction

The main focus of this thesis is to study the physics of Ultra Low Frequency (ULF) pulsations and how they transfer energy from solar wind to the magnetosphere. Under this, I will talk about their manifestation and their characteristics including the frequencies, amplitudes, spatial as well as temporal extent of the spectral components and the field line resonance (FLR) features. This will be done by applying data analysis techniques such as Fourier and wavelet analysis to HF radar data from Goose Bay and Syowa East HF radars and solar wind data from WIND and ACE satellites. I will then look for their possible source particularly in the solar wind by looking for some correlations between solar wind data and HF radar data. To start with, I will discuss the background theory of the ULF pulsations and their possible excitation mechanisms.

ULF pulsations are magnetohydrodynamic (MHD) waves that are excited on and propagate along earth's magnetic field within the magnetosphere (Hughes, 1994). They were discovered more than 140 years ago by Stewart (1861), long before the postulation of ionosphere and magnetosphere. Dungey (1954) came with the real understanding of the ULF pulsations which was followed by their classification in 1963 which was done according to their frequencies (McPherron, 2005). They are divided into 2 classes that include pulsations continuous (Pc) and pulsations irregular (Pi). Pc pulsations are quasi-sinusoidal signals with well defined spectral peaks and Pi pulsations are irregular signals containing power in many different frequencies. Each class is further divided into subclasses as shown in Table 1.

Table 1: The classification of ULF pulsations according to their period ranges.

Continuous pulsations (Pc)	
Class	**Period range (s)**
Pc1	0.2-5
Pc2	5-10
Pc3	10-45
Pc4	45-150
Pc5	150-600
Irregular pulsations (Pi)	
Pi1	1-40
Pi2	40-150

In this thesis, ULF pulsations which have frequencies that fall in a Pc5 band with a period range of (150-600 s) will be looked at and discussed in more detail.

1.2 Solutions of the MHD wave equations

In order to find solutions of the MHD waves one has to first consider the fluid and Maxwell's equations. The MHD waves are excited due to the movement of fluid (plasma consisting of charged particles) in the presence of electromagnetic fields (Kivelson and Russell, 1995). Fluid equations are:

$$\frac{\partial \rho}{\partial t} + \nabla \cdot \rho \mathbf{u} = 0$$
$$\rho\left(\frac{\partial \mathbf{u}}{\partial t} + \mathbf{u} \cdot \nabla \mathbf{u}\right) = -\nabla p + \boldsymbol{J} \times \boldsymbol{B}$$
$$\frac{p}{\rho^{\gamma}} = \text{constant}$$

Equation 1.1

Where ρ is the plasma density, $\mathbf{u}$ is the velocity, $\mathbf{J}$ is the current density, $\mathbf{B}$ is the magnetic flux density and γ is the ratio of specific heats. Maxwell's equations are:

$$\frac{\partial \mathbf{B}}{\partial t} = -\nabla \times \mathbf{E}$$
$$\nabla \times \mathbf{B} = \mu_o \mathbf{J}$$
$$\nabla \cdot \mathbf{B} = 0$$

Equation 1.2

Assume that the plasma is initially at rest such that $\mathbf{u} = 0 + \mathbf{u}$ and also assume that the wave introduces small perturbations **b,** $\delta\rho$ and δp in the appropriate quantities as well as quantities **E, u, and J** (Kivelson and Russell, 1995). The magnetic field, mass density and pressure can be written as the background value and small perturbation as $\mathbf{B} \rightarrow \mathbf{B} + \mathbf{b}$, $\rho \rightarrow \rho + \delta\rho$ and $p \rightarrow p + \delta p$. The perturbed quantities are assumed to be small enough that high powers and cross product of these quantities are dropped. Therefore the perturbed quantities should satisfy the equations:

$$\frac{\partial \delta\rho}{\partial t} + \rho\nabla \cdot \mathbf{u} = 0$$
$$\rho\frac{\partial \mathbf{u}}{\partial t} - \nabla\delta p + (\nabla \times \mathbf{b}) \times \mathbf{B}/\mu_o$$
$$\frac{\partial \mathbf{b}}{\partial t} = \nabla \times (\mathbf{u} \times \mathbf{B})$$
$$\nabla \cdot \mathbf{b} = 0$$

Equation 1.3

Assume that the waves propagate in the x-direction and all quantities oscillate proportional to $e^{i(kx-\omega t)}$ where $k = \frac{2\pi}{\lambda}$ and $\omega = 2\pi f_o$. Applying the plasma condition that p = 0 and, in addition, assume that the magnetic field and plasma density are constant. Replacing the time and x derivative by $-i\omega$ and $-ik$ respectively the above equations become

$$i(\omega\delta\rho - k\rho u_x) = 0$$
$$i\left[\omega\rho\mathbf{u} - k\frac{\left((\mathbf{b}\cdot\mathbf{B})\hat{x} - B_x\boldsymbol{b}\right)}{\mu_o}\right] = 0$$
$$i\left[\omega\mathbf{b} + k\left(B_x\mathbf{u} - u_x\mathbf{B}\right)\right] = 0$$

Equation 1.4

Assume that $\mathbf{B}$ lies in the ***x-z*** plane and k along x-direction and θ is the angle between $\mathbf{B}$ and k. By eliminating variables by substitution we end up with

$$\left[(\omega/k)^2 - V_A^{\,2}\sin^2\theta\right]u_x + V_A^{\,2}\sin\theta\cos\theta u_z = 0$$
$$\left[(\omega/k)^2 - V_A^{\,2}\cos^2\theta\right]u_y = 0$$
$$\left[(\omega/k)^2 - V_A^{\,2}\sin^2\theta\right]u_z + V_A^{\,2}\sin\theta\cos\theta u_x$$

Equation 1.5

where $V_A = \left(\mathrm{B}^2/(\mu_o\rho)\right)^{\frac{1}{2}}$ is the Alfven wave velocity.

In warm plasma where the plasma pressure is taken into account, the dispersion relation of the MHD waves is given by

$$\left((\omega/k)^2 - V_A\cos^2\theta\right)\left[\omega^4/k^2 - \omega^2(C_s^{\,2} + V_A^{\,2}) + V_A^{\,2}C_s^{\,2}\cos^2\theta\right] = 0$$

Equation 1.6

where C_s is the speed of sound. Equation 1.6 has three solutions corresponding to three waves that propagate through the plasma.

The first solution corresponds to shear Alfven waves which do not change plasma pressure or density, they only cause the magnetic field lines to bend. The dispersion relation of these waves is given by $(\omega/k)^2 = V_A^{\,2}\cos^2\theta$. This implies that Alfven waves never propagate perpendicular to the magnetic field but only along it.

The second solution corresponds to fast waves which propagate in any direction and at the same time transport energy in any direction. These waves carry perturbations in which particle pressure and density vary in phase with the magnetic perturbation parallel to the background field. The dispersion relation of the fast waves depends on the direction of propagation such that for propagation perpendicular to the magnetic field, the dispersion relation is given by $(\omega/k)^2 = \sqrt{V_A^{\,2} + C_s^{\,2}}$. For propagation parallel to the magnetic field, $(\omega/k)^2$ is the larger of V_A and C_s.

The third solution corresponds to slow waves which carry perturbations in which plasma pressure and density vary out of phase with the magnetic pressure. The waves have phase velocity that is less than V_A and is approximately parallel to the background magnetic field.

In cold plasma the pressure term becomes unimportant and the properties of the shear Alfven waves are unchanged from those found in the warm plasma. In this limit the dispersion relation of the fast mode reduces to $(\omega/k)^2 = V_A^2$ and the slow waves cease to exit.

1.3 Properties of solar wind and the magnetosphere

The solar wind is a flow of ionized solar plasma and a remnant of the solar magnetic field that pervades interplanetary space (Kivelson and Russell, 1995). The flow is the result of the huge difference in gas pressure between the solar corona and interstellar space, which then drives the gas outward despite the restraining influence of solar gravity. This highly conducting plasma travels at a supersonic speed of ~450 km.s^{-1} as a result of supersonic expansion of the solar corona. Other properties of the solar wind at 1- Astronomical Unit (AU which is the distance from the sun to the earth) are listed in Kivelson and Russell (1995). When the solar wind magnetic field which is frozen into the plasma encounters an obstacle, for example dipole magnetic field lines of the earth that it cannot penetrates, the solar wind is slowed down and to a large extent deflected around it. As the solar wind hits the earth's magnetic field at supersonic speed, a shock wave which is known as bow shock is formed as shown in Figure 1.1. The region that is formed underneath the bow shock which is denser and hotter than the solar wind plasma is known as a magnetosheath. The shocked solar wind plasma in the magnetosheath cannot penetrate the earth's magnetic field and is thus deflected around it. The boundary that separates the magnetosheath and magnetosphere is called the magnetopause. The magnetosphere is the cavity in which most of the discussion in this thesis will be based. Other regions that are formed during the interaction of the solar wind and the earth's magnetic field are shown in Figure 1.1 for completeness although they are of less importance in this thesis.

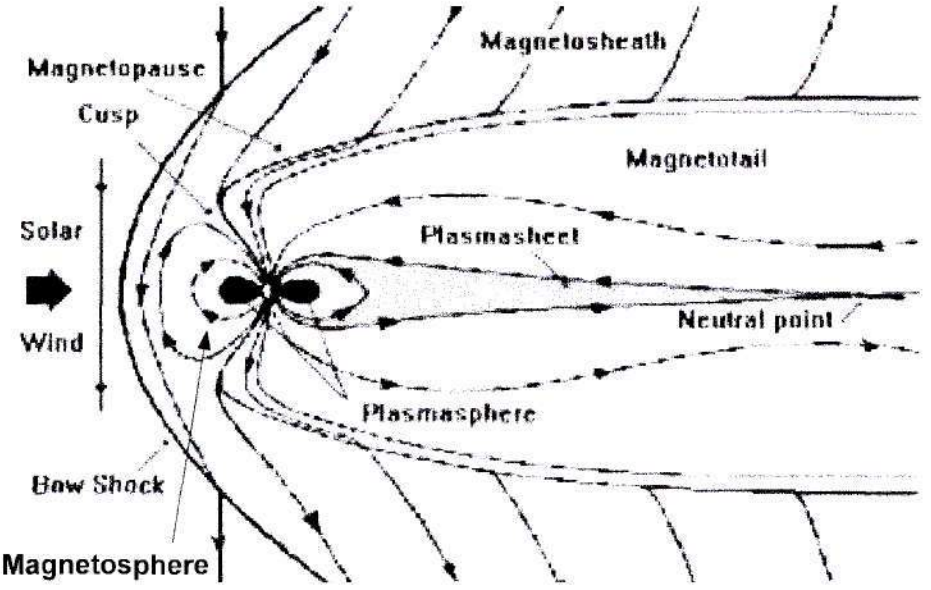

Figure 1.1: Modified schematic cross-section of the magnetosphere in the noon-midnight meridian. Also shown are different regions formed during the deflection of solar wind by the earth magnetic field, URL: http://www.spaceweather.com/glossary/imf.html.

There are numerous magnetospheric processes that occur in the magnetospheric cavity which are excited by different factors, among those are Ultra Low Frequency (ULF) pulsations. Numerous waves that are seen at the surface of the earth originate outside the magnetosphere (Yumoto, 1988). The solar wind, ion foreshock, bow shock and magnetopause are some of the external sources of ULF pulsations (McPherron, 2005). ULF pulsations are the mechanism that is believed to transfer a certain percentage of energy from the sun to the earth. Field line resonance and waveguide or cavity resonance (as will be discussed at length in Sections 1.6.2 and 1.6.3) are processes that are believed to transform the ULF wave energy that enters the magnetosphere from outside (McPherron, 2005). The characteristics of the ULF pulsations being excited depend on the properties of the magnetosphere which includes the size of the magnetospheric cavity, the length and strength of the magnetic field lines and mass density distribution (Fenrich et al., 1995; Kepko and Spence, 2003). Longer field lines as well as field lines with more or heavier particles will have longer resonant period (lower frequencies) and vice versa (McPherron, 2005). The magnetospheric size and the internal wave speed determine the frequency of the oscillations that are excited, for example they place the limit of the global oscillations at approximately 1 mHz (Kepko and Spence, 2003). This idea is still going to be discussed in length later.

1.4 Field line resonance

The field line resonance can be explained by assuming that the earth's magnetic field lines behave like vibrating strings which are frozen in the ionosphere and can not move (McPherron, 2005). In the absence of the force the field lines attain equilibrium. However if some processes that may develop in the magnetosphere happens to displace them, tension force would develop and tries to restore them back to their equilibrium position. Since the magnetic field lines are frozen into the plasma (which consist of heavy particles), they pick up momentum that cause them to overshoot the equilibrium position and thus oscillate until other processes damp them.

In a cold uniform plasma, two modes of oscillations can exist, which include poloidal or compressional oscillations and toroidal or field aligned oscillations (Walker et al., 1992). The toroidal mode is the displacement in an azimuthal direction and it is shown in Figure 1.2.

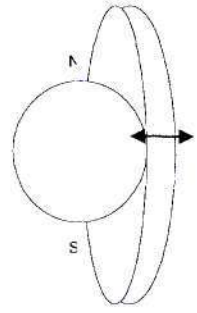

Figure 1.2: The toroidal mode of oscillations showing field lines displaced in an azimuthal direction. This mode of oscillation is excited with ease due to the fact that azimuthally adjacent field lines oscillate in-phase.

This mode of oscillation is commonly observed in space due to the fact that azimuthal oscillations do not change the magnitude of the magnetic field or cause plasma density changes (McPherron, 2005). The field line azimuthally adjacent to the vibrating field line consists of nearly the same frequency and so vibrates in-phase with it. These properties identify this mode as an Alfven wave. On the other hand, the poloidal mode is the displacement in a radial direction and it is shown in Figure 1.3.

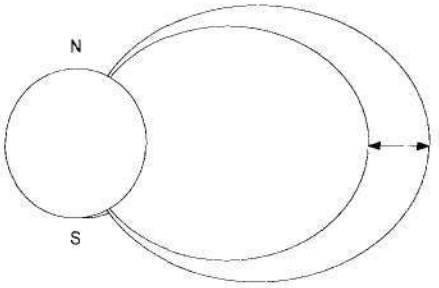

Figure 1.3: The poloidal mode of oscillations showing field lines displaced in a radial direction. This mode of oscillation is hard to excite due to the fact that radially adjacent field lines oscillate out of phase.

This mode is hard to excite because the field lines are vibrating in a radial direction and radially adjacent field lines are vibrating at different frequencies, as a result the field lines will vibrate out of phase (McPherron, 2005). These properties identify this mode as a fast MHD wave. As it was stated above that the frequency and the Alfven velocity of the field lines is dependent on the length and strength of the field lines such that longer field lines as well as field lines with heavier particles will resonate with low frequencies (McPherron, 2005). Thus it is expected that the Alfven velocity and resonant frequency of the field lines should increase as one moves from the magnetosphere to the earth (from right to left of the figure). However there are some deviations in the expected behaviour as shown in Figure 1.4.

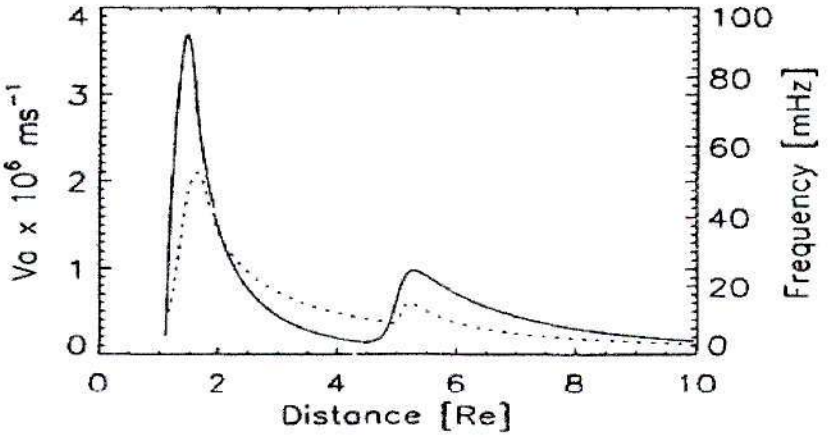

Figure 1.4: The radial profile of Alfven velocity (solid) and frequency (dotted) of the field lines Waters et al. (2000).

In Figure 1.4 the magnetopause is located at 10 Re, plasmapause at 5 Re and ionosphere at 1.1 Re. The frequency and Alfven velocity are expected to increase smoothly from the magnetosphere to ionosphere but there are some deviations in the plasmasphere region as well as in the ionosphere region. The sudden decrease in frequency across plasmapause region is due to the increase in plasma density and another decrease in the ionosphere is caused by the presence of heavy particles such as oxygen.

1.5 Latitude profile of amplitude and phase of the ULF pulsations

According to Walker (1995) some external influence such as Kelvin-Helmholtz instability or abrupt change in solar wind dynamic pressure or any other influence which has a well defined frequency can excite the field lines inside the magnetosphere into oscillations. The field lines at a certain *L*-shell (e.g. *L*-shell D in Figure 1.5) with characteristic frequency matching that of the driver will resonate, and large oscillations will be set up over a narrow range of latitudes. The schematic representation of this mechanism is shown in Figure 1.5 where in this case Kelvin-Helmholtz instability is responsible for the excitation of field lines into resonance.

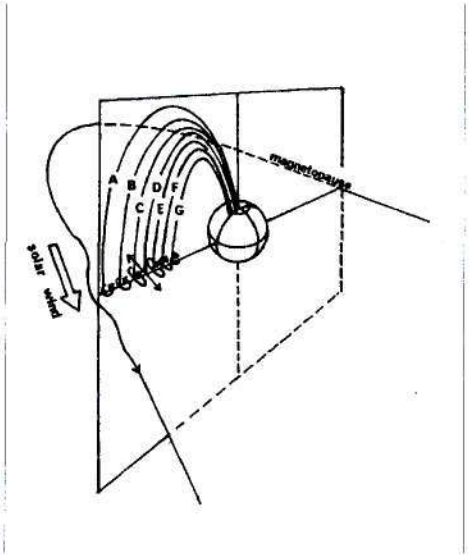

Figure 1.5: Schematic representation of a resonance showing how Kelvin-Helmholtz instability wave on the magnetopause excites a particular *L*-shell into resonance (Walker, 1995)

This theory was studied independently by Southwood (1974) and Chen and Hasegawa (1974) where they predicted that an enhancement in amplitude at the resonance L-shell is accompanied by a phase change of approximately 180°. This behaviour is the result of the fact that L-shells nearer the earth have higher frequencies than the driver and lead it in phase and those that are near magnetopause have lower frequencies than the driver and lag it in phase. Walker et al. (1979) provided the confirmation of this theory where they used STARE radar data to plot amplitude and phase of an electric field as shown in Figure 1.6.

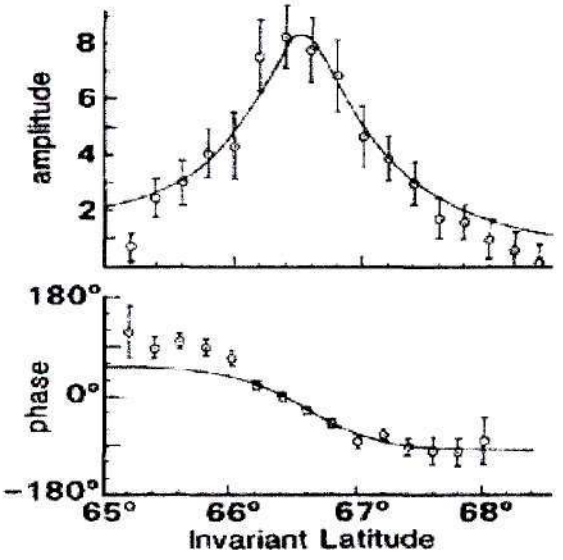

Figure 1.6: The theoretical prediction of resonance theory compared with STARE radar observations. The solid lines represent the theoretical prediction and the points represent the real data (Walker et al., 1979).

In Figure 1.6 the solid lines represent the theoretical prediction and the points represent the real data. The ULF pulsations that show this behaviour are classified as field line resonance (FLR). The field lines are observed to be oscillating at discrete frequencies that are close to 1.3, 1.9, 2.7 and 3.3 mHz similar to those observed by e.g. Samson et al. (1991); Walker et al. (1992); Fenrich et al. (1995); Stephenson and Walker (2002); Kepko and Spence (2003). The occurrence of these discrete frequencies will be discussed later.

1.6 The review of excitation mechanisms of ULF pulsations

ULF pulsations which have frequencies that fall in a Pc5 band with a period range of (150-600s) are often observed to occur at discrete frequencies in the magnetosphere. These oscillations were observed by satellites, ground magnetometers and radars (Taroyan and Erdélyi, 2003). The physical processes responsible for their excitation are still unknown but their possible excitation mechanisms will be discussed below.

1.6.1 Kelvin-Helmholtz instability

The first proposition was made by Dungey (1955) that solar wind could excite Kelvin-Helmholtz (KH) vortices travelling along magnetosphere. The flow of the solar wind around the magnetosphere can create surface waves. These surface waves are similar to the waves created in the lake when the strong wind is blowing (Kivelson and Russell, 1995). The schematic representation of this process is shown in Figure 1.7 (a) where the wiggly lines represent the ULF waves that are created and the thickness of the lines represent the wave amplitudes which decrease anti-sunward but peaks at the resonance L-shell. The field lines at the magnetopause compressionally couple to field lines inside the magnetosphere, setting them into oscillation and at the same time transmitting energy to them. These waves propagate down until other magnetospheric processes damp them.

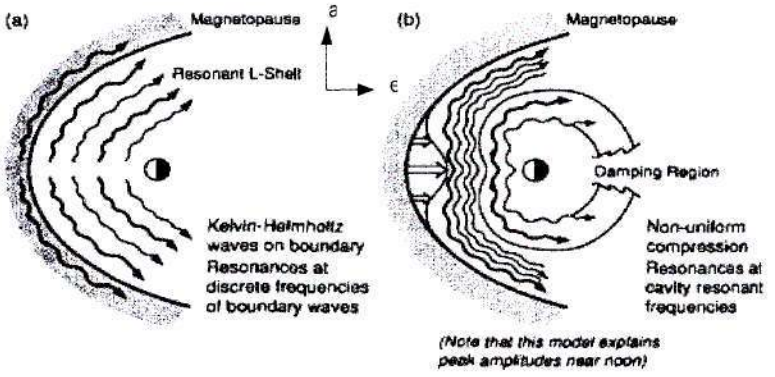

Figure 1.7: Shows schematically how Kelvin-Helmholtz instability excites the surface waves which then excite ULF pulsations in the magnetosphere (b) solar wind dynamic pressure excites ULF pulsations in the magnetosphere. (Kivelson and Russell, 1995)

The theoretical study of the resonant coupling process was carried out independently by Southwood (1974) and Chen and Hasegawa (1974). Although the theory proved successful in explaining many of the observed features, it failed to explain the reproducibility of the observed discrete frequencies of FLRs (Provan and Yeoman, 1997).

1.6.2 Cavity mode

The shortcoming mentioned above led Kivelson and Southwood (1985) to propose that a cavity mode is responsible for the excitation of FLRs. They proposed that the magnetosphere can be considered to be a cavity that can resonate at its discrete frequencies (Taroyan and Erdélyi, 2003). This resonance may be caused by numerous processes, including a change in solar wind dynamic pressure. In this process the ULF pulsations are created as the magnetosphere responds to an abrupt change in solar wind dynamic pressure as illustrated in Figure 1.7 (b). If the solar wind compresses the magnetosphere, changes in the components of the field in the directions â and ê as shown in Figure 1.7 (b) are created thereby creating the ULF pulsations which propagate along the filed lines and at the same time the fast mode oscillations will couple to inner field lines (Kivelson and Russell, 1995). The northern and southern hemisphere ionosphere serve to confine the signals between the two ionospheres on the other hand the near-equatorial ionosphere and the magnetopause confines the signals between them. As a result the frequencies of the signals that propagate radially will be quantized as much as the frequencies of the field aligned signals will be quantized. The schematic representation of the coupling of fast mode to field line resonance is shown in Figure 1.8.

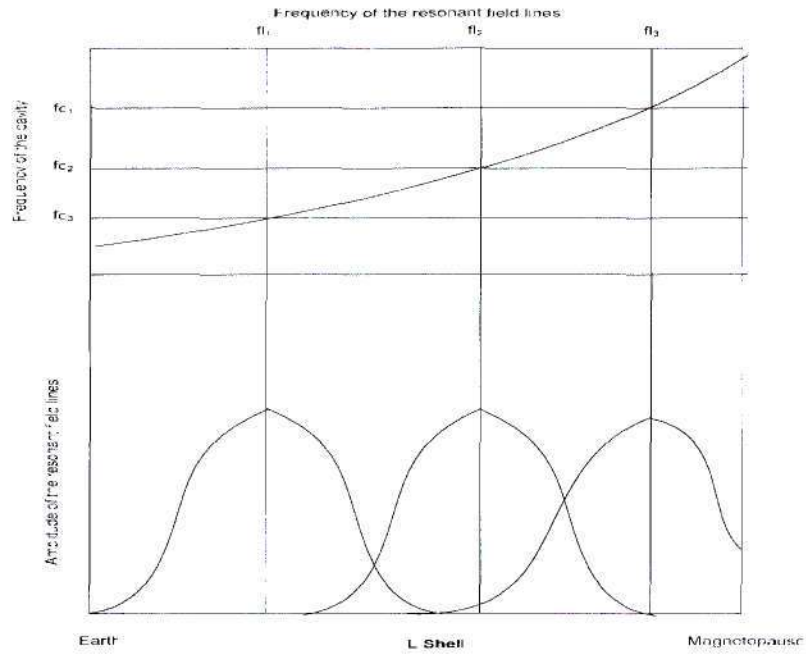

Figure 1.8: The schematic representation of field line resonance driven by resonant magnetospheric cavity mode. The figure shows 3 frequencies of the cavity fc_1, fc_2 and fc_3 and the frequencies of the field lines fl_1, fl_2 and fl_3. When frequencies of the cavity matched that of the field lines, oscillations with large amplitude are excited on the field line as shown.

For simplicity, 3 resonant frequencies of the cavity fc_1, fc_2 and fc_3 are shown in the top panel. Three field lines at different L-shells are also shown and they resonate at frequencies fl_1, fl_2 and fl_3 also shown in the top panel. When the characteristic frequency of the resonating field lines match that of the cavity modes, the energy of the fast modes is transferred to the field lines which then resonate with greater amplitude as shown in the bottom panel. This excitation mode has managed to explain the excitement of the observed discrete frequencies of the field line resonance, but it was lacking the observational evidence.

1.6.3 Waveguide mode

The lack of observational evidence of the cavity mode led Walker et al. (1992) to propose another new model that could be responsible for the excitation of FLRs. They assumed that the magnetospheric cavity is not closed but represent an open-ended waveguide with boundaries at the magnetopause and the turning point as shown in Figure1.9.

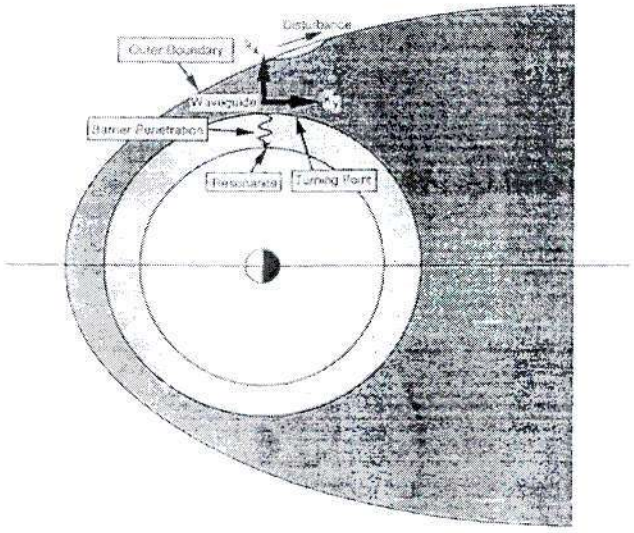

Figure 1.9: The schematic diagram of the equatorial plane in the waveguide model (Walker et al., 1992).

The impulse excitation mechanism in the waveguide magnetosphere is insufficient to explain the almost constant presence of the Pc5 FLRs (Taroyan and Erdélyi, 2003). Anderson et al. (1990) had used the Active Magetospheric Particle Trace Explorer/Charge Composition explorer (AMPTE/CCE) magnetic field data and showed that the Pc5 FLRs are continuously present in the dawn flank. The steady supply of energy has been proposed to be coming from the solar wind moving along magnetopause thereby producing a disturbance on the boundary which is propagated tailward. This mechanism is similar to the one illustrated in Figure 1.7 (a) where solar wind excites FLR through Kelvin-Helmholtz instabilities. However, the difference is that the excited waves are reflected between the magnetopause and the turning point as shown in Figure 1.9. During this reflection some of the energy can penetrate through the barrier and excites FLR in the inner magnetic fields. This model was supported by observations which revealed some correlations between solar wind speeds and the power of the Pc5 FLR (Engebretson et al., 1998; Mathie and Mann, 2001).

1.6.4 Solar wind sources

Samson et al. (1991) noted that the observed frequencies of the ULF pulsations were very stable and reproducible. If we consider the cavity or waveguide mode picture we would require a cavity that has constant dimensions and unvarying properties. Due to the variability

of magnetospheric properties it is very difficult to attribute the observed stable frequencies to cavity modes. Secondly, it was stated in Sections 1.3 that the magnetospheric size and the internal wave speed place the limit of the global oscillations at approximately 1 mHz (Kepko and Spence, 2003). But global magnetospheric oscillations with frequencies of less than 1 mHz are common and have been observed in radar measurements by e.g. Walker et al. (1992). The simultaneous observation of the frequencies of less than 1 mHz and discrete frequencies noted by Samson et al. (1991) would call into question the proposal that the discrete frequencies are the manifestation of the cavity or waveguide mode since oscillations with frequency of less than 1 mHz are not associated with the cavity or waveguide modes (Kepko and Spence 2003). For this reason, a search for sources of the ULF pulsations outside the magnetosphere was undertaken. Walker (2002) proposed that the source of the observed frequencies seen in the field line resonances were the fast MHD waves incident on the bow shock from upstream solar wind. Observational evidence was provided independently by Stephenson and Walker (2002) and Kepko and Spence (2003). They did some correlation between HF radar data and satellite data and found some oscillations with frequencies which lay in the Pc5 band in both data. It is believed that the oscillations in the solar wind excited the field lines into resonances there by transferring the energy from the solar wind to the magnetosphere

Having covered the introduction and the background theory of the ULF pulsations, I will discuss the techniques that will be used to analyze the data and the observational techniques that were used to collect it. Thereafter, I will present the results of the analysis and conclude with a brief discussion of them.

Chapter 2 Data analysis techniques

2.1 Introduction

In this chapter data analysis techniques such as Fourier analysis, analytic signal, wavelet analysis and cross-spectral density will be discussed. Although the Fourier transformation is a powerful technique for determining the frequency content of the signal, it is unable to provide the time of occurrence and the time evolution of individual spectral components. Later in the analysis correlation between radar and satellite data will be done to check if the oscillations observed on the ground could have been caused by the ones in the solar wind. In order to determine that, time of occurrence of these oscillations is required. This information can be obtained by making use of wavelet transform. The analytic signal which is used to determine the time evolution of amplitude and phase of the spectral component will also be discussed. And lastly the cross-spectral density will be discussed which quantifies the spectral components present in two signals.

2.2 Fourier Transform

Fourier transformation (FT) is a technique that is used to investigate the frequency content of a signal. It actually decomposes the signal into sinusoids of different frequencies which add to the original signal. Brook and Wynne (1998) defined the Fourier transform of a signal $x(t)$ as

$$X(f) = \int_{-\infty}^{\infty} x(t)\, e^{-i2\pi ft}\, dt$$

Equation 2.1

and the inverse Fourier transform as

$$x(t) = \frac{1}{2\pi} \int_{-\infty}^{\infty} X(f)\, e^{i2\pi ft}\, d\omega$$

Equation 2.2

Equation 2.1 gives us the frequency content of the signal (i.e. which frequency components exist in the signal) over the whole duration of the signal without telling us the time of occurrence of each component. Consequently the technique works well when we are investigating stationary signals whose characteristics do not change with time. The analysis of nonstationary signals can be done using other techniques such as Short-Time Fourier Transform (STFT) and wavelet transform (WT) which will be dealt with in more details in Sections 2.4 and 2.5 respectively

2.3 Analytic Signal

The analytic signal of the real function *f(t)* can be defined as the complex function which is given by the sum of the function itself and its quadrature function (Bracewell, 1986). According to Smith (2003) the Hilbert transform can be considered as an ideal filter consisting of the amplitude of one at all frequencies and an infinite bandwidth, that introduces a phase shift of $+90^{\circ}$ on the negative frequency components and phase shift of -90° on the positive frequency components. The phase shift of $+90^{\circ}$ can be introduced by multiplying the negative frequency components by $e^{j\frac{\pi}{2}} = j$, and the phase shift of -90° can be introduced by multiplying the positive frequency components by $e^{-j\frac{\pi}{2}} = -j$. The Hilbert transform which is given by *Hi(t)* is referred to as the quadrature function of *f(t)*. Therefore the analytic signal is given by

$$AS(t) = f(t) + jHi(t)$$

Equation 2.3

In Figure 2.1 the function *f(t)* is plotted along the real axis and its quadrature function along the imaginary axis. The analytic signal is the complex function which is represented by a helix that is slowly contracting and dilating. It can be considered as a phasor with a slowly varying length and phase. The length and phase of the phasor represents the instantaneous amplitude and phase respectively. The rate of change of the phase represents the instantaneous frequency.

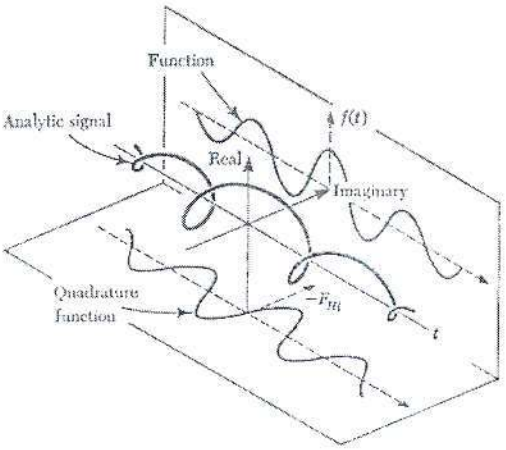

Figure 2.1: The function *f(t)* plotted along the real axis and the quadrature function F_{Hi} plotted along the imaginary axis. The complex analytic function represented by a helix that is slowly contracting and dilating (Bracewell, 1986).

The analytic signal is used to determine the time evolution of amplitude and phase of the selected frequency component of the signal. Since the method is applied on the quasi-monochromatic signals, the signals have to be filtered prior to the calculation of the analytic signal. To illustrate, consider a non-stationary process consisting of the signal $f(t)$ plus some noise given by

$$f(t) = \sum_{j=0}^{n-1} A_j(t)\, e^{+i\omega_j t} + \sum_{j=0}^{n-1} B_j(t)\, e^{-i\omega_j t}$$

Equation 2.4

where $A_j(t)$ and *B(t)* indicate a variation of amplitude while $\omega_j t$ indicate a variation phase of the j^{th} component with time. The signal is passed through a band-pass filter centred on the frequency component of interest ω_o and the filtered signal would be

$$f_f(t) = \sum_{j=k}^{l} A_j(t)\, e^{+i\omega_j t} + \sum_{j=k}^{l} B_j(t)\, e^{-i\omega_j t}$$

Equation 2.5

where k and l are the indexes corresponding to lowest and highest cut-off frequencies respectively.

The Hilbert transform of function $f(t)$ would be

$$Hi(t) = -i\sum_{j-k}^{l} A_j(t)\, e^{+i\omega_j t} + i\sum_{j-k}^{l} B_j(t)\, e^{-i\omega_j t}$$

Equation 2.6

Thus from equation 2.3 the analytic signal is given by

$$\begin{aligned} \mathrm{AS}(t) &= \sum_{j-k}^{l} A_j(t)\, e^{+i\omega_j t} + \sum_{j-k}^{l} B_j(t)\, e^{-i\omega_j t} + i\left[-i\sum_{j-k}^{l} A_j(t)\, e^{+i\omega_j t} + i\sum_{j-k}^{l} B_j(t)\, e^{-i\omega_j t} \right] \\ &= \sum_{j-k}^{l} 2A_j(t)\, e^{+i\omega_j t} \end{aligned}$$

Equation 2.7

There is a gain of two at the positive frequency components and the negative frequency components were filtered out.

Having deduced the analytic signal, the variation of amplitude with time is given by

$$A(t) = \left| A_j(t) \right|$$

Equation 2.8

Particular care needs to be taken when extracting the phase information because of a $2n\pi$ ambiguity where n is an integer (Walker et al., 1992). The phase of the analytic signal is given by

$$\phi(t) = \omega_j t$$

Equation 2.9

The phase of the analytic signal has a 2π phase ambiguity which was rectified by adding multiples of 2π .Thereafter, the phase difference between the analytic signal and a pure sinusoid with central frequency ω_o is determined from the phase factor of equation 2.10.

$$AS(t)\, e^{-i\omega_0 t} = \sum_{j-k}^{l} 2A_j(t)\, e^{+i\omega_j t}\, e^{-i\omega_0 t} = \sum_{j-k}^{l} 2A_j(t)\, e^{i(\omega_j - \omega_0)t}$$

Equation 2.10

where ω_0 is the central frequency of the filter.

Therefore the variation of phase with time is given by

$$\phi(t) = (\omega_j - \omega_0)t$$

Equation 2.11

The variation of the frequency with time can be evaluated from the rate of change of the phase, and the results yield

$$f_j(t) = \frac{\left(\frac{\partial\phi(t)}{\partial t} + \omega_0\right)}{2\pi}$$

Equation 2.12

2.4 Short Time Fourier Transform

Although the FT can give us the spectrum of the signal, it cannot give the time of occurrence of the spectral components but the Short-Time Fourier Transform (STFT) can give us both. For this reason STFT can be used to analyze a signal whose spectral components vary with time. When applying this technique, the signal is divided into small segments, and these segments are assumed to be stationary. The signal can be segmented by multiplying it with the window function of the fixed length. Ideally, the window length should be equal to the segment of the signal where the assumption of it being stationary is valid (Polikar, 2002).

The STFT is calculated by applying the FT on the windowed signal and then advancing the window in time. This process is repeated until the whole signal is covered. The whole procedure can be summarized in one equation which is given by

$$STFT(t', f) = \int_t \left[x(t) \bullet W^*(t - t')\right] e^{-j2\pi ft} dt$$

Equation 2.13

where $x(t)$ is the signal being analyzed, $W(t)$ is the window function and * denote a complex conjugate. The result of this operation is the time-frequency representation of the signal which shows frequency components that are present in the signal and their times of

occurrences. The precision of the time-frequency representation depends on the length of the window function. In FT there is a good frequency resolution and no time resolution because the window function last for the whole duration of the signal. In STFT the narrower the window the better the time localization of the spectral component, but this is at an expense of the frequency resolution. Basically there is a trade-off between the time localisation and the frequency resolution in a sense that a good time-frequency representation of the signal can be achieved by using a narrow window when looking for high frequency and vice versa. The problem with this technique is that once the window length has been chosen, that window will be used in the STFT and it will be the same for all frequencies. To solve this problem, we need a technique with a window function that can be varied depending on whether we are analyzing high or low frequency spectral components.

2.5 Wavelet analysis

Wavelet transformation is the technique that can overcome the above mentioned problem of the STFT. The better time-frequency resolution capabilities of wavelet transform will be discussed in details in Section 2.5.3, but for now background theory of wavelet analysis will be presented.

2.5.1 Wavelet

The wavelet is a waveform that is effectively limited in duration and its average value is zero Misiti et al. (1996). This term is used to describe the set of functions $\psi_{ab}(t)$ that are deduced from shifted and dilated/scaled version of the mother wavelet or basic wavelet given by $\psi(t)$. The mother wavelet is defined as the prototype for the generation of other wavelets. There are different types of mother wavelets that can be used, which include among others, the Morlet, Paul, and DOG wavelets etc (Torrence and Compo, 1998). In this analysis Morlet wavelet was used because it gives a better defined and cleaner waveform than other wavelets.

2.5.2 Continuous wavelet transform

The continuous wavelet transform (CWT) of the signal $x(t)$ is defined as sum over time of the signal multiplied by the scaled and shifted wavelet and mathematically it is given by (Torrence and Compo, 1998)

$$WT(\tau,s)=\frac{1}{\sqrt{|s|}}\int x(t)\,\psi^{*}\left(\frac{t-\tau}{s}\right)dt$$

Equation 2.14

where $\psi\left(\frac{t-\tau}{s}\right)$ are the wavelet basis functions, * indicates a complex conjugate, s is the scale and τ is the translation. The scale parameter scales the function by dilating or compressing it. The scale parameter and the frequency are inversely related and the constant of proportionality is not the same for each wavelet. The proportionality constant can be deduced by finding the wavelet power spectrum of a cosine signal of known frequency and finding the scale of the largest power (Malinga, 2001). Then the ratio between the scale and the frequency of the cosine gives the proportionality constant. The translation parameter is related to time information and it gives the position of wavelet as it is shifted along the signal.

The result of equation 2.14 are the wavelet coefficients WT which depend on the s and τ. WT gives the degree of correlation between the wavelet and the portion of the signal around τ. If the wavelet closely resembles the portion of the signal, the value of WT will be high and if not then the WT will be small (Malinga, 2001). Once the CWT is deduced, the wavelet amplitude spectrum can be calculated according to (Torrence and Compo, 1998)

$$A(s,\tau)=|WT(s,\tau)|$$

Equation 2.15

and the corresponding phase is given by (Torrence and Compo, 1998)

$$\phi(s,\tau)=\arctan\left[\frac{\mathrm{Im}(WT(s,\tau))}{\mathrm{Re}(WT(s,\tau))}\right]$$

Equation 2.16

2.5.3 Time-Frequency localization

Having looked at the theory of the wavelets, the time-frequency localisation of the wavelet transform will be discussed. The wavelet transform has a good time-frequency representation due to the fact that it has a variable 'window' function. It should be noted that wavelet does not use the window function in the sense of the one used in STFT. The window in the

inverted commas refers to the wavelet which has a compact support (that is it has a finite length). It performs correlation and windowing at the same time. This can be illustrated using Figure 2.2 similar to the one used by Polikar (2002).

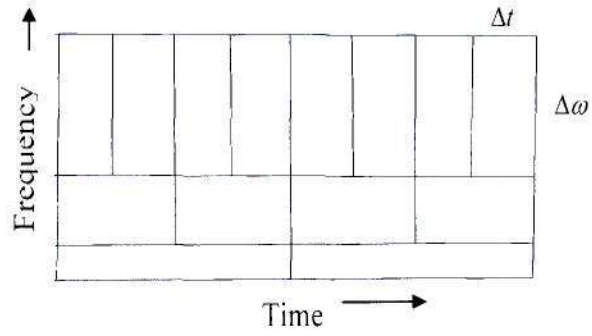

Figure 2.2 The vertical and horizontal dimensions of the figure represent frequency and time respectively where frequency increase upward and time to the right. [Similar to the one from Torrence and Compo (1998)].

The horizontal dimension of each cell is Δt and the vertical dimension is $\Delta\omega$ and the area is given by $\Delta t\Delta\omega$. Although the dimensions of the cells change, the area is constant and represents one value of the wavelet transform. For high frequencies (i.e. small scale) the horizontal dimension of the cells are shorter which correspond to shorter window length. In this case the signal is better resolved in time and poorly resolved in frequency. For low frequencies (large scale) the horizontal dimensions are longer which correspond to longer 'window' length. And for this case the signal is better resolved in frequency and poorly resolve in time. Wavelet analysis is designed to give good time resolution and poor frequency resolution at high frequencies and vice versa.

2.6 Cross-spectral Density

The cross-spectral density (CSD) is used to quantify the frequency components that are common between two signals. Consider two signals $x(t)$ and $y(t)$, their Fourier transforms are given by $X(\omega)$ and $Y(\omega)$, then the corresponding CSD is given by

$$S_{xy} = \frac{X_n \cdot {}^{*}Y_n}{\omega_0} = A_{xy}(\omega)\exp\left[i\phi_{xy}(\omega)\right]$$

Equation 2.17

The cross-spectrum amplitude quantifies the average product of the amplitudes of the spectral components in $x(t)$ and $y(t)$ at a specific frequency f while the cross-spectrum phase quantifies the average value of the phase shift between spectral components of two signals at that frequency. This information can be used to find the time lag for a particular component f between two signals. The time lag can be given by

$$\Delta t = \frac{\Delta\varphi}{360^{o} \times f}$$

Equation 2.18

where $\Delta\varphi$ is the phase shift in degrees.

Chapter 3 Observational techniques

3.1 Introduction

Having discussed the data analysis technique used to analyze the data, I will now discuss the observational techniques used to collect it. The major analysis in this thesis will be conducted using SuperDARN High Frequency (HF) radar data and some satellite data. The technology and operation of these instruments will be discussed. The major discussion in this chapter will be based on the SuperDARN HF radar operation and brief discussion on the WIND and ACE satellites.

3.2 HF radar principles

3.2.1 Description and operation of radars

The Super Dual Auroral Radar Network (SuperDARN) is a collaborative network of HF radars that monitor the ionospheric plasma convection over the Northern and Southern polar regions. SuperDARN HF radars are very important instruments that are used to investigate high latitude ionosphere and magnetosphere (Walker, 2002). They are capable of sending signals to the atmosphere and receiving reflected signals from ionospheric irregularities in the *E*- and *F*-regions of the high latitude ionosphere.

The standard SuperDARN HF radar antenna array consists of 16 booms each supporting a log-periodic antenna (Greenwald et al., 1995). Signals from these antennas are phased using an electronically-controlled time-delay element that allows the beam to be steered into 16 directions. The width of each beam depends on the radar operating frequency, and ranges from 2.5° at 20 MHz to 6° at 8 MHz. The nominal sector covered by one complete scan of the HF radar is about 52°. The dwelling time of the beam in one direction is about 7 s resulting in a time resolution of one complete scan being 120 s and the field of view being about 2000×2000 km^2. The analysis of the returned signal from the irregularities allow the determination of line of sight Doppler velocity, backscatter power, and spectral width and other spectral information for up to 75 range gates along beam where each range gate is equal

to 45 km. This implies that the measurement can be made from a few kilometres to more than 3000 km in range.

Many SupperDARN HF radars have additional secondary 4 antenna arrays that are used to determine the vertical angle of arrival of the backscattered signal (Greenwald et al., 1995). The secondary array also uses a phase matrix and it functions as an interferometer to determine the relative phases of the backscatter signals arriving at the two arrays. The phase information is converted to an elevation angle which is used to determine the propagation modes of the returning signals as a function of range, as well as the approximate altitude of the scatters. There is total of 11 radars in the Northern Hemisphere and 6 in the Southern Hemisphere and their fields of view are shown in Figure 3.1 and 3.2 respectively. The field of view of the HF radar located at Goose Bay is highlighted in red in Figure 3.1 and the one at Syowa East is highlighted in Figure 3.2. This thesis is based on data collected from these two radars.

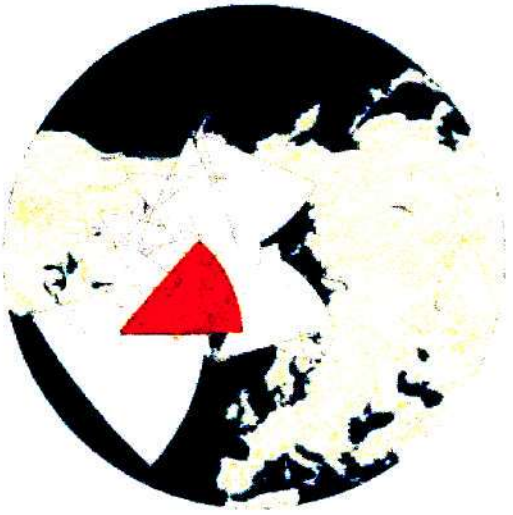

Figure 3.1: Fields of view of the HF radars in the Northern Hemisphere with Goose Bay highlighted in red.

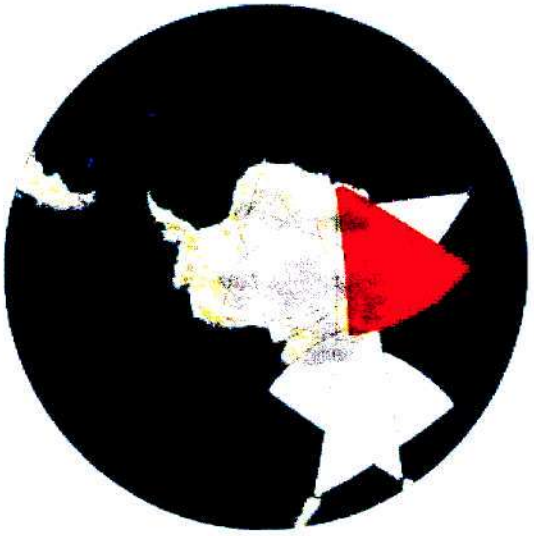

Figure 3.2: Fields of view of the HF radars in the Southern Hemisphere with Syowa East Highlighted in red.

The antenna arrays of all SuperDARN HF radars are similar and as an example Figure 3.3 shows the view of an antenna array of the þykkvibær HF radar located at UK (Iceland).

Figure 3.3: view of the antenna array of the þykkvibær HF radar located at UK (Iceland).

The operation of the SuperDARN HF radars is controlled according to a protocol signed by the representatives of all radars. In this protocol, three modes of operation were agreed upon which include standard/normal, special and discretionary mode (Walker, 2002). A more detailed description on the modes is given on the SuperDARN web site that could be found on URL: http://sd-www.jhuapl.edu/programs. In the standard mode the radars operate by sweeping successively through all beam directions for an integration time corresponding to a 2-minute scan. In the special mode the radars have a special scanning pattern chosen for

particular experiment. In the discretionary mode the principal investigators are at liberty to operate the radars at their own discretion to suit their own experiments. The HF radars are controlled by a fast computer system that is flexible and can be used to modify all operating parameters of the radar (Greenwald et al., 1995). The operation of the radar can be changed by an operator under program control in response to a scientific schedule, or changing ionospheric conditions as observed by the radar. HF radars can also be operated using remote controllers without the operator being actually at the radar station.

3.2.2 Analysis of the backscatter returns

The SuperDARN HF radars use a variety of multipulse transmission sequences consisting of 5 to 7 pulses transmitted over a 100 ms interval (Greenwald et al., 1995). The return signal from the irregularities is sampled and processed to produce multilag autocorrelation functions (ACF's) as a function of range. Walker (2002) has explained in more detail how the ACF are calculated. The ACF's are fitted to determine the backscatter power, the line of sight velocity and the spectral width for each range for which there are significant returns. These estimates are produced and stored on dics and DVDs. The data is distributed to all (SuperDARN) collaborators. An example of the data that can be obtained from the SuperDARN HF radar is shown is Figure 3.4 This figure shows the three-parameter plots of backscatter power (top), line of sight Doppler velocity (middle) and the spectral width (bottom) are shown in Figure3.4 as the function of range and universal time. Although the SuperDARN data were used to investigate the ULF pulsations in this thesis, the data have plenty of other applications which include the study of substorm convection patterns (Bristow et al., 2001), determination of polar cap boundary (Chisham et al., 2003), fluctuations in the spectral distribution of near range meteor echoes (Arnold et al., 2001) etc.

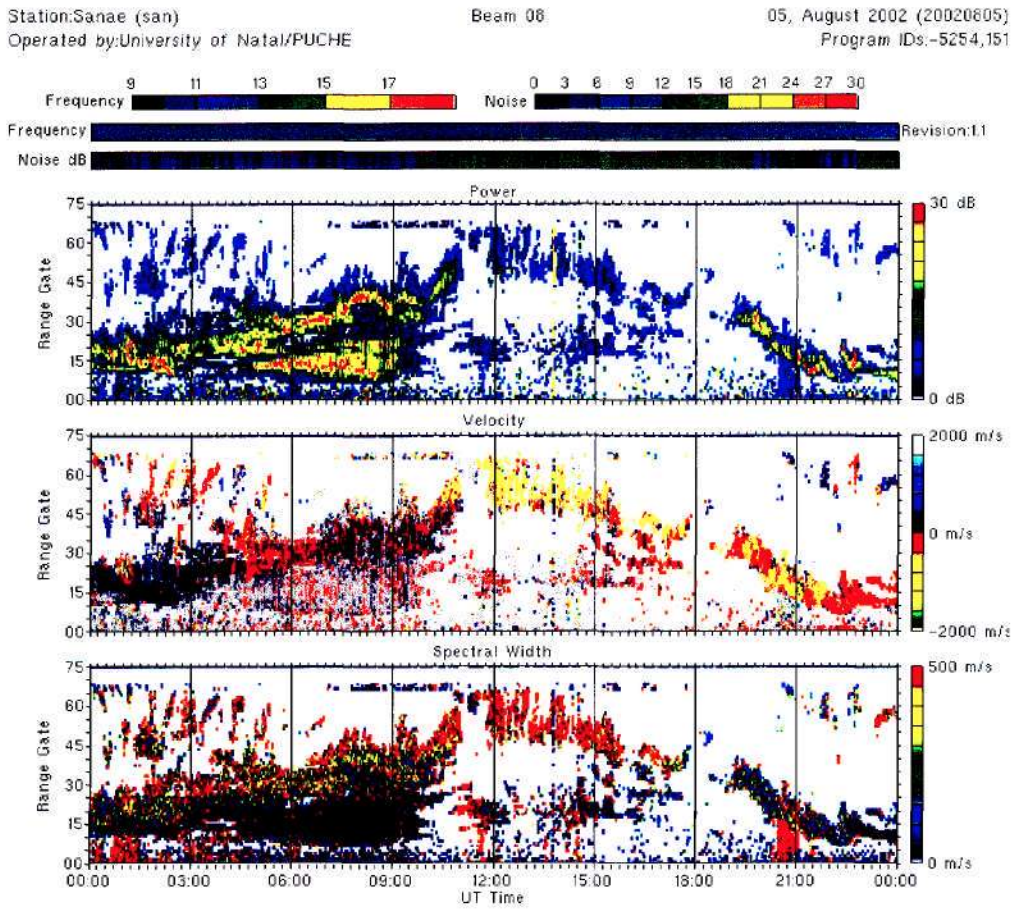

Figure 3.4: The three dimensional summary plots of backscatter power (top), line of sight Doppler velocity (middle) and the spectral width (bottom) produced from the data received from SANAE HF radar located at Antarctica.

3.3 Satellite Data

3.3.1 Interactive Physics Laboratory (WIND) and the Advanced Composition Explorer (ACE) satellites

Part of the analysis in this thesis will be conducted using the WIND and ACE satellites. These satellites are part of the contribution of the National Aeronautics and Space Administration (NASA) to the International Solar-Terrestrial Physics (ISTP) programme that makes coordinated observations of the complex sun-solar wind-magnetosphere-ionosphere system

(Kessel et al., 1995). These satellites carry an array of instruments which include the Solar Wind Experiment (SWE) (in WIND) and Solar Wind Electron, Proton and Alpha Monitor (SWEPAM) (in ACE) which measures protons and electrons in the solar wind. These instruments provide nearly continuous monitoring of the solar wind conditions and these measurements are being used to investigate the disturbances and changes in the solar wind that drive important phenomena in the near-earth environment. The data from these satellites are collected and pasted on the ISTP data Web site that can be obtained from the URL: http://cdaweb.gsfc.nasa.gov/cdaweb/istp_public/. The data is posted as Key Parameters and is available to all researchers. The example of the data that can be obtained from these satellites is shown in Figure 3.5 which shows the three components of the velocity of the solar wind in Geocentric Solar magnetic (GSM) coordinates. This data was collected from the WIND satellite on the 29th of October 2005 for a time interval 0:00 to 10:00 h. Although this is not the only data that can be obtained from the satellites, these data are shown because they were used in this thesis.

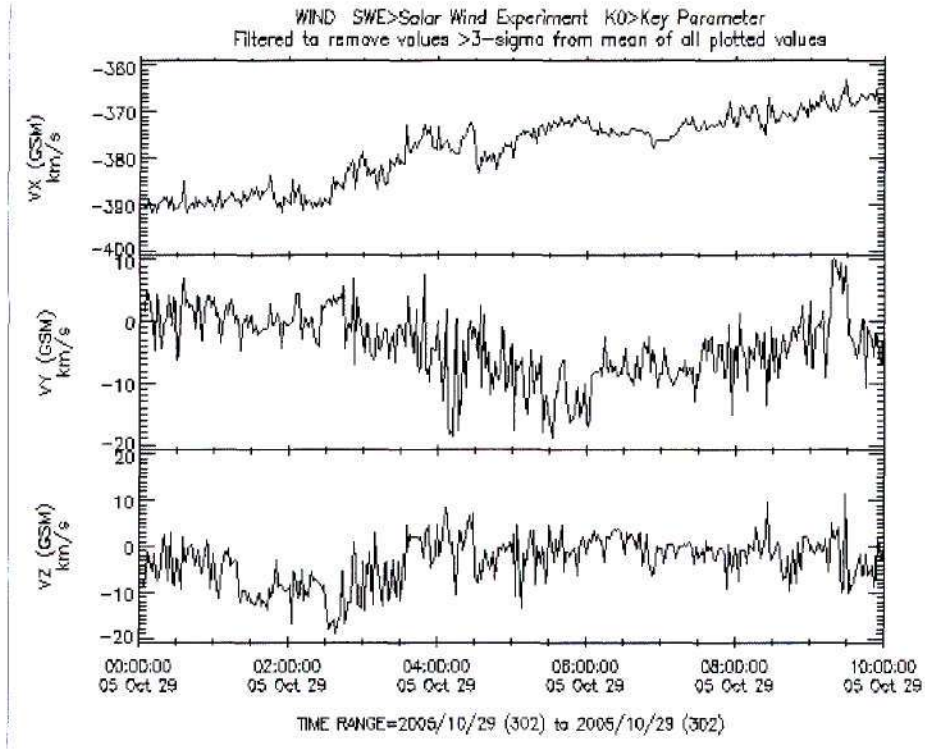

Figure 3.5: The three components of the solar wind velocity in Geocentric Solar Magnetic (GSM) coordinates collected from the WIND satellite on the 29th of October 2005 for the time interval from 0:00 to 10:00 h.

HF radars and satellites are not the only instruments that are used to investigate ULF pulsations, magnetometers are also used. Unlike magnetometers, HF radars can be steered in different directions yielding spatial resolution that will be exploited to investigate FLR characteristic. This is one reason among others that HF radar data were used in this work. Satellite data was primarily used to capture oscillations in the solar wind so as to do some correlations with HF radar data.

Chapter 4 Data analysis

4.1 Introduction

In this chapter I will apply the theoretical ideas and the techniques of the analysis developed in chapter 1 and chapter 2 to the HF radar data from Goose Bay and Syowa East HF radars and to the solar wind data from WIND and ACE satellites. The first step will be to determine the spectral content of signal using Fourier transform to confirm that the observed oscillations can be classified under Pc5 ULF pulsations. I will use the analytic signal to determine whether the observed ULF pulsations are FLR's and then investigate their possible source by making use of wavelet analysis to correlate HF radar data and solar wind data. I will then examining the temporal extent of the observed FLRs using the analytic signal.

4.2 Signature of ULF pulsations

The investigation of the ULF pulsations was conducted using the data collected from the HF radar located at Goose Bay (53.32° N, 60.46° W, geographic), Syowa East (69.01° S, 39.61° E, geographic), the WIND and ACE satellites. The field of view of the Goose Bay HF radar is shown in Figure 4.1 with beam 2 highlighted in red and Figure 4.2 shows the field of view of the Syowa East HF radar with beam 6 highlighted in blue. These beams are highlighted to show their locations because most of the analysis was done using the data from them. The data from the Goose Bay HF radar were collected on the 11th of November 2002 during the time interval 6:00 to 8:00 Universal Time (UT) with a sampling period of 120 s and the Syowa East data were collected on the 17th of June 2000 during time interval 04:00 to 07:00 UT with a sampling period of 75 s. Data from these days and times were used for no particular reason other than that the signature of the pulsations were apparent.

The investigation started by scanning through range-time summary plots of line-of-sight Doppler velocity. The activity of the ULF pulsations is observed as alternating bands of positive and negative velocity as shown in Figure 4.3 for Goose Bay data as well as in Figures 4.4 and 4.5 from Syowa East data. Note that the data in Figure 4.5 is the continuation of the data in Figure 4.4.

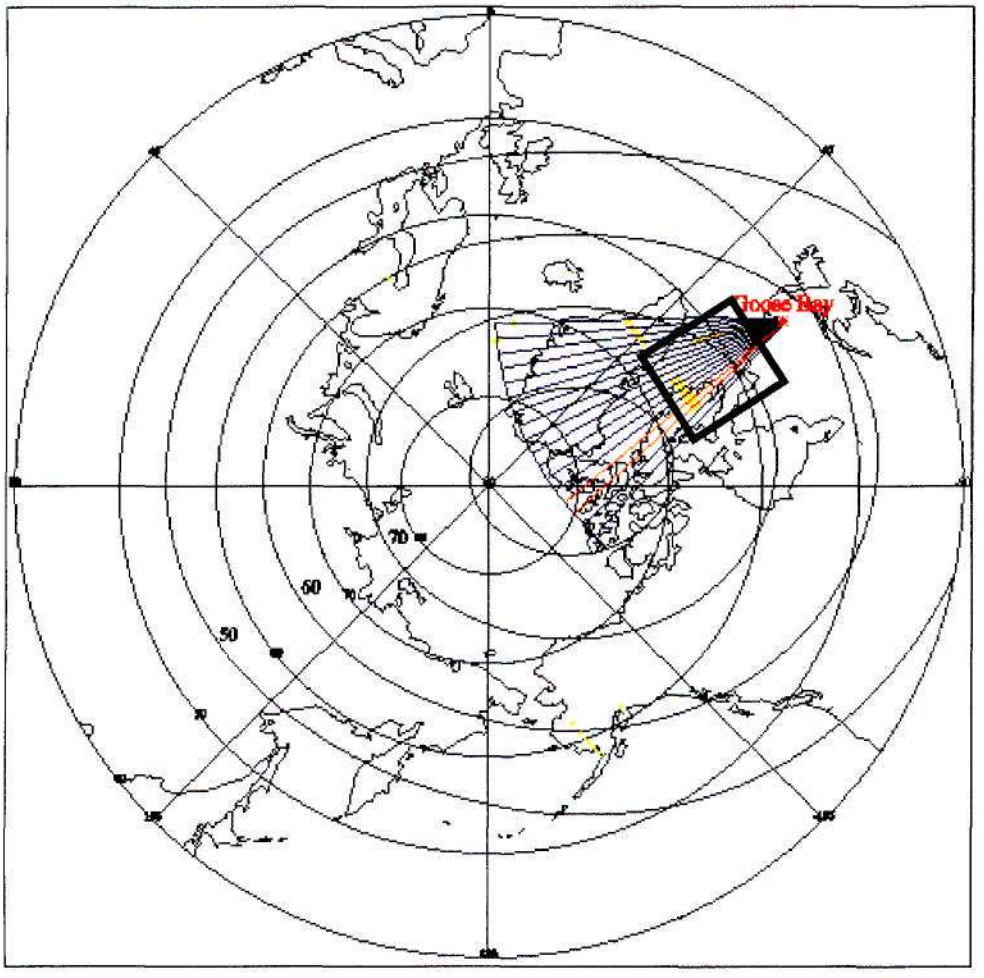

Figure 4.1: The field of view of the Goose Bay HF radar with beam 2 highlighted in red and rectangle shows region where signals were received. The figure shows geographic and geomagnetic latitude where geographic North Pole is at the centre of the inner circle and geomagnetic North Pole is slightly shifted.

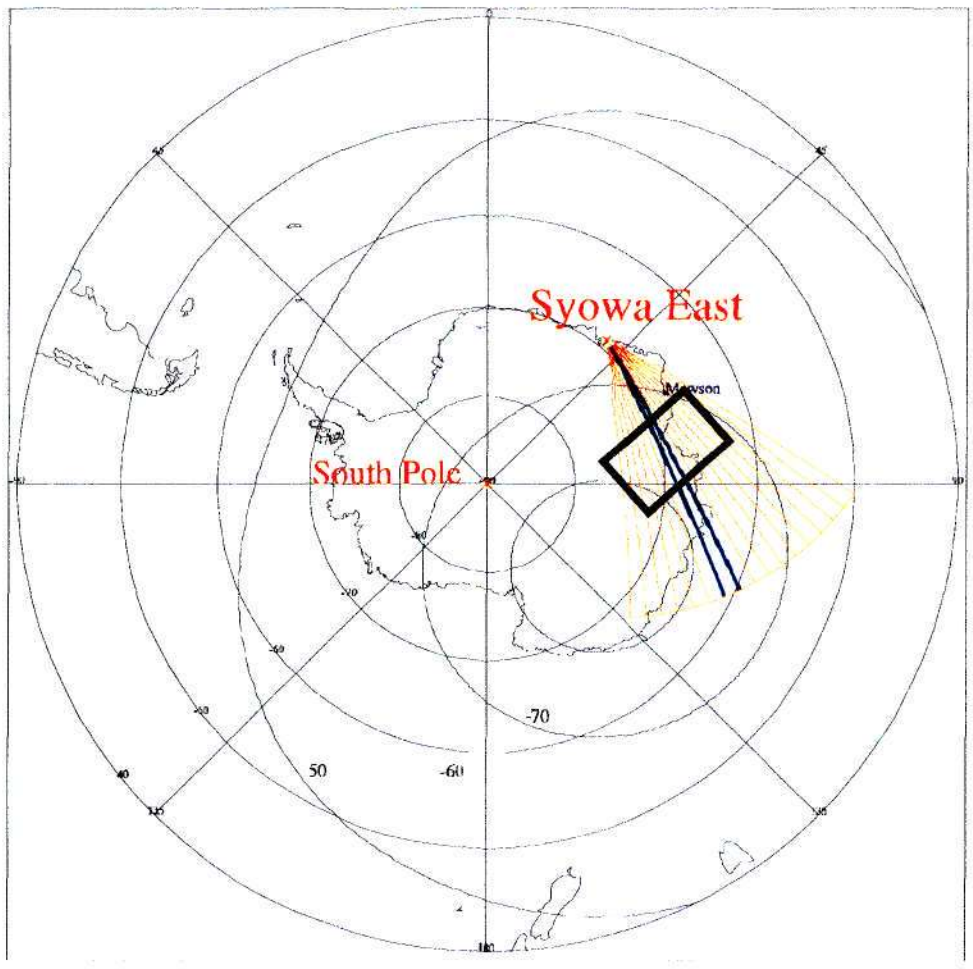

Figure 4.2: The field of view of the Syowa East HF radar with beam 6 highlighted in blue and rectangle shows region where signals were received. The figure shows geographic and geomagnetic latitude where geographic South Pole is at the centre of the inner circle and geomagnetic South Pole is slightly shifted.

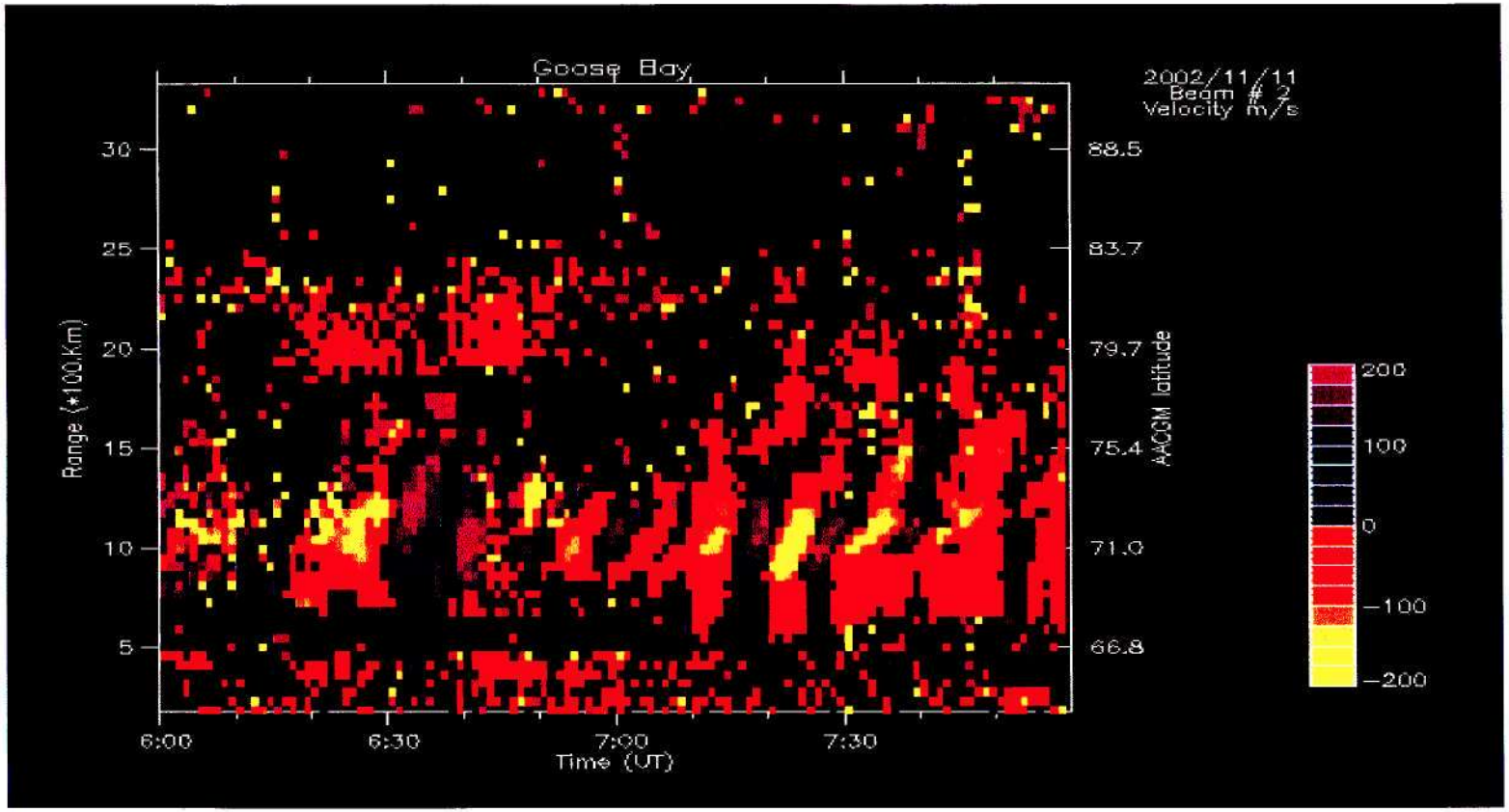

Figure 4.3: The summary plot of line-of-sight Doppler velocity collected from the Goose Bay HF radar on the 11th of November 2002 from 6:00 to 8:00 UT. The data were sampled every 120 s

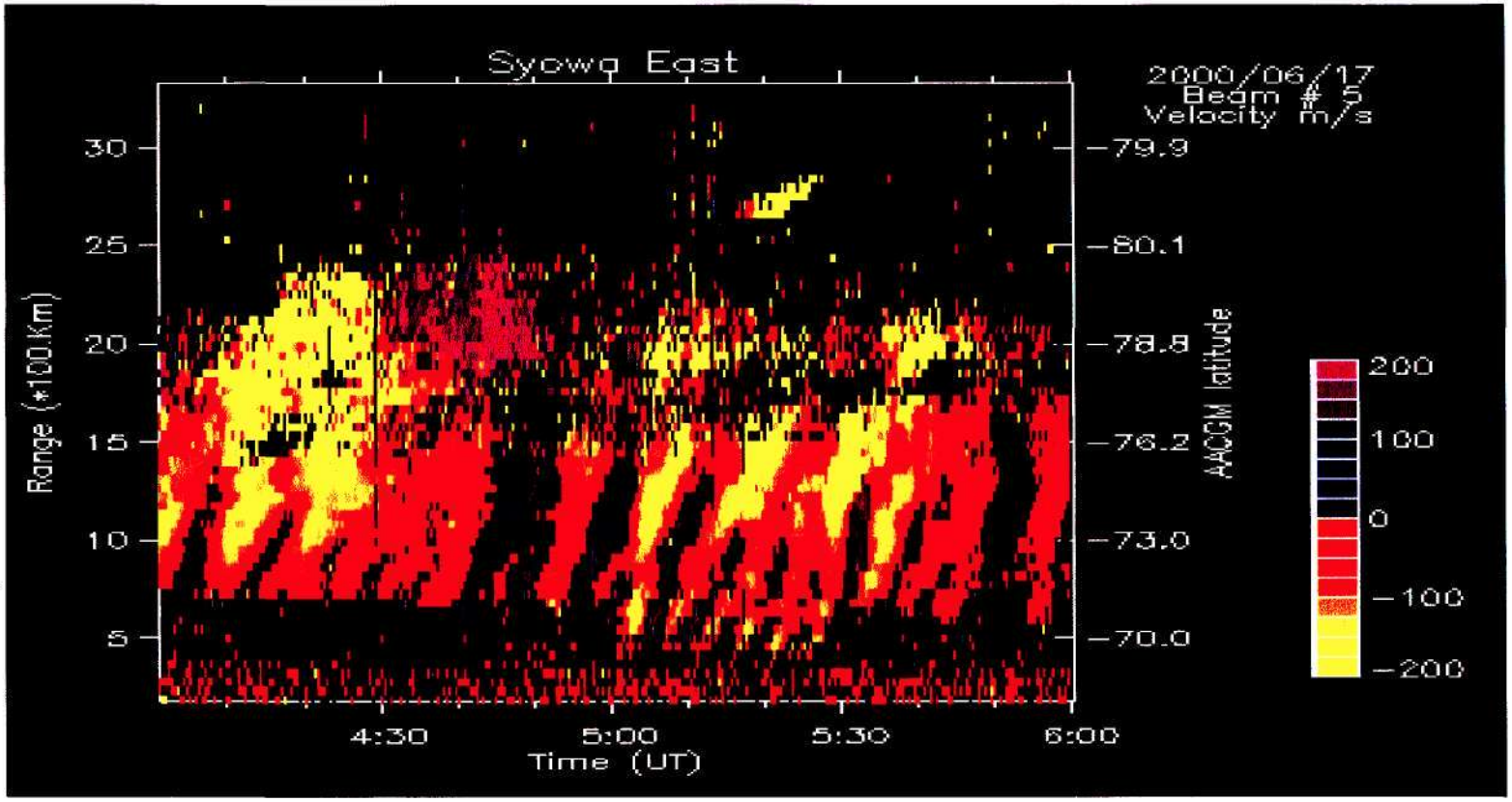

Figure 4.4: The summary plot of the line-of-sight Doppler velocity collected from the Syowa East HF radar on the 17th of June 2000 from 4:00 to 6:00 UT. The data were sampled every 75 s

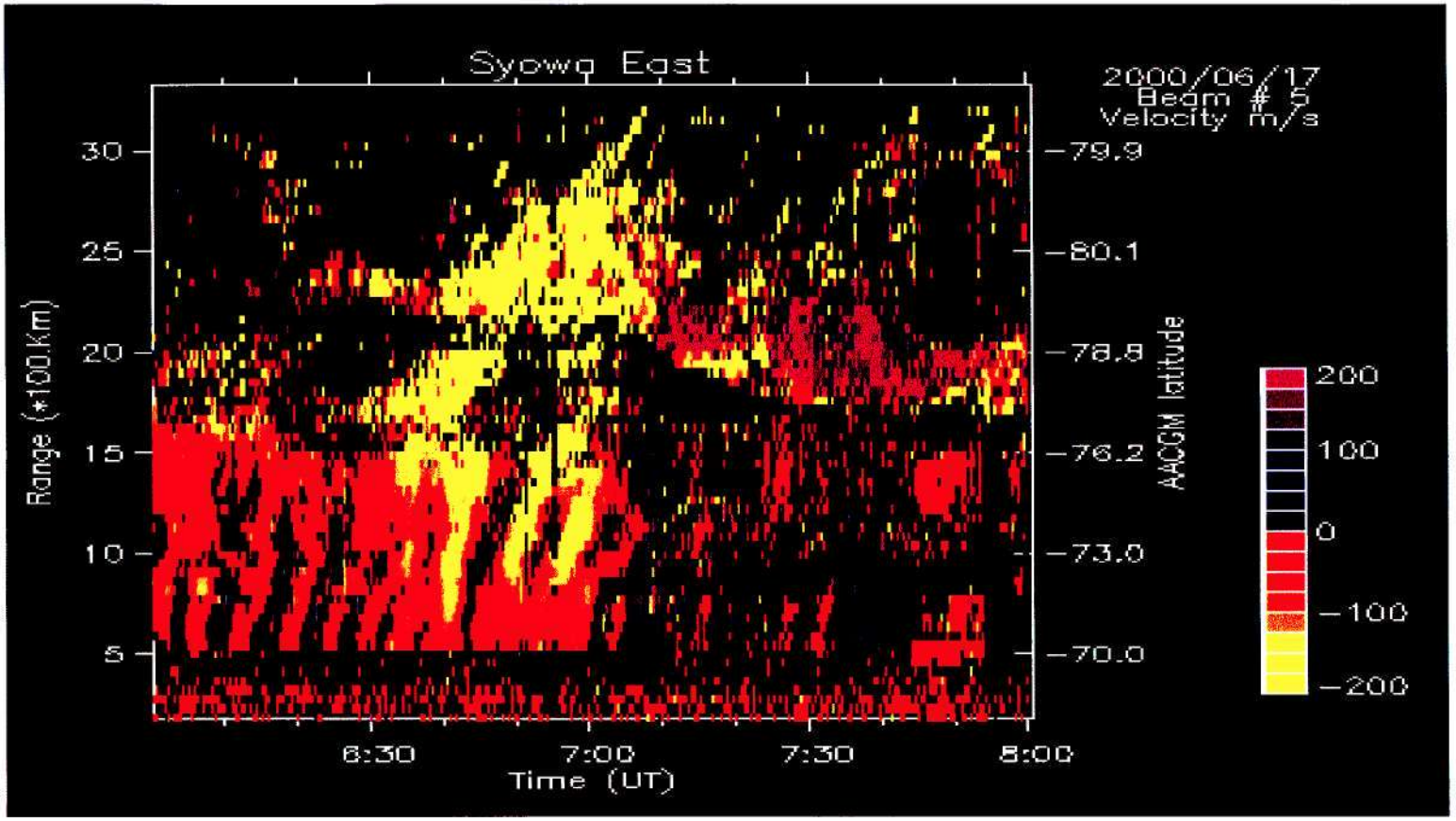

Figure 4.5: The summary plot of the line-of-sight Doppler velocity collected from the Syowa East HF radar on the 17th of June 2000 from 6:00 to 8:00 UT. The data were sampled every 75 s. This figure is a continuation of data in Figure 4.4.

Figure 4.1 shows the field of view of the Goose Bay HF radar with beam 2 highlighted in red. This beam was chosen because it is aligned with the magnetic meridian and the black rectangle indicates the region where strong signals were received. The choice of the beam to be used depends on what one is looking for and in this case the 180° phase change of the FLRs was of particular interest, so the beam that is aligned with the magnetic meridian was chosen. For Syowa East HF radar all beams are not aligned with the magnetic meridian but beams 0 to 6 makes the smaller angle with the meridian and beam 6 highlighted in blue in Figure 4.2 was chosen for intensive analysis. The black rectangle in this figure indicates the region where strong signals were received. The Goose Bay data plotted in Figure 4.3 shows the activity of the ULF pulsations observed for about an hour from 6:50 to 7:50 UT with the stronger activity from about 7:00 to 7:45 UT. The ULF pulsation activity is observed over a latitudinal range of about 9° from 67° to 76°.

The activity of ULF pulsations in the Syowa East data shown in Figure 4.4 and 4.5 is observed for about 3 hour from 4:00 to 7:00 UT with the strongest activity from about 4:30 to 6:30 UT. These pulsations had a latitudinal span of about 6° from 70° to 76°. Although the signature of the pulsations is clear in Goose Bay data, it stands out more clearly in the Syowa East data.

4.3 Amplitude Spectrum

Before any analysis, linear interpolation of the velocity data was performed to fill in small data gaps that were not more than 30% of the data and the data with large data gaps were not used. The 30% mentioned above refers to the total missing data with the individual data gaps being shorter than 10 points. Other than that the data were not filtered.

In order to determine which spectral components are present in the data, the Fourier transform was used to calculate the amplitude spectra of the Goose Bay data (beam 2) and Syowa East data (beam 6). This was done for a number of latitudes where there was enough data and the contour plots of the spectra are shown in Figure 4.6 for Goose Bay data and Figure 4.7 for Syowa East data. The red lines in these figures indicate the resonance latitude while the ellipse in Figure 4.7 highlights the relationship between frequency and latitude and circles in Figure 4.7 indicate the peaks. All these features will be discussed later.

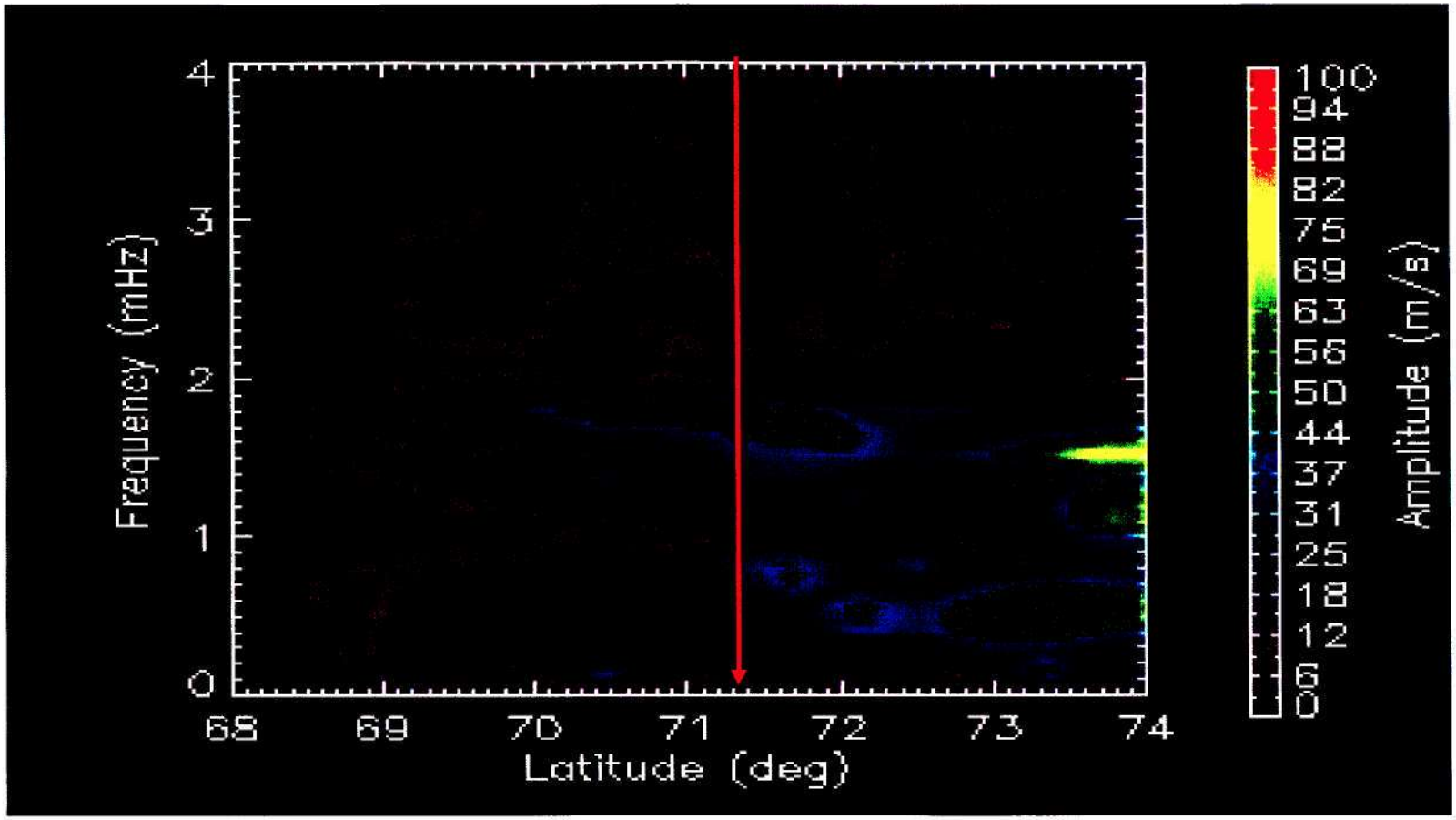

Figure 4.6: The amplitude spectra of the line-of-sight Doppler velocity calculated using Goose Bay data collected on the 11th of November 2002 from beam 2. The frequency resolution is 0.14 mHz.

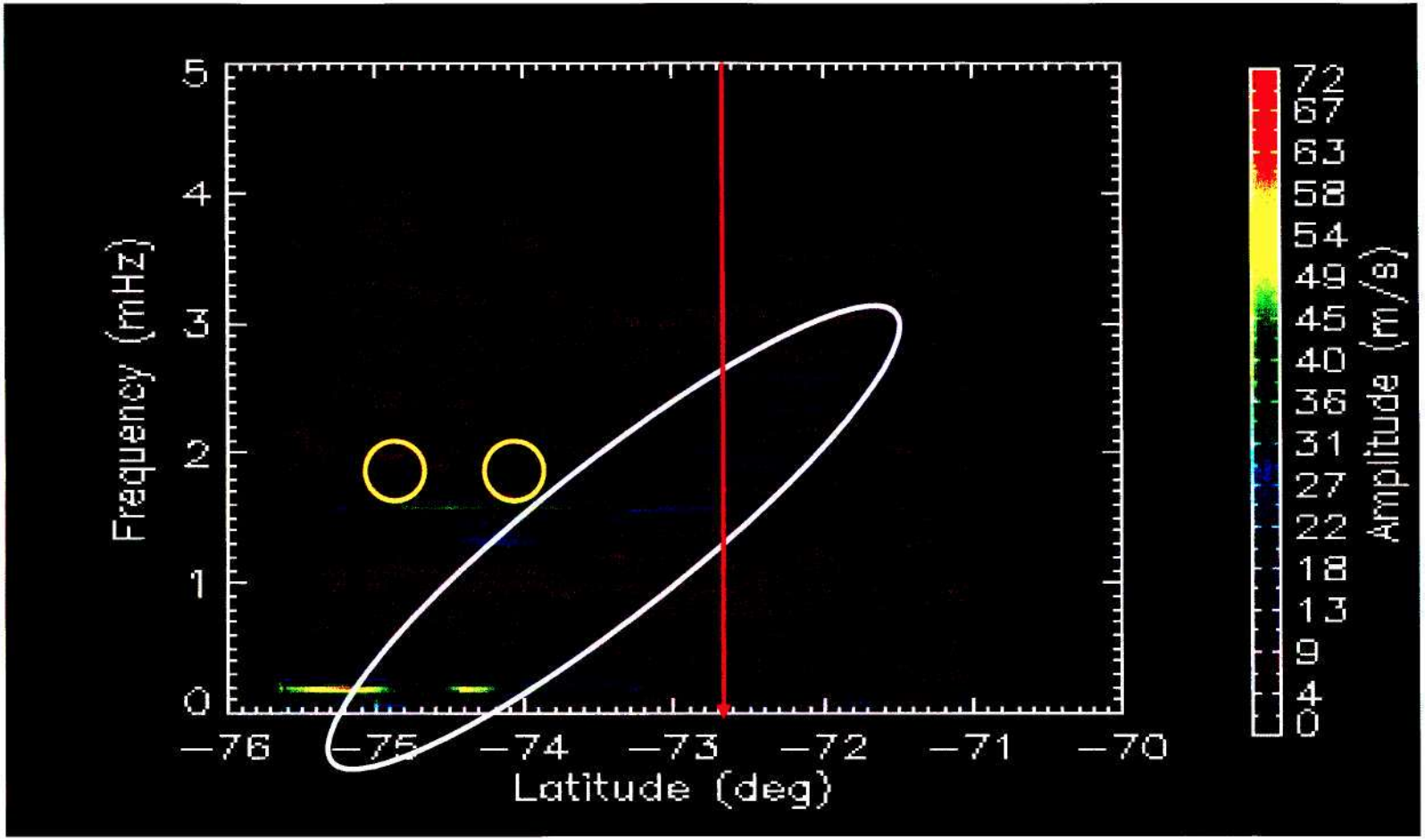

Figure 4.7: The amplitude spectra of the line-of-sight Doppler velocity calculated using Syowa East data collected on the 17th of June 2000 from beam 6. The frequency resolution is 0.093 mHz.

During the day of the event the Goose Bay radar was operating under normal mode and it was taking samples every 120 s. The sampling frequency was 8.3 mHz resulting in a Nyquist frequency of 4.15 mHz which is more than a maximum frequency of interest (4 mHz). Thus the requirements of the sampling theorem were met. The frequency resolution is 0.14 mHz which is suitable to resolve the frequencies (1.3, 1.9, 2.3, 2.7 and 3.3 mHz). On the other hand the Syowa East radar was operating on special mode and was taking samples every 75 s. The sampling frequency is 13.3 mHz resulting in a Nyquist frequency of 6.65 mHz which is also more than a maximum frequency of interest. Again the sampling theorem is met. The frequency resolution is 0.093 mHz which is even more suitable to resolve the frequencies of interest. Both spectra in Figures 4.6 and 4.7 are plotted from 0 to 4 mHz because this range includes the frequencies of interest and moreover there are no spectral components above 4 mHz.

Goose Bay data and Syowa East data show peaks near frequencies which are close to the discrete frequencies observed by Samson et al. (1991); Walker et al. (1992); Fenrich et al. (1995); Stephenson and Walker (2002); Kepko and Spence (2003) which are assumed to be excited by magnetospheric cavity or waveguide mode. The observations suggest that ULF pulsations occurred at discrete frequencies close to 1.3, 1.9, 2.3, 2.7 and 3.3 mHz with small deviations from these values. This deviation was also noted by Kepko and Spence (2003); Ziesolleck and Mcdiarmid (1995); Francia and Villante (1997). For example Francia and Villante (1997) examined spectra from low-latitude L'Aquilla (L=1.6) ground station and found oscillations occurring over a band width ~ 0.2 mHz such that f = 1.2-1.4, 1.8-2.0, 2.2-2.4, 2.6-2.8 mHz. Such observations are in line with what is observed here, for example Goose Bay data show peaks near 1.3 and 1.9 mHz and Syowa East data show peaks near 1.3, 1.9, 2.3 and 2.7 mHz. Intensive analysis was done on the spectral component near 1.9 mHz from both data sets which will henceforth be referred to as the 1.9 mHz component and the results will be shown in the next sections.

The spectral components that are less than 1 mHz which are near 0.6 and 0.9 mHz in Goose Bay data and near 0.3 mHz in Syowa East data are also observed and these frequencies were also observed by Walker et al. (1992). As mentioned in the Section 1.6.4, these oscillations are not associated with cavity or waveguide mode. The 0.6 mHz component from Goose Bay data could

not be analyzed to check for FLRs characteristics because there is not enough data but the 0.9 mHz component from Goose Bay data and 0.3 mHz components from Syowa East data were analyzed and they were found not to show any FLR characteristics.

Peaks near less common frequencies such as 1.5 mHz in Goose Bay data and near 1.6 mHz in Syowa East data are observed. These peaks were also observed by Fenrich et al. (1995). The spectral component near 1.5 mHz from Goose Bay data were not analyzed because there is not enough data whereas the components near 1.6 mHz from Syowa East data was analyzed and found to exhibit FLRs characteristics.

Field lines emanating from high latitudes are longer and oscillate with low frequency while the opposite is true for field lines emanating from low latitudes. Although it is not possible to deduce whether this relationship exist in Figure 4.6 because there is not enough data, it is clearly observed in Figure 4.7. High frequencies maximize at low latitudes and vice versa. For example 0.3 mHz has a prominent peak near a latitude of -75.3°, 1.3 and 1.6 mHz near -74.2°, 1.9 mHz near - 72.6° while 2.3 and 2.7 mHz maximize near latitude of -72°. This inverse relationship is also illustrated by a white ellipse in Figure 4.7.

The peak near 1.9 mHz is observed in beams 1 to 9 of the Goose Bay data and in beams 2 to 7 in Syowa East data. Although other beams show similar results, further analysis was done using Goose Bay data from beam 2 and Syowa East data from beam 6. The spectral component near 1.9 mHz was examined in more details in both data.

4.4 Instantaneous amplitude and phase

The nature of the field line resonance (FLR) will be discussed in Section 4.4.1, so it is necessary to have a spatial as well as the temporal information of the signal. Temporal information at each latitude can be acquired by making use of the analytic signal. As mentioned in Section 2.3 the analytic signal can be applied when interpreting signals that are quasi-monochromatic. As was said that intensive analysis will be done using the 1.9 mHz component, this component was first isolated by band-pass filtering data around it using an IDL's digital filter which was constructed

using Kaiser's window which is in turn based on the modified Bessel function. This filter is nearly optimum in a sense of having the largest energy in the mainlobe (IDL's manual, 1997). Therefore the amplitude of the spectral component was minimally attenuated. The bandwidth of the filter is 0.4 mHz which was narrow enough to exclude the neighbouring components, yet wide enough so as not to force the resonance frequency to appear stable. The investigation of the time evolution of the 1.9 mHz frequency component was done by the calculating the instantaneous amplitude and phase i.e. the amplitude and phase of the analytic signal. The contour plots of the instantaneous amplitude and phase spectra of the Goose Bay data and Syowa East data are shown in Figures 4.8 to 4.11. The rectangles as well as the lines in the following figures illustrate FLR characteristics which will be discussed in more details in the next section and the 2 ellipses in Figure 4.10 indicate peaks that will also be discussed.

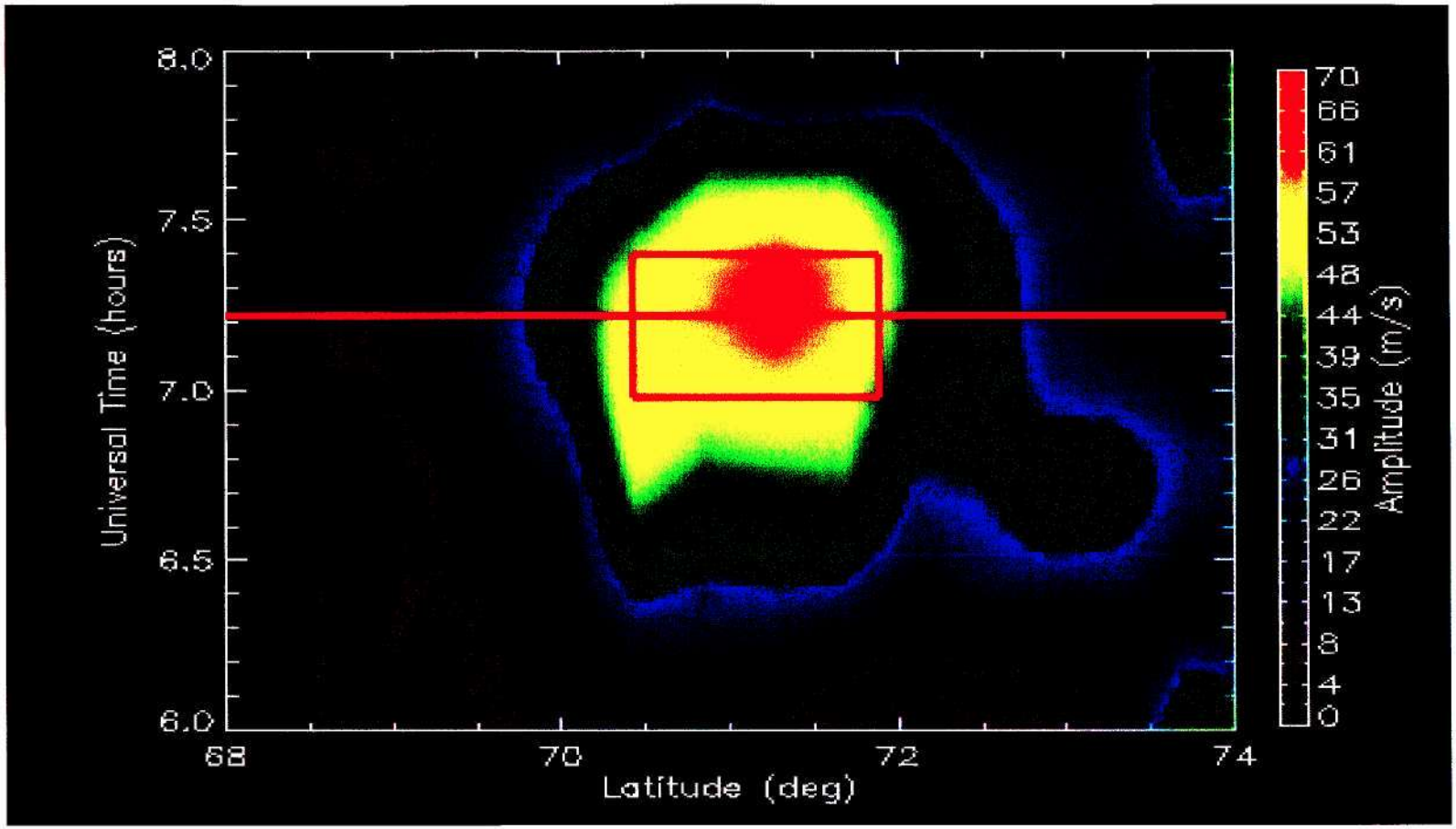

Figure 4.8: The instantaneous amplitude of the 1.9 mHz component from Goose Bay data calculated as the amplitude of the analytic signal. The length of the signal is 2 h with a time resolution of 120 s.

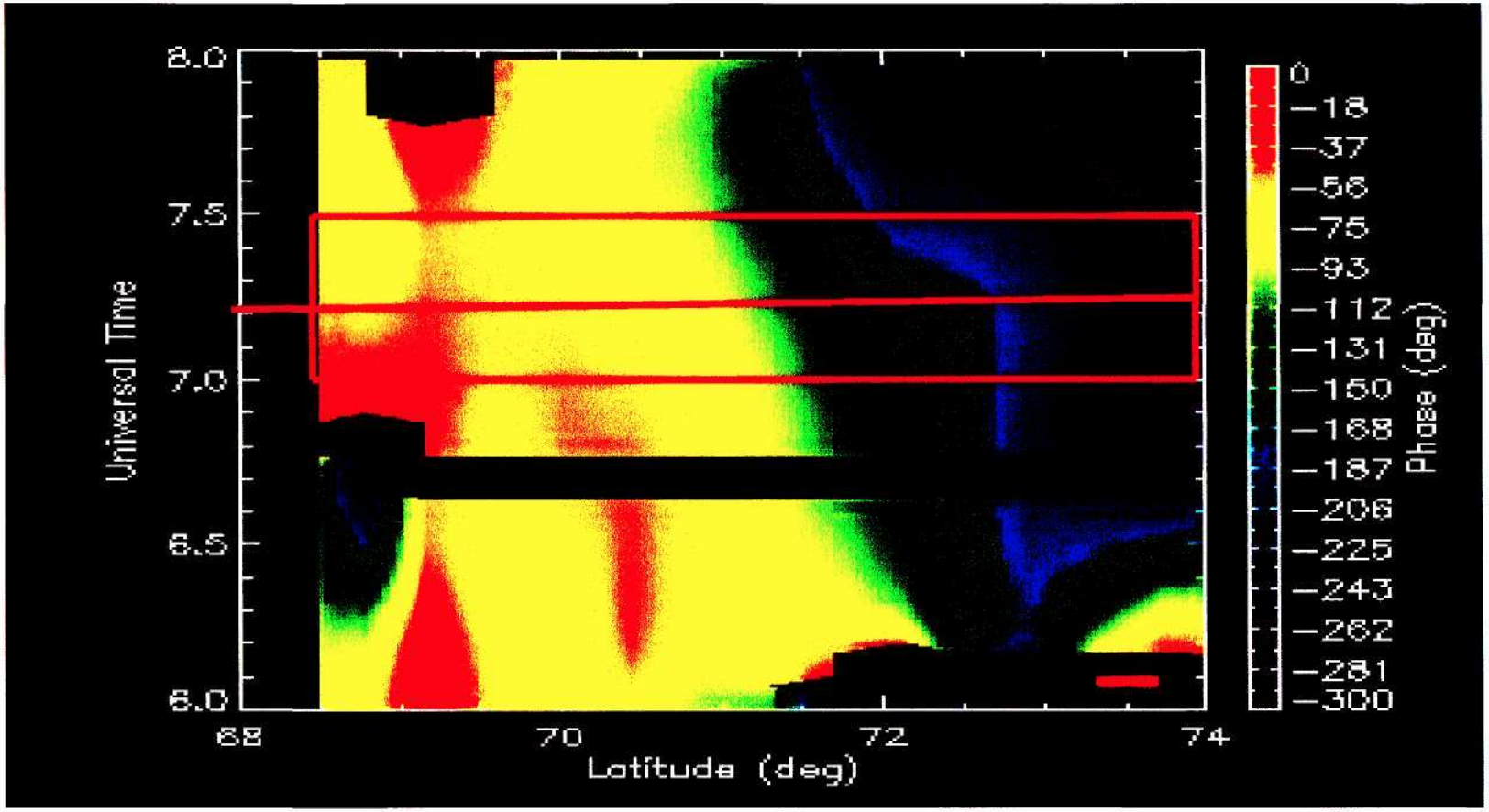

Figure 4.9: The instantaneous phase of the 1.9 mHz component from Goose Bay data calculated as the phase of the analytic signal. The length of the signal is 2 h with a time resolution of 120 s.

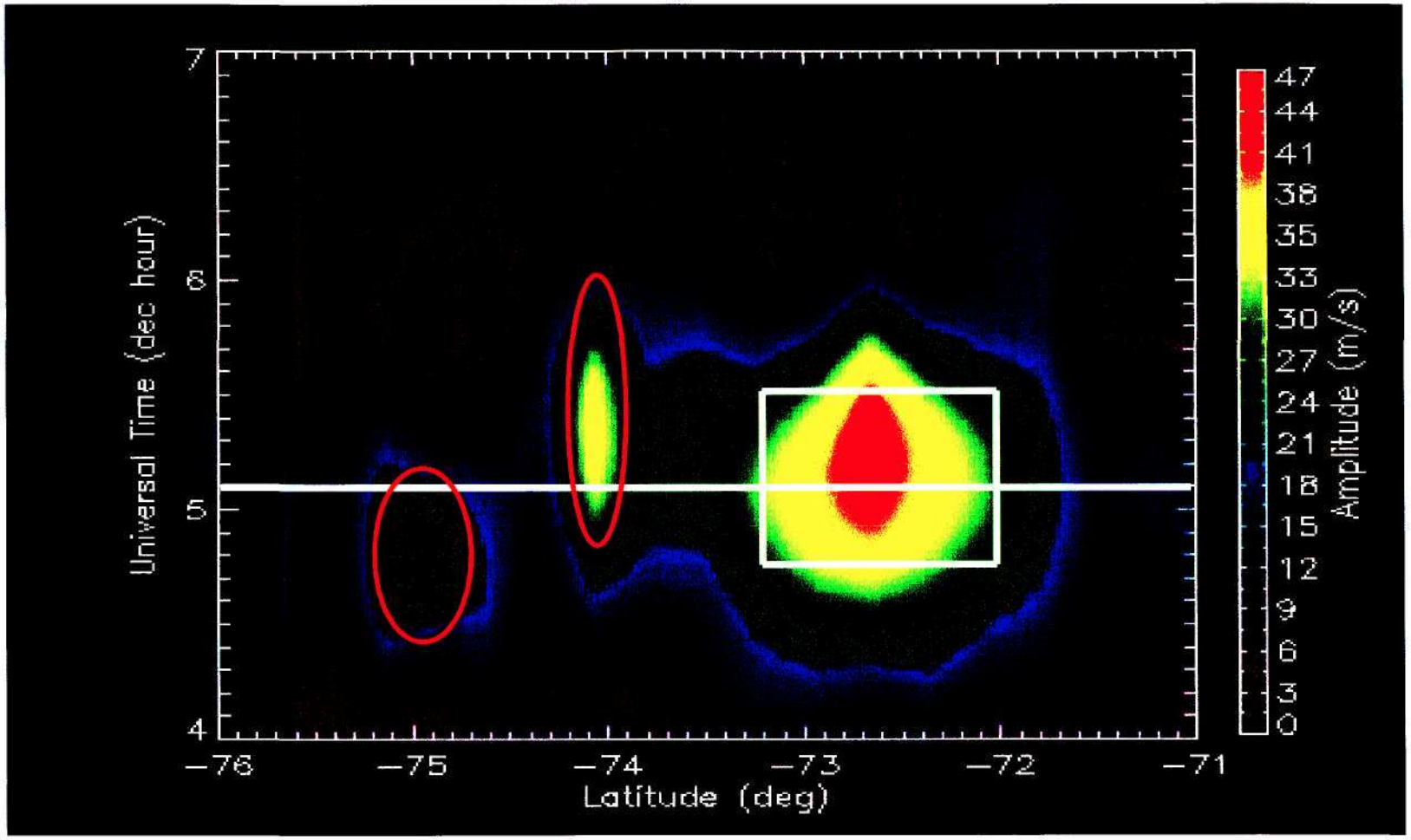

Figure 4.10: The instantaneous amplitude of the 1.9 mHz component from Syowa East data calculated as the amplitude of the analytic signal. The length of the signal is 3 h with a time resolution of 75 s.

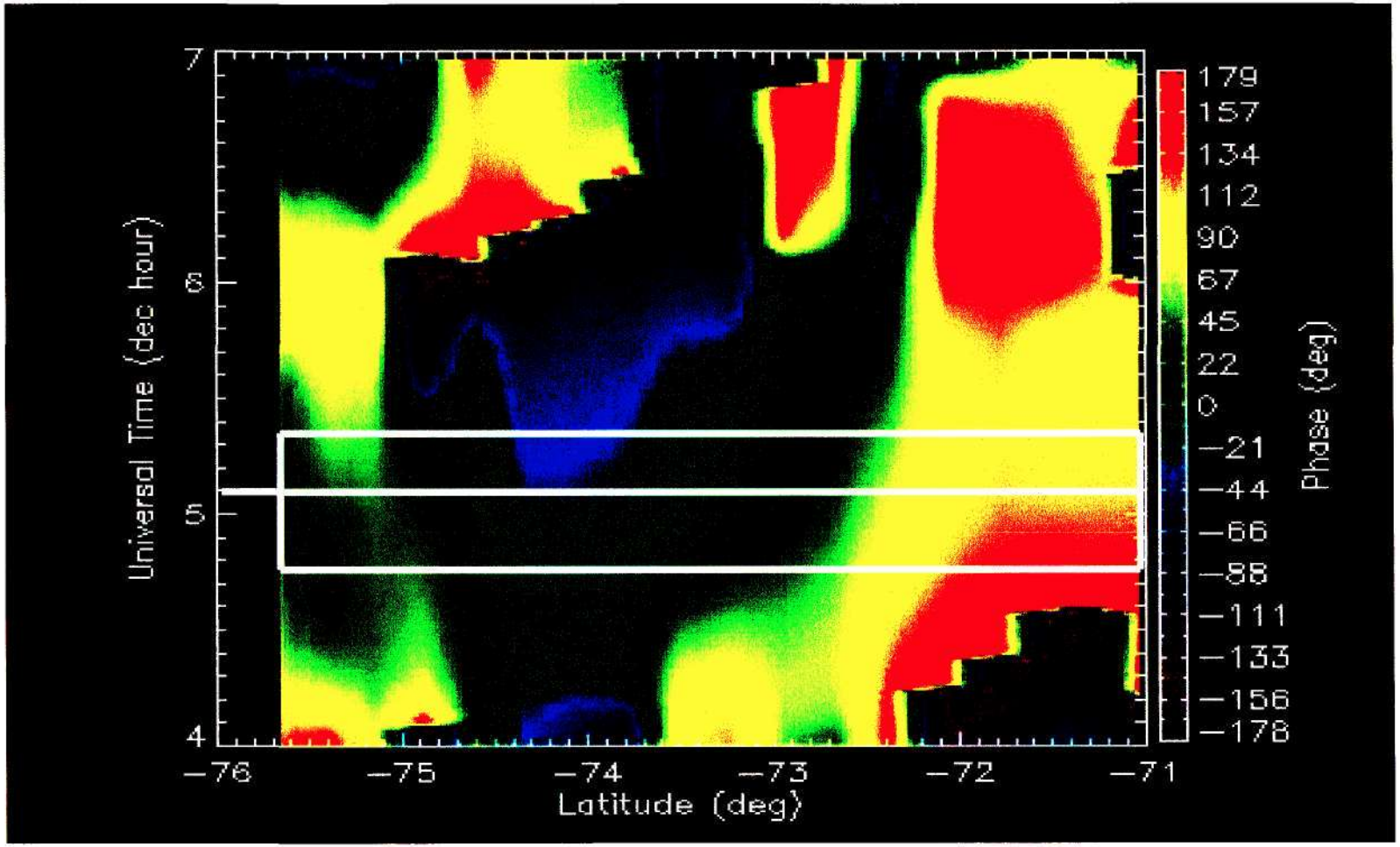

Figure 4.11: The instantaneous phase of the 1.9 mHz component from Syowa East data calculated as the phase of the analytic signal. The length of the signal is 3 h with a time resolution of 75 s.

Figure 4.8 shows the evolution of amplitude of the 1.9 mHz component with time as well as its latitudinal extent from Goose Bay data. This figure shows that the 1.9 mHz frequency component was observed for about an hour from 6.5 to 7.7 UT with a strongest activity that lasted for about 30 min from 7.0-7.5 UT illustrated by a red rectangle. The latitudinal extent of this component was about 2° from 70° to 72° geomagnetic with the strongest activity in the range 71° to 72°. ULF pulsations with latitudinal extent similar to these were also observed by Fenrich et al. (1995). Figure 4.9 shows the variation of the phase of the spectral component with time and latitude from Goose Bay data. In this figure the phase were unwrapped and plotted from -300° to 0° as the results the discontinuities were created during the exclusion of the data above 0° and below -300°. The phase was unwrapped and scaled so as to clearly show its variation especially in the time interval of interest (i.e. from 7.0 to 7.5 UT) where the amplitude is maximum. It is observed that the phase decreased from low to high latitude for example the phase is about -50 ° (at latitude of 68.5°) and it is about -250 ° (at latitude of 74 °) yielding the phase change of about 200°.

In Figure 4.10 the 1.9 mHz frequency component from Syowa East data has a latitudinal extent of about 1.5° from geomagnetic latitude of -72° to -73.5° with the strongest activity having a latitudinal spread of 1° near latitude -73°. This component has a temporal extent of about 2 hours from about 4.0-6.0 UT with a strongest activity that last for 45 min from 4.8 to 5.6 UT illustrated by a white rectangle. Apart from the main instantaneous peak at the latitude of -72.6° which I believe is the instantaneous resonance peak, there are 2 additional peaks near latitudes of -74° and -75° illustrated by 2 ellipses in Figure 4.10. These peaks are also observed in the amplitude spectra in Figure 4.7 illustrated by 2 yellow circles. In trying to explaining this behaviour, consider the plot in Figure 4.12.

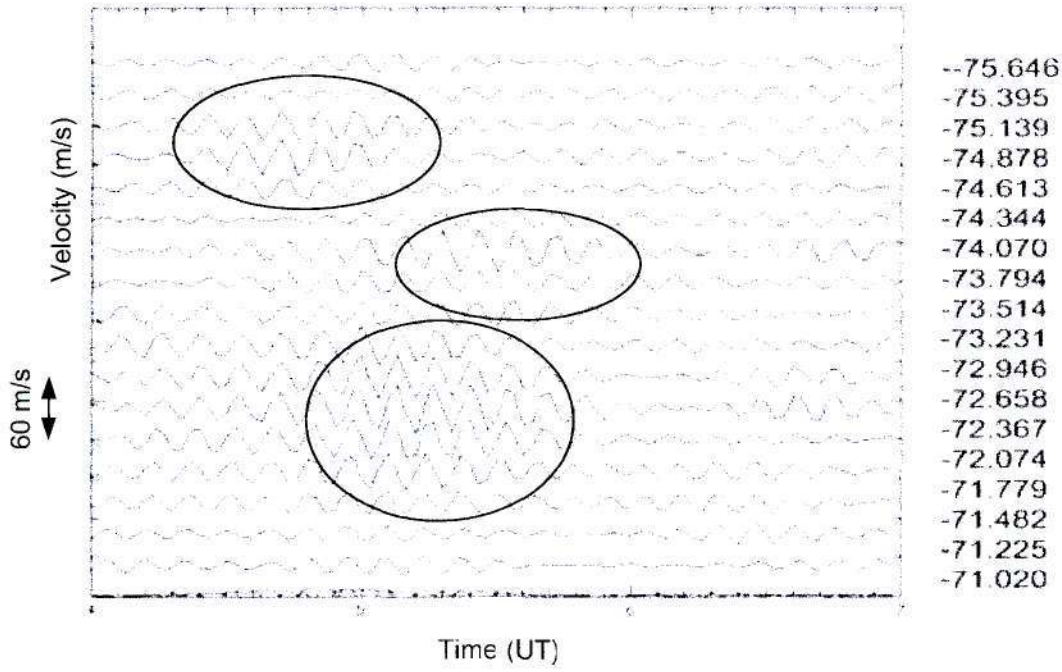

Figure 4.12: The velocity data from beam 2 of the Goose Bay radar being filtered around 1.9 mHz. Data were shifted by the same factor and the length of the arrow to the left indicates the magnitude of the amplitude. The values on the right indicate the latitude in degrees from which the signals were received.

This figure shows the HF radar velocity data which was filtered around 1.9 mHz, plotted by shifting the velocity from different latitude by the same factor and the length of the arrow indicates the magnitude of the amplitude. In this figure it can be seen that there are three oscillations at this frequency but at different latitudes near -72.6°, -74° and -75° illustrated by 3 ellipses in Figure 4.12. The possible explanation for this behaviour is a change in density which happened to alter the latitude of the resonant field lines. To illustrate this consider Figure 4.13 which shows the variation of the frequency with latitude. Consider moving from higher *L*-shell (latitude) at the right of Figure 4.13 to lower *L*-shell (latitude) at the left of Figure 4.13. As the latitude decreases the frequency increases and under normal conditions the frequency increases linearly as shown by the top line in Figure 4.13. When the density suddenly increases as shown by the middle curve, the frequency suddenly decreases and increases again as shown by the bottom curve. This curve shows that it is possible to have 3 field lines oscillating at the same frequency but at different *L*-shells or latitudes as illustrated by 3 circles on the lower curve in Figure 4.13.

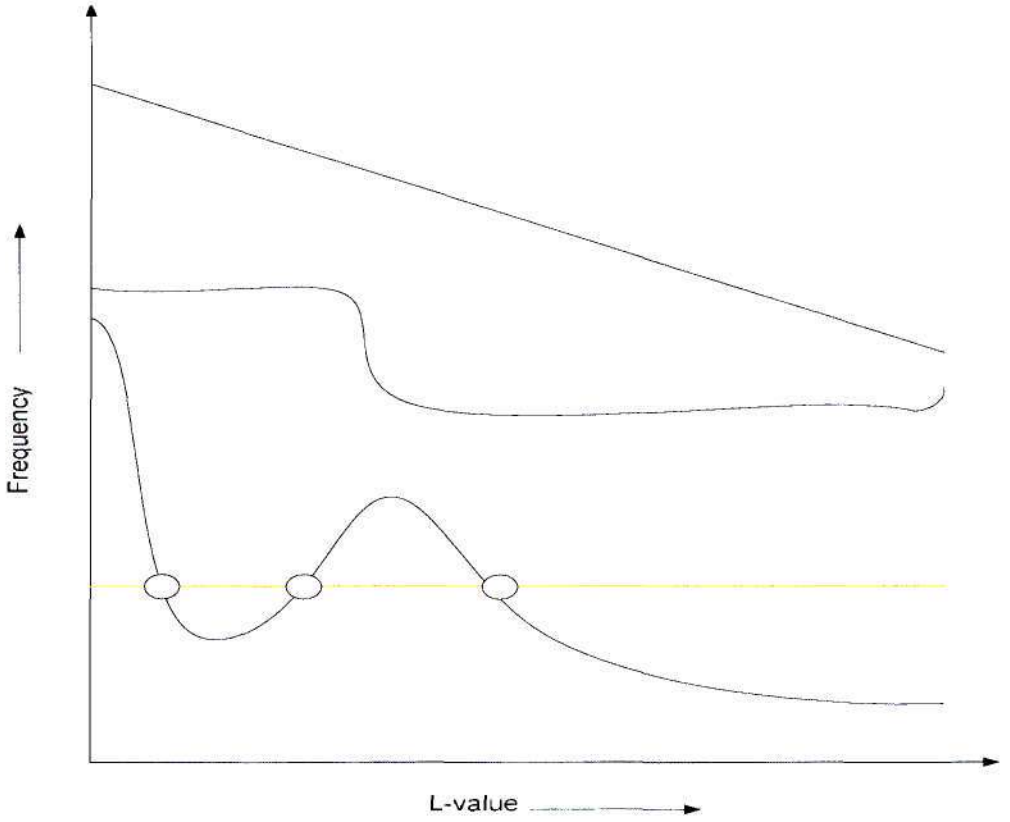

Figure 4.13: Shows the frequency dependent on the *L*-value or latitude where the top line shows the behavior of the frequency under normal conditions, the middle curve indicate the change in density and the bottom curve indicate the resulting variation of frequency. The 3 circles on the curve illustrate that it is possible to have 3 field lines at different latitudes oscillating at the same frequency.

Figure 4.11 shows the variation of the phase of 1.9 mHz component with time and latitude from Syowa East data. Even though there are some phase jumps as shown in the figure, the phase was not unwrapped because there are no jumps in the time interval of interest (i.e. from 4.8 to 5.6 UT) where the amplitude is maximum. Just like in the Goose Bay data the phase decrease from low latitude to high latitude for example it decrease from about 130 ° (at latitude of -71 °) to -40 ° (at latitude of -74 °) resulting in the phase change of about 170°. The phase increase again from -50 ° (at the latitude -74°) to 50 ° (at latitude of -76 °) resulting in the phase change of about 100°. While there is no phase change across the latitude of -74 °, there is a phase change across latitude of -75 °. Since this phase change is less than 180°, the instantaneous peak at the latitude of -75° can not be considered as the resonance peak.

4.4.1 Field line resonance (FLRs)

The variation of amplitude and phase of the observed spectral component with time and latitude from Goose Bay and Syowa East data was calculated and plotted in Figures 4.6 to 4.9 to identify possible FLR characteristics. As it was stated by Fenrich et al. (1995) that if an observed spectral component corresponds to FLR, it should exhibit narrow maximum in amplitude at certain latitude and a phase change of approximately 180° across that latitude. This behaviour is similar to a driven damped simple harmonic oscillator.

According to Walker (1995) if any influence which has a well defined frequency excites the field lines inside the magnetosphere into oscillations, field lines at certain latitude with the frequency matching that of the influence will resonate, and large oscillations will be set up over a narrow range near that latitude. This behaviour is observed in Figure 4.8 (Goose Bay data) and 4.10 (Syowa East data) where an unknown mechanism with frequency near 1.9 mHz seem to have excited the magnetic field lines inside the magnetosphere. Large oscillations are observed over a narrow range from 71° to 72° (in Goose Bay data) and from -72.2° to -73° geomagnetic latitude (in Syowa East data). The phase change of approximately 180° is observed in Figure 4.9 (Goose Bay data) across the latitude of 71.3° and in Figure 4.11 (Syowa East data) across the resonance latitude of -72.6°. The 1.9 mHz frequency component observed in the Goose Bay data and Syowa East data appears to be a FLR because of the above mentioned characteristics.

These features become even more apparent when considering a cut through a contour plot of instantaneous amplitude and phase of the spectral component from Goose Bay data at 7.2 UT illustrated by a red line in Figures 4.8 and 4.9 and from Syowa East data at 5.1 UT illustrated by a white line in Figures 4.10 and 4.11. These times are chosen because that was when the amplitudes were maximum. The behaviour of the amplitude and phase as a function of latitude from Goose Bay data at 7.2 UT is shown in Figures 4.14 and 4.15 respectively and in Figure 4.16 and 4.17 from Syowa East data respectively.

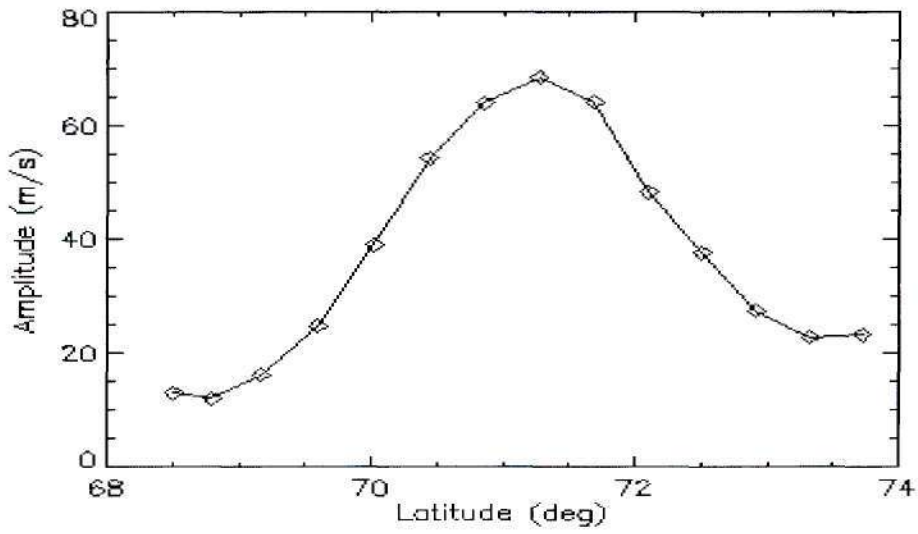

Figure 4.14: The amplitude spectrum of the 1.9 mHz spectral component from Goose Bay data at 7.2 UT showing the enhancement in amplitude across the resonance latitude of 71.3°.

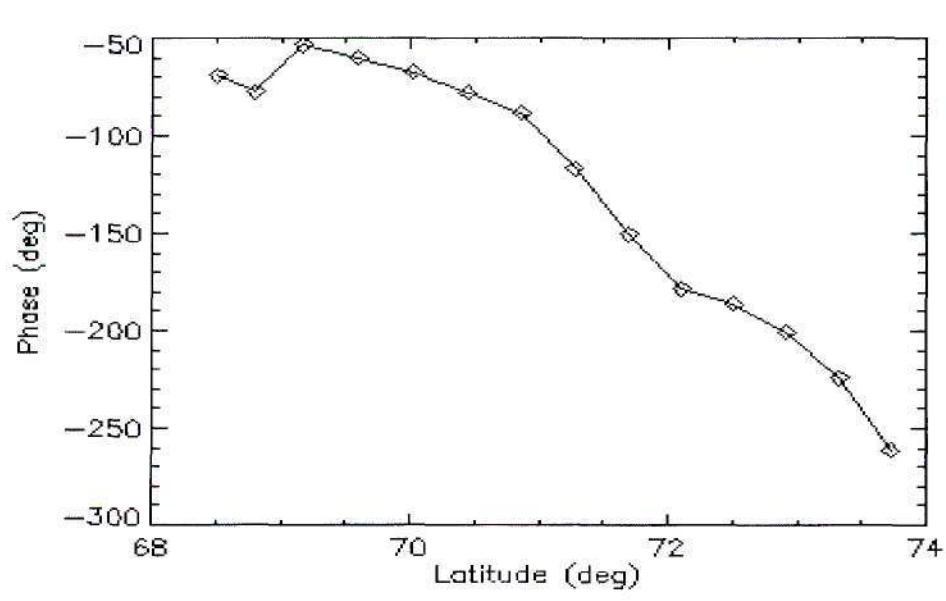

Figure 4.15: The phase spectrum of the 1.9 mHz spectral component from Goose Bay data at 7.2 UT showing the phase change of approximately 180° across the resonance latitude of 71.3°.

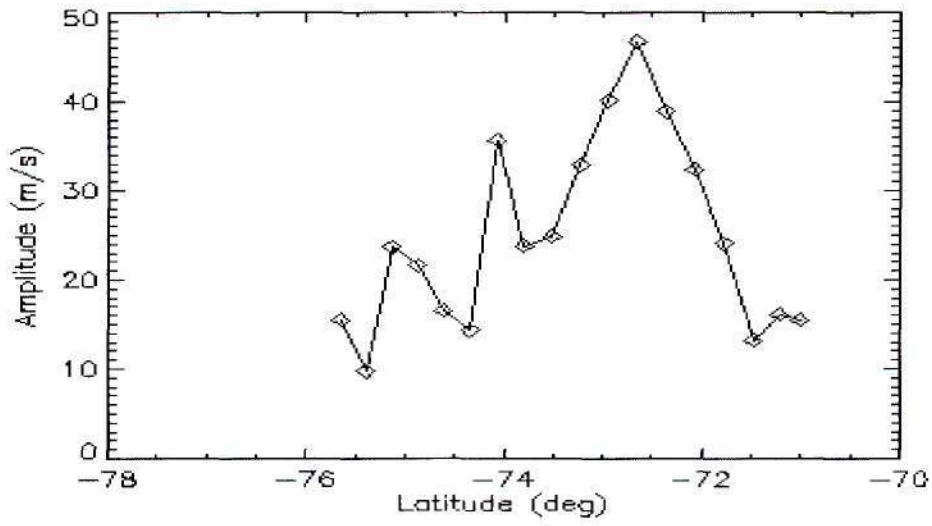

Figure 4.16: The amplitude spectrum of the 1.9 mHz spectral component from Syowa East data at time 5.1 UT showing the enhancement in amplitude across the resonance latitude of -72.6°.

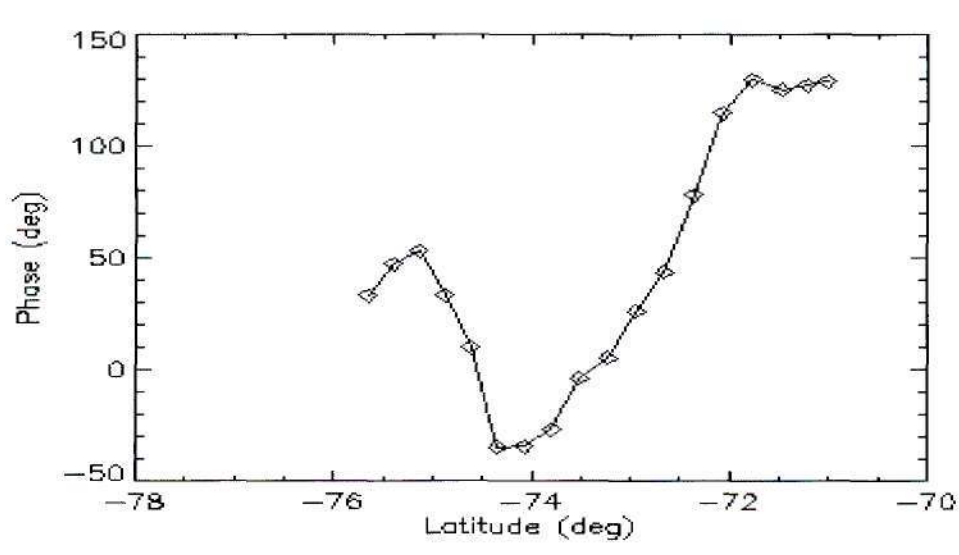

Figure 4.17: The phase spectrum of the 1.9 mHz spectral component from Syowa East data at time 5.1 UT showing the phase change of approximately 180° across the resonance latitude of -72.6°.

Now Figure 4.14 clearly shows that the amplitude of the 1.9 mHz component (from Goose Bay data) at 7.2 UT increases slowly with latitude from 68.5° and peaks at resonance latitude of 71.3°

and then decreases again. Across this resonance latitude the phase changes by approximately 200° as shown in Figure 4.15.

The 2 small peaks near latitude of -74° and -75° in the Syowa East data shown in Figure 4.16 are the same peaks that were discussed in Section 4.4. Other than that, similar behavior is observed in Syowa East data where the amplitude of 1.9 mHz component increases from the latitude of -74° and peaks at resonance latitude of -72.6° and then decreases again as shown in Figure 4.16. The 170° phase change is observed across this resonance latitude as shown in Figure 4.17. The fact that the resonance latitude are so close to each other is just a coincident because firstly, the data were not collected on the same day, secondly these stations are not at conjugate sites. The Syowa East radar does not have conjugate station whereas the conjugate station of Goose Bay radar is Halley radar, unfortunately the quality of the data from Halley during the day of the event was very poor.

4.4.2 Spatial extent of ULF pulsations

So far the investigation of the 1.9 mHz component has been done over a narrow range of longitude along one beam, in this section the amplitude and phase of this component will be looked at simultaneously using all beams covering a longer longitudinal range. This was done to establish the FLR characteristics over the longer range of longitudes. The behaviour of this component is observed at exactly 7.2 UT at Goose Bay and at 5.1 UT at Syowa East. These times are chosen because the amplitude of this component is at its maximum in most of the beams. The contour plots of the amplitude and phase spectra computed from Goose Bay data are shown in Figures 4.18 and 4.19 while the spectra computed from Syowa East data are shown in Figures 4.20 and 4.21. Essentially these plots show a snapshot of the instantaneous amplitude and phase of the 1.9 mHz component in all beams taken by Goose Bay HF radar and by Syowa East HF radar. The white squares in the figures show the field of view of the radars and the directions of the beams given by the coordinates of geomagnetic longitude and latitude. Goose Bay data from beam 0 was not plotted because there was an error in the data. Thus Figures 4.18 and 4.19 show data from beam 1 (leftmost) to beam 15 (rightmost). Figures 4.20 and 4.21 show Syowa East data from beam 0 (leftmost) to beam 13 (rightmost). Beams 14 and 15 are not plotted because of limited data. The rectangles and lines in following figure are illustrating FLR features which will be discussed later.

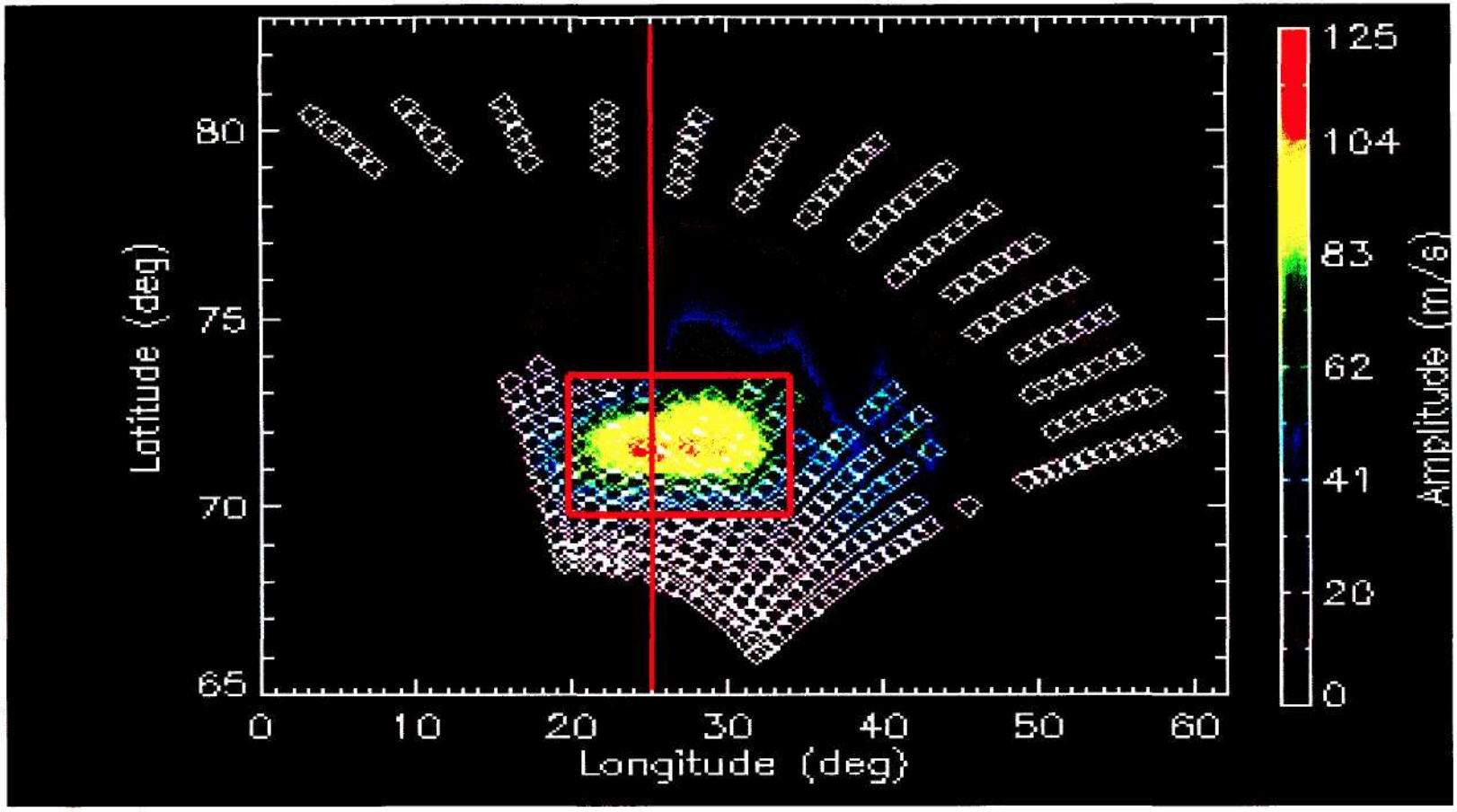

Figure 4.18: A snapshot of the amplitude of the 1.9 mHz frequency component from Goose Bay data from beams 1 to 15 (left to right) taken at 7.2 UT. The white squares representing the coordinates of the magnetic longitude and latitude show the field of view of the radar and directions of the beams.

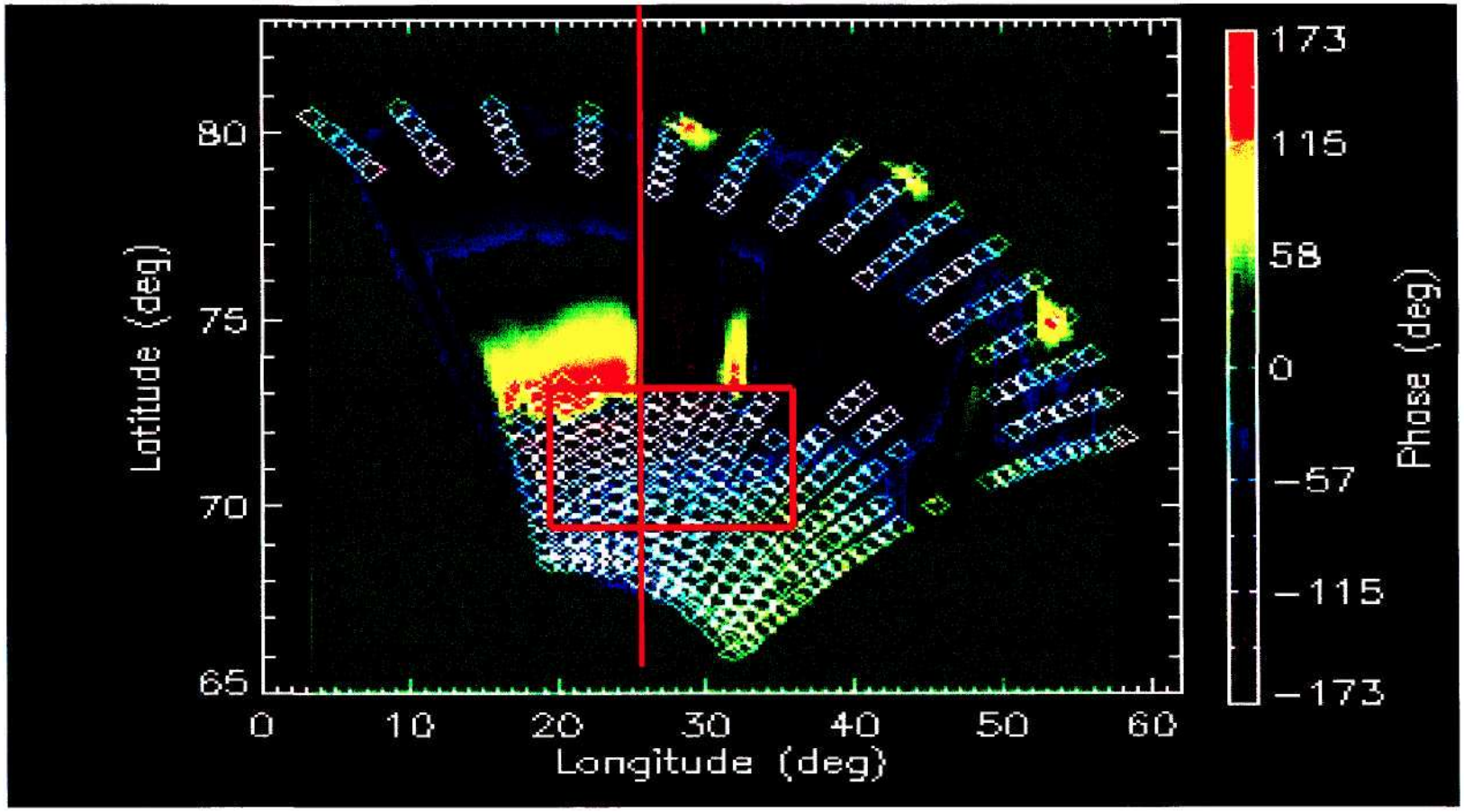

Figure 4.19: A snapshot of the phase of the 1.9 mHz frequency component from Goose Bay data from beams 1 to 15 (left to right) taken at 7.2 UT. The white squares representing the coordinates of the magnetic longitude and latitude show the field of view of the radar and directions of the beams.

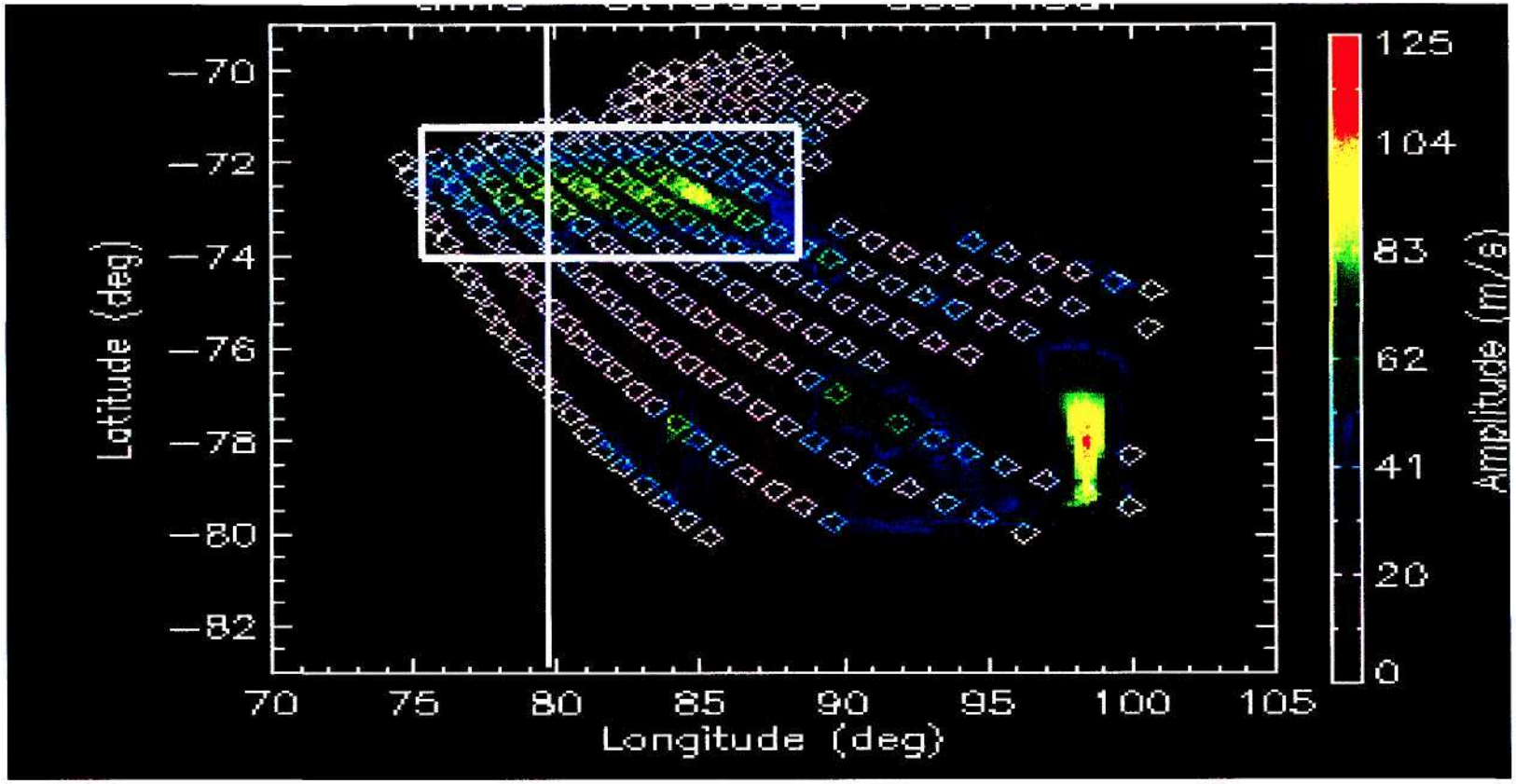

Figure 4.20: A snapshot of the amplitude of the 1.9 mHz frequency component from Syowa East data from beams 0 to 13 (left to right) taken at 5.1 UT. The white squares representing the coordinates of the magnetic longitude and latitude show the field of view of the radar and directions of the beams.

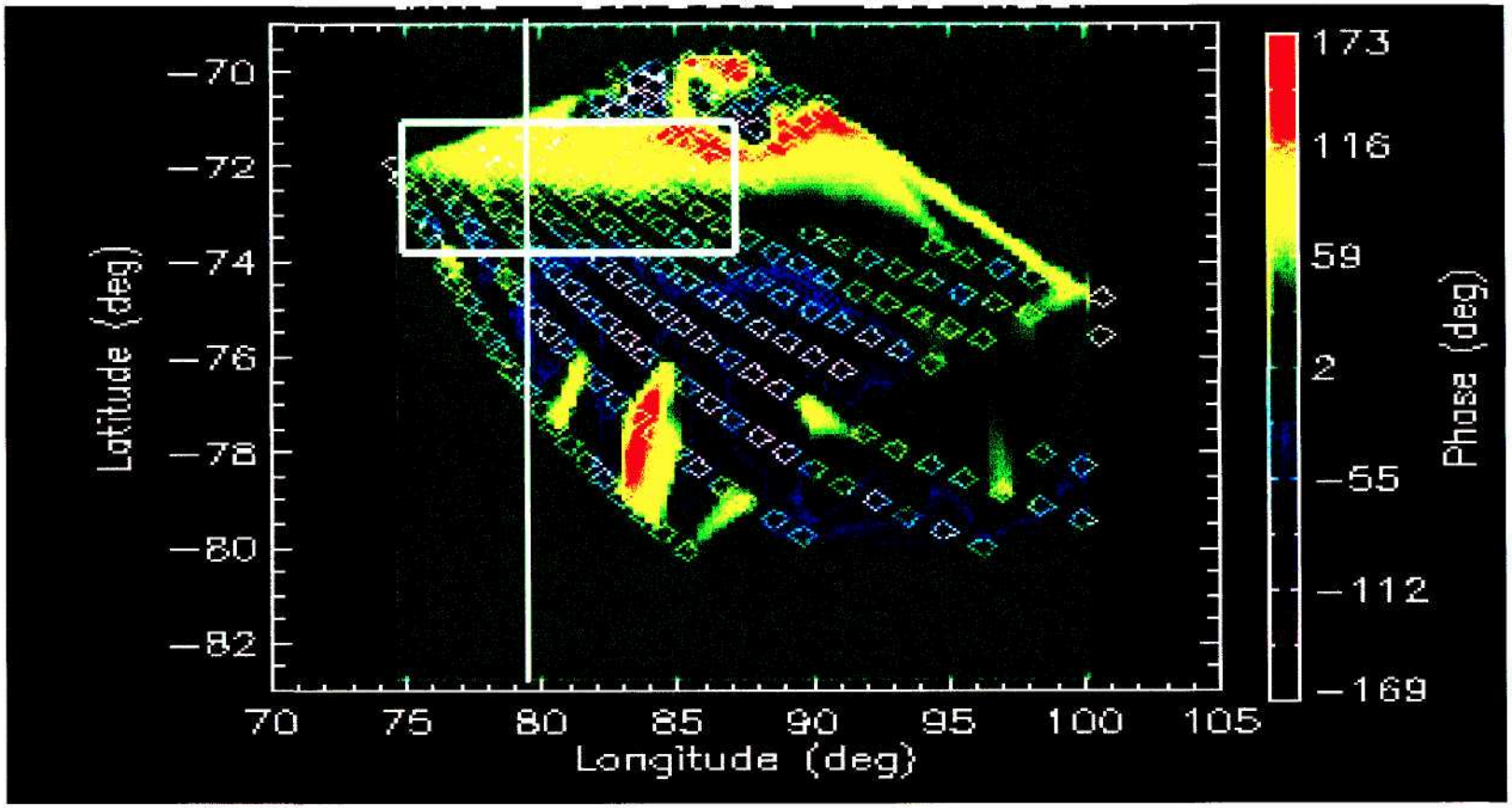

Figure 4.21: A snapshot of the phase of the 1.9 mHz frequency component from Syowa East data from beams 0 to 13 (left to right) taken at 5.1 UT. The white squares representing the coordinates of the magnetic longitude and latitude show the field of view of the radar and directions of the beams.

If we assume that the earth's magnetic field has a dipole configuration with unvarying magnetospheric properties, field lines emanating from the same latitude have equal magnetic strength and length and thus are expected to oscillate at the same frequency and with equal amplitudes. Again considering the theory by Walker (1995) which states that when a certain driver with a well defined frequency excites the magnetic field lines, oscillations with greater amplitudes will be set up at a very narrow band of latitude where characteristic frequency of the field lines matches that of the driver. This enhancement in amplitude is expected to be observed in all field lines from that band of latitudes.

It is assumed that on the 11th of November 2002 at 7.2 UT a certain driver of the frequency ~ 1.9 mHz excited the field lines and it happened to match the characteristic frequency of the magnetic field lines near the latitude of 71.3°. As it was expected, it is observed in Figure 4.18 that there is an enhancement in amplitude of the 1.9 mHz spectral component near this latitude. This enhancement in amplitude is not observed over the whole field of view of the radar but rather over 13° longitudinal range from about 20° as shown by a red rectangle in Figure 4.18. Nevertheless this longitudinal range is still long enough considering the fact that the properties of the magnetosphere are always changing. On top of that the earth's magnetic field is not a dipole configuration as it was assumed above but the field lines are compressed on the day side and elongated on the night side. The above mentioned factors may have caused the amplitude not to be enhanced over a longer longitudinal range. Figure 4.19 shows the phase change of approximately 180° across this latitude and this behaviour is observed over longitudinal range from about 20° to 33°. Moreover Figures 4.18 and 4.19 shows that this behaviour is observed in the data from beam 2 to 9 of the Goose Bay radar.

On the 17th of June 2000 at 5.1 UT it is also assumed that a certain driver of the frequency ~ 1.9 mHz excited the field lines and the behaviour similar to that mentioned above is observed. The difference is that the enhancement in amplitude of the 1.9 mHz component is observed at the resonance latitude of -72 6° and is observed over the longitudinal range of about 12° from 76° as shown by a white rectangle in Figure 4.20. Figure 4.21 shows the phase change of approximately 180° across this latitude and this behaviour is observed over 12° of longitude from 76°. On this day this behaviour is observed in the data from beams 1 to 7 of Syowa East radar.

As it was done for the single beam, FLR features become even more apparent by considering the cuts through the instantaneous amplitude and phase spectra of this component along longitude near 25° across different latitude from Goose Bay data. The cuts are considered as illustrated by the red lines in Figures 4.18 and 4.19 and this longitude is just chosen from the range where the amplitude is maximum and the results are shown in Figures 4.22 and 4.23. Same thing is also done in Syowa East data where the cuts are illustrated by the white lines in Figures 4.20 and 4.21 along longitude near 80° and the results are shown in Figures 4.24 and 4.25.

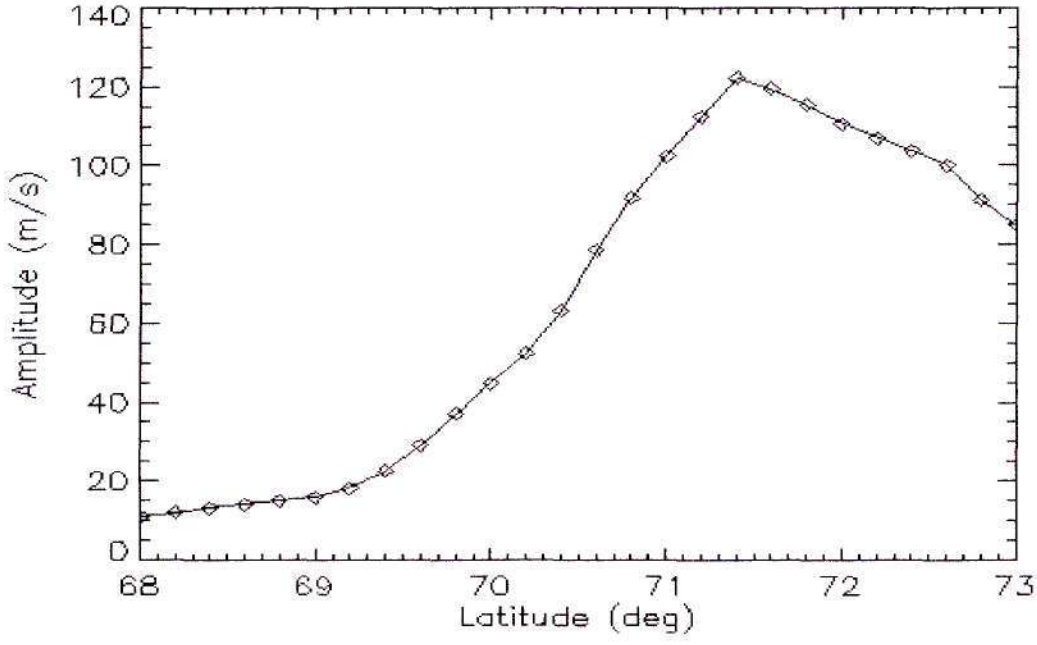

Figure 4.22: The amplitude spectrum of the 1.9 mHz spectral component observed in Goose Bay data at 7.2 UT along longitude near 25°.

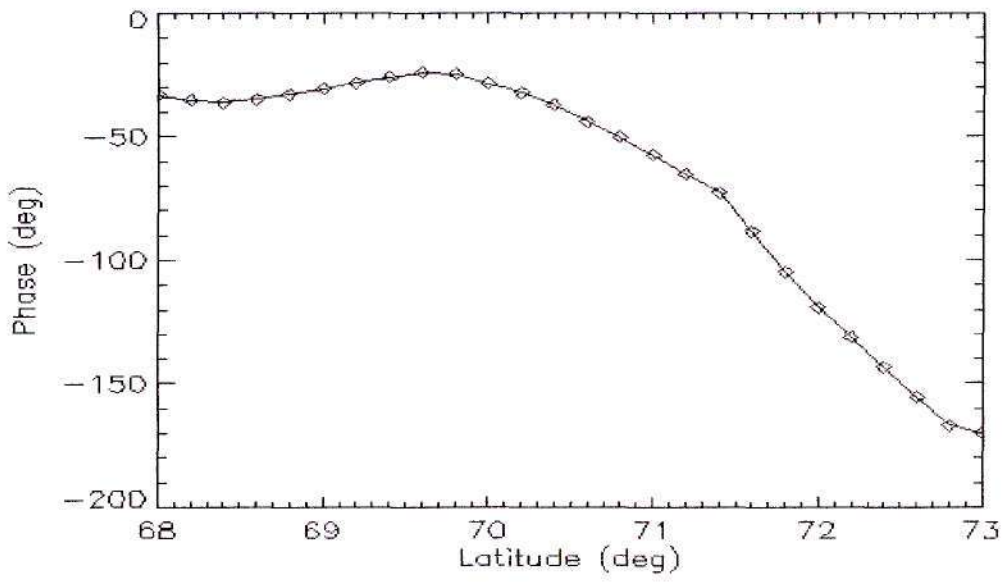

Figure 4.23: The phase spectrum of the 1.9 mHz spectral component observed in Goose Bay data at 7.2 UT along the longitude near 25°.

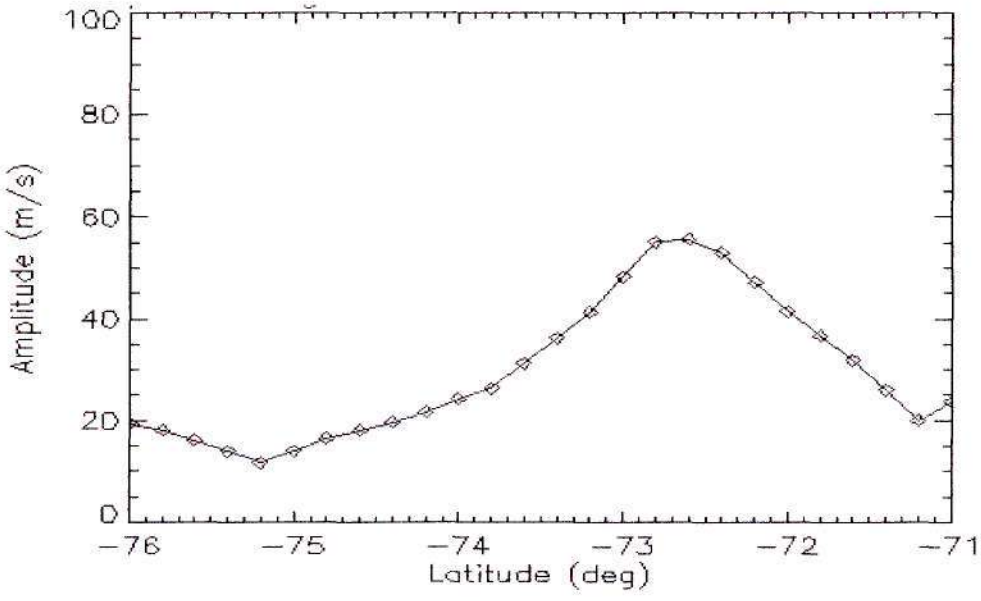

Figure 4.24: The amplitude spectrum of the 1.9 mHz spectral component observed in Syowa East data at 5.1 UT along longitude near 84°.

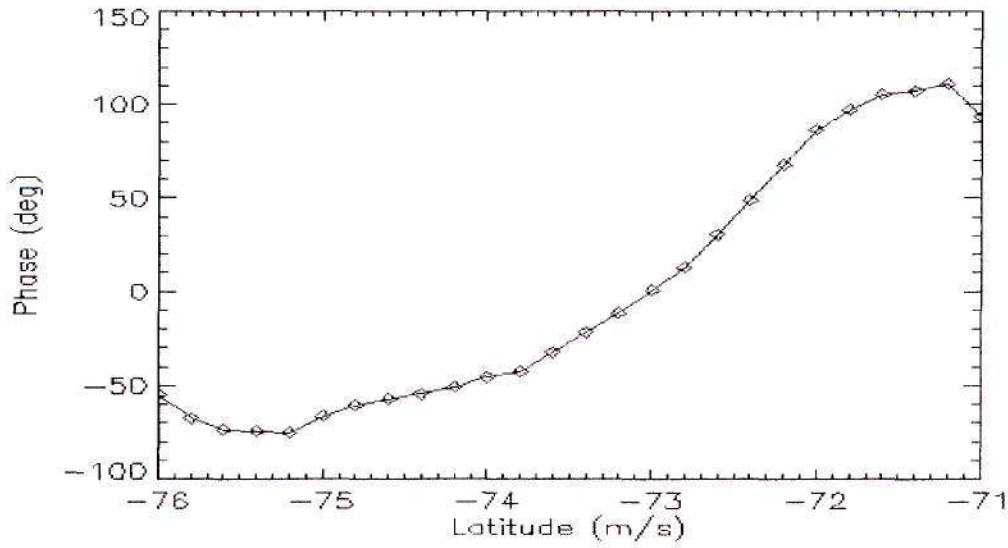

Figure 4.25: The phase spectrum of the 1.9 mHz spectral component observed in Syowa East data at 5.1 UT along longitude near 25°.

Figures 4.22 and 4.23 are plotted from latitude of 68° to 73° while Figures 4.24 and 4.25 are plotted from latitude of -76° to -71° because there are no data above and below these ranges. Compared to Figures 4.14 and 4.15 which show the latitude profile of the amplitude and phase of the 1.9 mHz spectral component at 7.2 UT along beam 2 of Goose Bay radar, Figures 4.22 and 4.23 show similar spectra plotted at the same time but along the longitude of 25°. Although the amplitude (~60 m/s) in Figure 4.14 is about half the amplitude (~120m/s) in Figure 4.22, the amplitude still peaks at the same latitude of 71.3°. The amplitude in Figure 4.14 was measured by beam 2 which is close to longitude of 20° as can be seen in Figure 4.22 the amplitude is less there than the amplitude near the longitude of 25° as shown in Figure 4.22. This difference in amplitude of the field lines may be attributed to the difference in plasma density around each magnetic field such that the greater the density around the field lines the lower the amplitude. Figure 4.23 shows that the phase change of ~180° is still observed along the longitude of 25°.

While Figures 4.16 and 4.17 shows the latitude profile of the amplitude and the phase of the 1.9 mHz spectral component at 5.1 UT along beam 6 of the Syowa East radar, Figures 4.24 and 4.25 shows a similar spectra plotted at the same time but along the longitude of 80°. The amplitude (~50 m/s) in Figure 4.14 (relative to amplitudes in Goose Bay mentioned above) is approximately equal to the amplitude (~60 m/s) in Figure 4.24 moreover the amplitude still peaks at the same latitude of -72.6°. The difference in amplitude may be due to the same reason as stated above. The

phase change of approximately 180° is also observed as shown in Figure 4.25. The reason why the spectra in Figures 4.14, 4.15 and Figures 4.22, 4.23 and also Figures 4.16, 4.17 and Figures 4.23, 4.24 are not so similar is that they were not taken from the same longitude.

4.5 Possible sources of ULF pulsations

There are numerous possible sources of ULF pulsations which include ones that are internal as well as those external to the magnetosphere (McPherron, 2005). The internal sources include gyro resonance, drift and bounce resonance, earthward directed plasma flows and modulation of Auroral electrojet whereas the external sources include solar wind, ion foreshock and bow shock. In this thesis the sources of the observed pulsations were looked for outside the magnetosphere and more especially in the solar wind.

Walker (2002) proposed that the frequencies of MHD wave incident on the bow shock from upstream solar wind may be responsible for the frequencies of the FLRs seen on the ground. If this is the case then the oscillations on the ground should have similar characteristics as oscillations in the solar wind especially the frequency. In order to determine this, the wavelet transform of the line-of-sight velocity from the HF radar data and the x-component of the velocity from the satellite data were used. The x-component of the velocity was chosen because solar wind velocity is the greatest in the x-direction and also greater than the group velocity of the MHD waves in the solar wind. Thus the group velocity in the sun-earth line is approximately in the x-direction.

Figures 4.26 and 4.27 shows a 4-day orbit of the satellites which include WIND, ACE and others which are indicated in these figures. In this thesis, data from instruments on board WIND and ACE satellites will be used. On the 11th of November 2002 the WIND satellite was located at (102, -29, 0.5) Re (GSE) and was close to the sun-earth line as illustrated by a red ring in Figure 4.26. On the 17th of June 2000 the ACE satellite was located at (236, 39, 5) Re (GSE) and was close to this line as illustrated by a red ring in Figure 4.27.

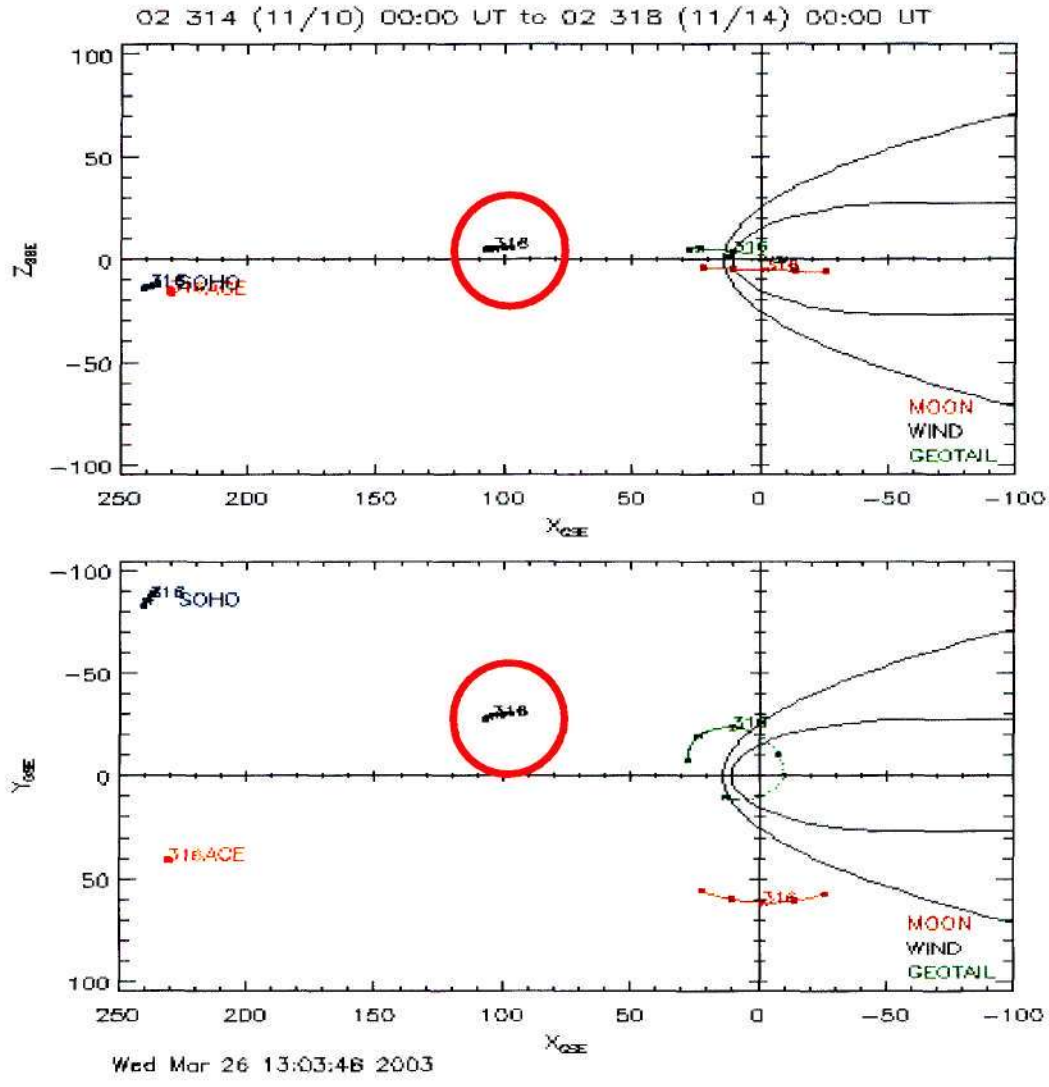

Figure 4.26: The location of the satellites during the 4-day orbit with WIND satellite being close to the sun-earth line from the 10th to the 14th of November 2002. The data analyzed were taken on the 11th of November 2002.

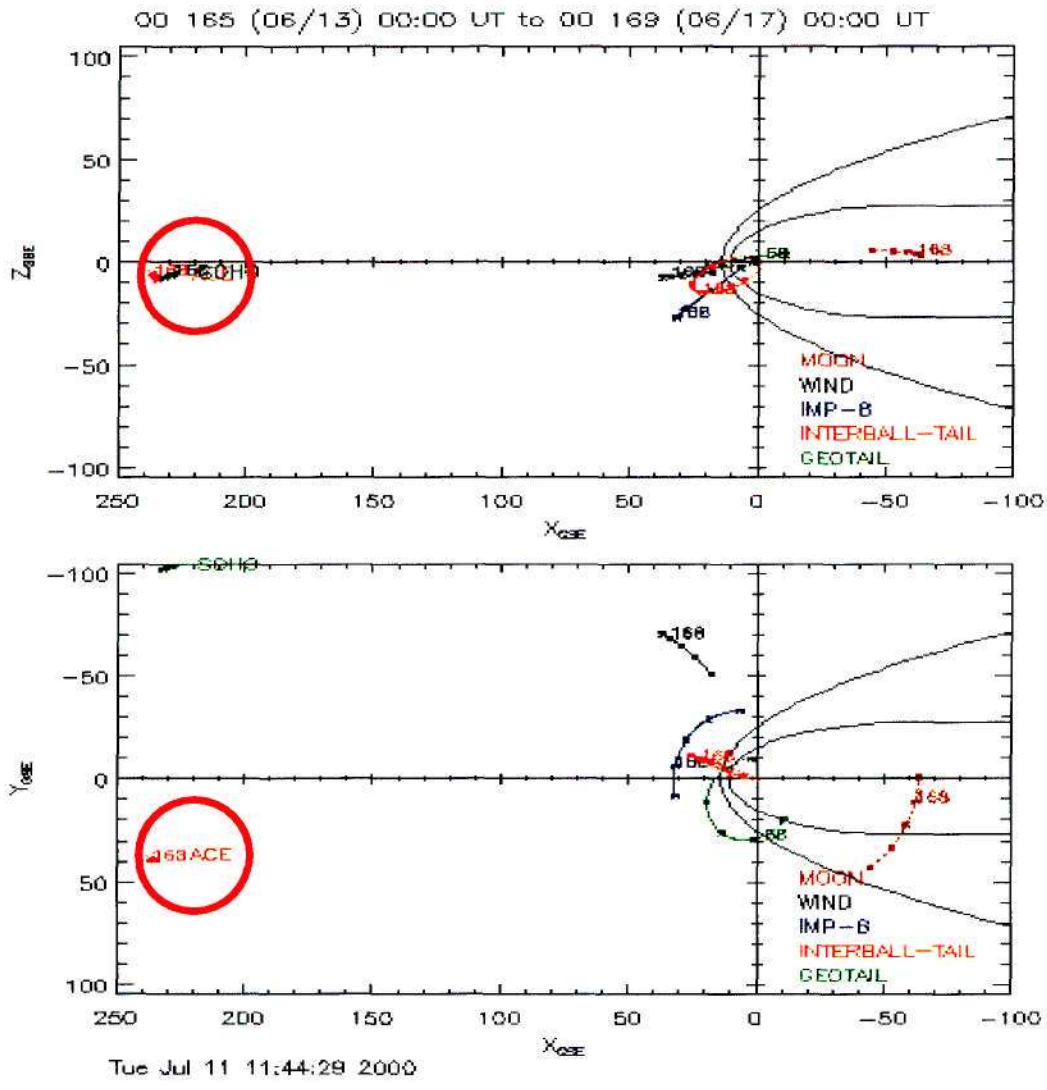

Figure 4.27: The location of the satellites during the 4 day orbit with ACE satellite being close to the sun-earth line from the 13th to the 14th of June 2000. The data analyzed were taken on the 17th of June 2000.

Figure 4.28 shows data from the Solar Wind Experiment (SWE) collected by instruments on board WIND satellite on the 11th of November 2002 from 6.0 to 8.0 h with a sampling period of 120 s and Figure 4.29 shows data from Solar Wind Electron, Proton and Alpha Monitor (SWEPAM) collected by instruments onboard ACE satellite on the 17th of June 2000 from 4.0 to 7.00 h with the same sampling period.

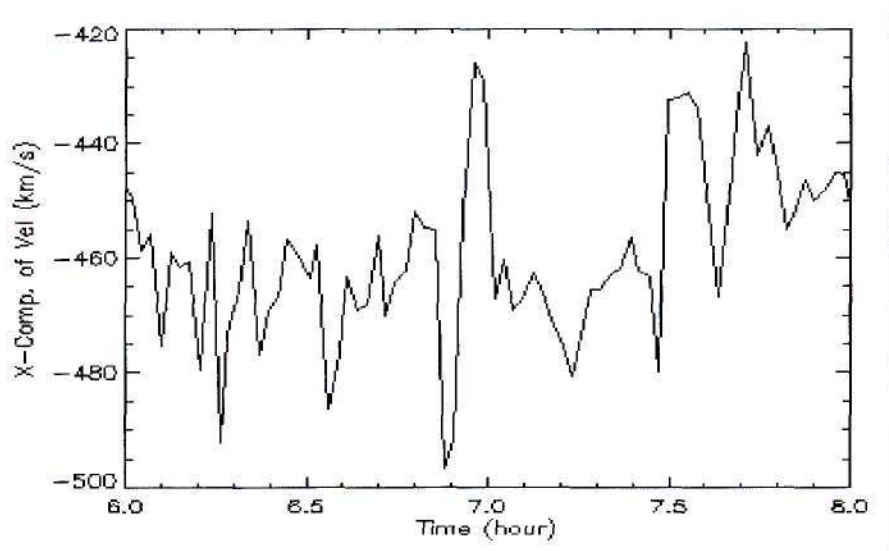

Figure 4.28: The x-component of the velocity data collected by instruments on board WIND satellite (102, -29, 05) Re (GSE) on the 11th of November 2002 for the time interval 6.0 to 8.0 h with a sampling period of 120 s.

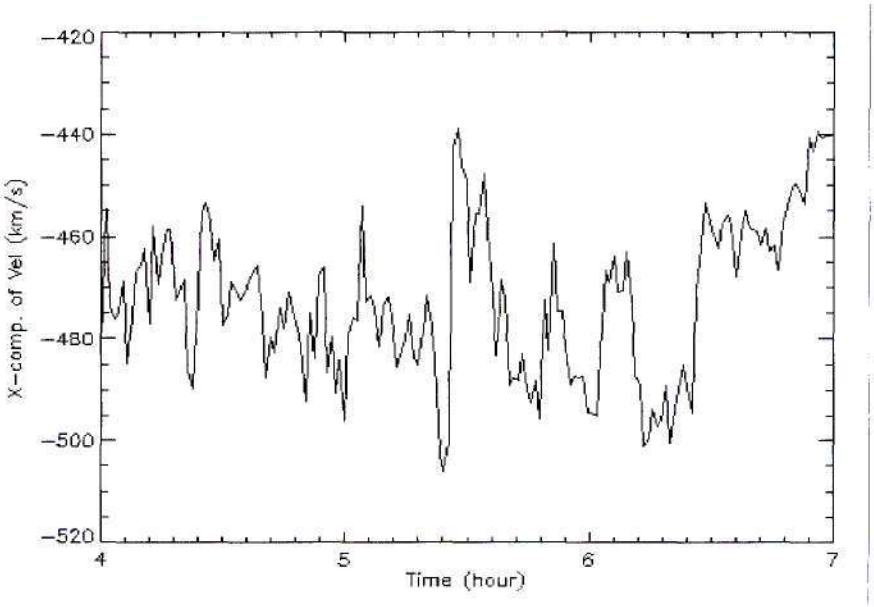

Figure 4.29: The x-component of the velocity data collected by instruments on board ACE satellite (38, -70, 7.5) Re (GSE) on the 17th of June 2000 for the time interval 4.0 to 7.0 h with a sampling period of 120 s.

4.5.1 Solar wind as the possible source of the ULF pulsations

Correlation between HF radar data and satellite data was done using wavelet analysis to investigate the hypothesis that MHD waves in the solar wind are possibly responsible for the ULF pulsations that are observed on the ground. For this to be true, the signal observed at the ground should be delayed by a time approximately equal to the travel time of the solar wind from the satellite to the earth.

4.5.2 Time delay calculations

The calculations below were done using data obtained from the Coordinated Data Analysis website (CDAWeb) that can be found from the URL:

http://cdaweb.gsfc.nasa.gov/cdaweb/istp_public/

On the 11th of November 2002 from 6.0 to 8.0 h the average x-component of the distance of the WIND satellite from the earth was 650878 km and the magnitude of the average x-component of the solar wind speed was 458 km.s^{-1}. This corresponds to a travel time of about 24 min calculated from (time = distance / velocity). For the ACE satellite the average x-component of the distance from the earth on the 17th of June 2000 was 1.508×10^6 km and the magnitude of the average x-component of the solar wind velocity was 473 km.s^{-1} and this corresponds to a travel time of about 53 min.

The wavelet transform of the x-component of the velocity data from the WIND satellite and the line-of-sight velocity data from beam 2 of the Goose Bay radar at the resonance latitude of 71.3° were calculated and the spectra are shown in Figure 4.30 and 4.31 respectively. The same was done using the ACE data and the data from beam 6 of the Syowa East at the resonance latitude of -72.6° and the results are shown in Figure 4.32 and 4.33 respectively.

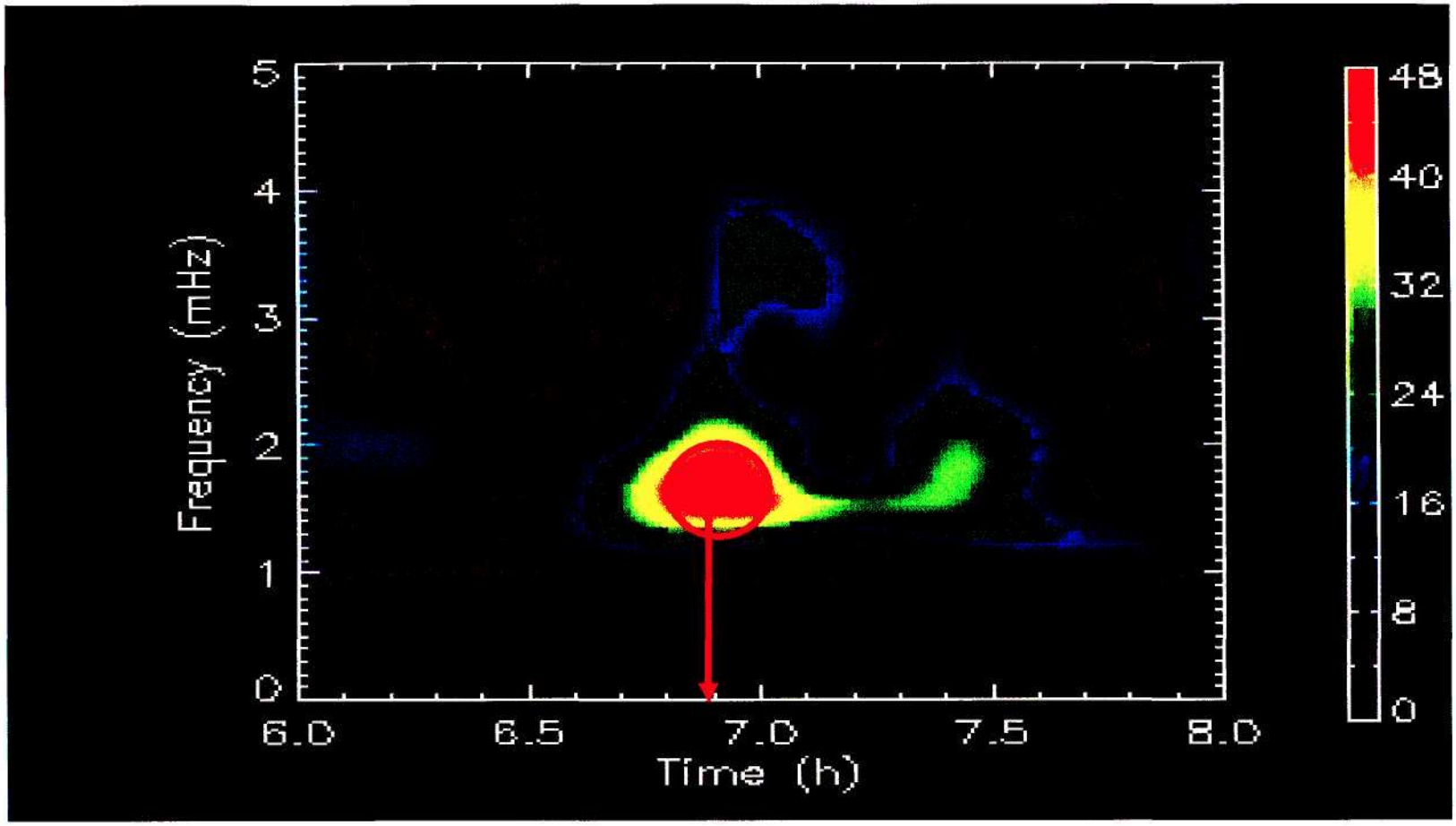

Figure 4.30: The wavelet amplitude spectra of the *x*-component of the velocity data collected by instruments onboard the WIND satellite on the 11th of November 2002. The figure shows the 1.9 mHz component observed at about 6.9 h and the amplitudes have arbitrary units.

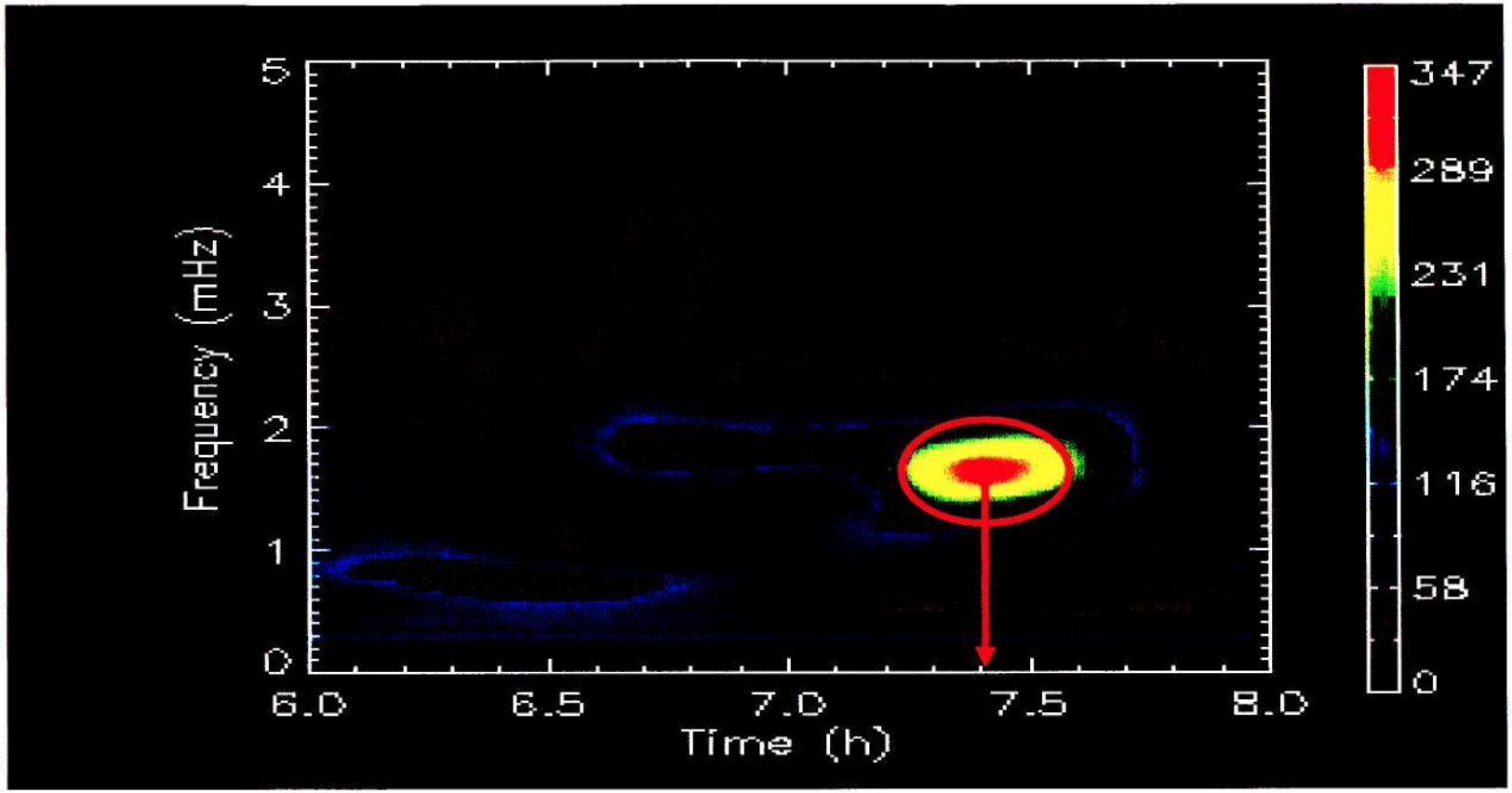

Figure 4.31: The wavelet amplitude spectra of the line-of-sight velocity from beam 2 of the Goose Bay data at resonance latitude of 71.3°. The data were collected on the 11th of November 2002. The figure shows the 1.9 mHz component observed at about 7.4 UT and the amplitudes have arbitrary units.

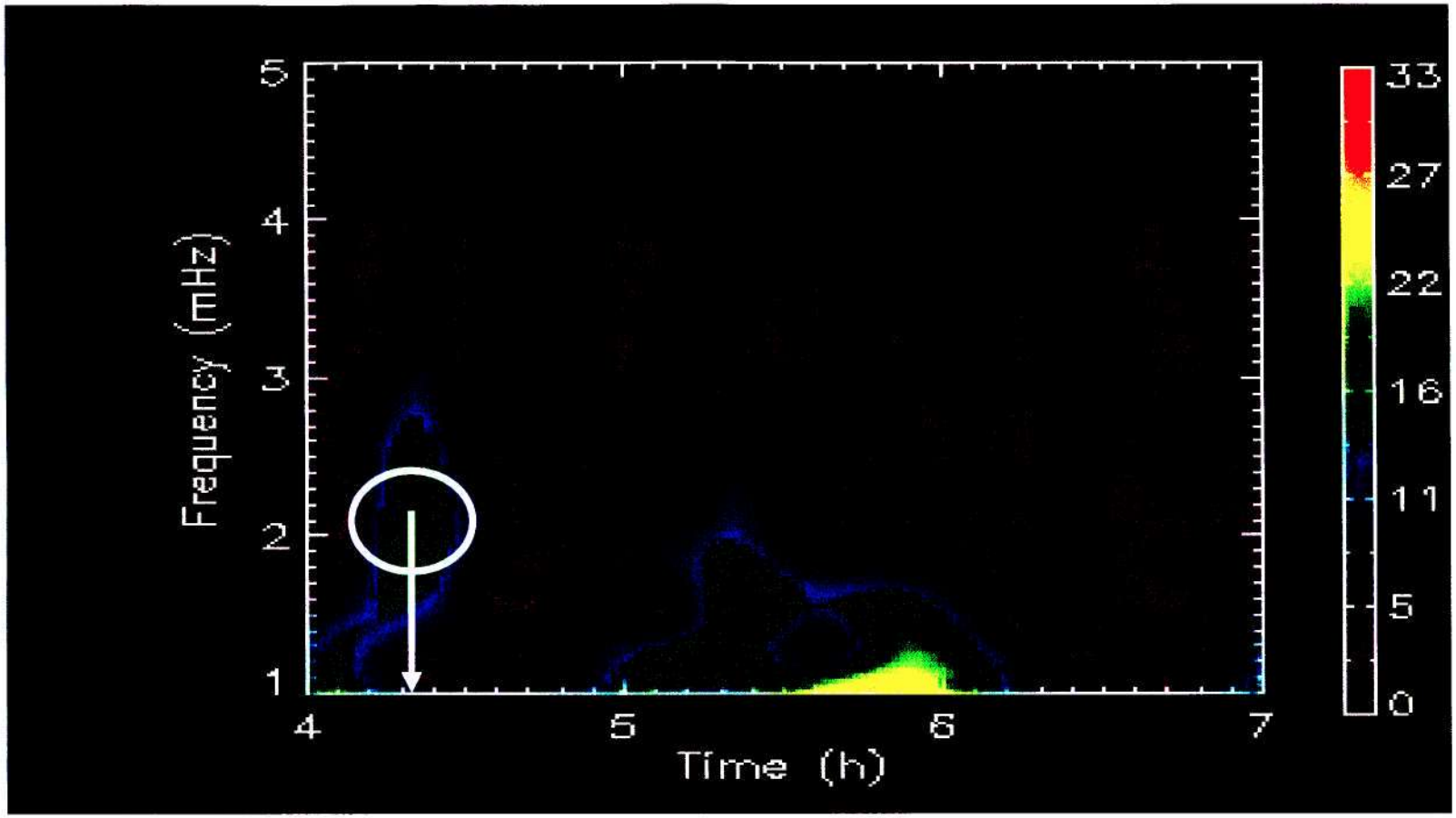

Figure 4.32: The wavelet amplitude spectra of the x-component of the velocity data collected by instruments onboard the ACE satellite on the 17th of June 2000. The figure shows the 1.9 mHz component observed at about 4.3 h and the amplitudes have arbitrary units.

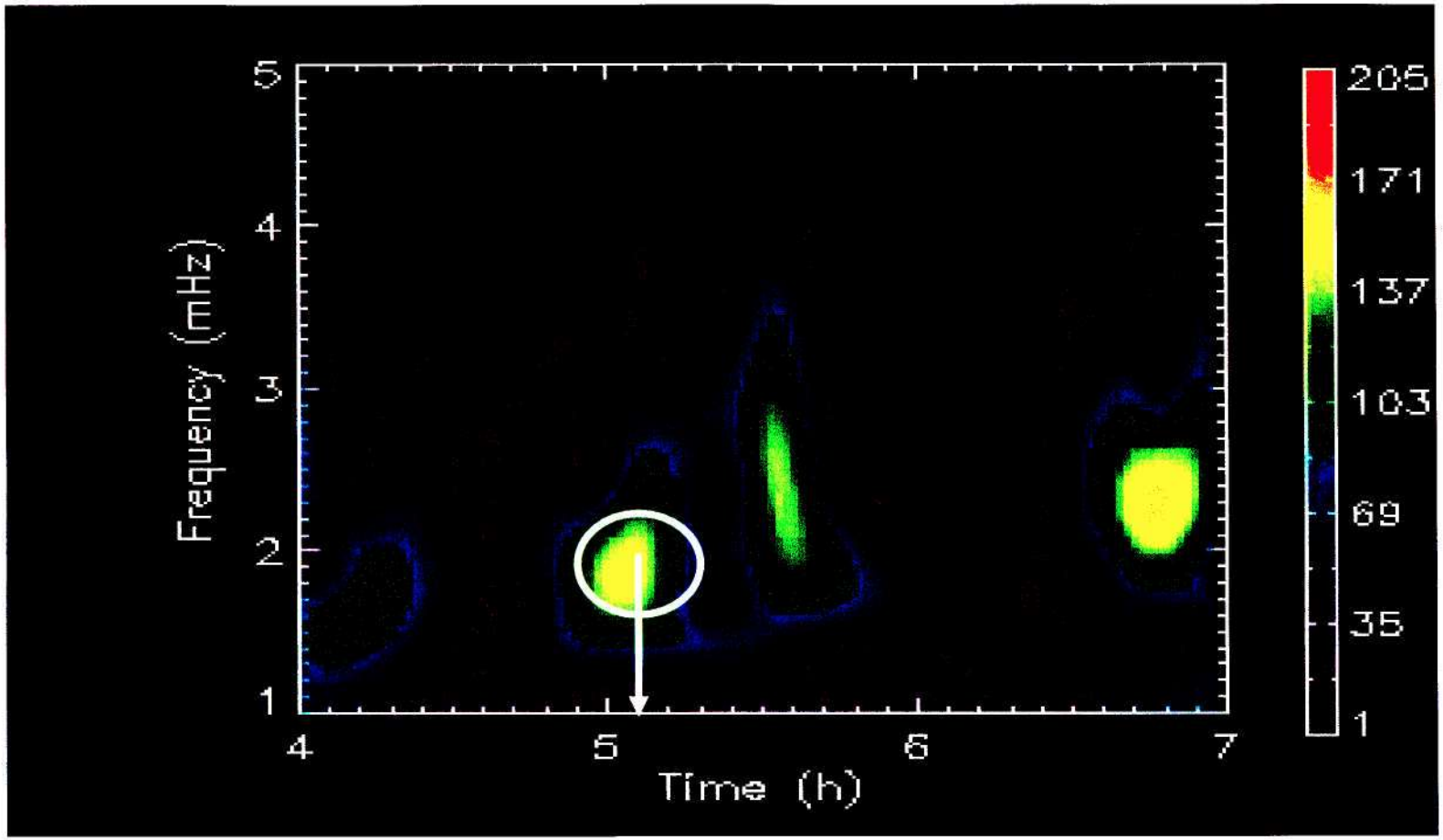

Figure 4.33: The wavelet amplitude spectra of the line-of-sight velocity from beam 6 of the Syowa East data at resonance latitude of -72.6°. The data were collected on the 17th of June 2000. The figure shows the 1.9 mHz component observed at about 5.1 UT and the amplitudes have arbitrary units.

Wavelet analysis is not the only technique that could be used to correlate data sets, for example, I could have used STFT or cross-spectral density (CSD). The reason why STFT was not used was that the duration of the data being analysed was short (2 h for Goose Bay and 3 h for Syowa East). Since in the STFT the signal is segmented into smaller signals, the length of the segmented signals would be extremely short. As a result their Fourier transform would have a very poor frequency resolution such that the discrete frequencies of interest which, as we saw early, are in close proximity, could not be adequately resolved. On the other hand, CSD is able to compute a phase shift between 2 signals and from it, time delay can be deduced. This can be done correctly only if the period of the 2 signals overlap. But during these events the time delay was very much longer than the periods of the ULF pulsations and there were no such overlaps and consequently the CSD gives incorrect results. To illustrate this I will consider the ULF oscillations with maximum period corresponding to 1.3 mHz component and the shorter time delay of the 2 events (30 min for the 11th November 2002).

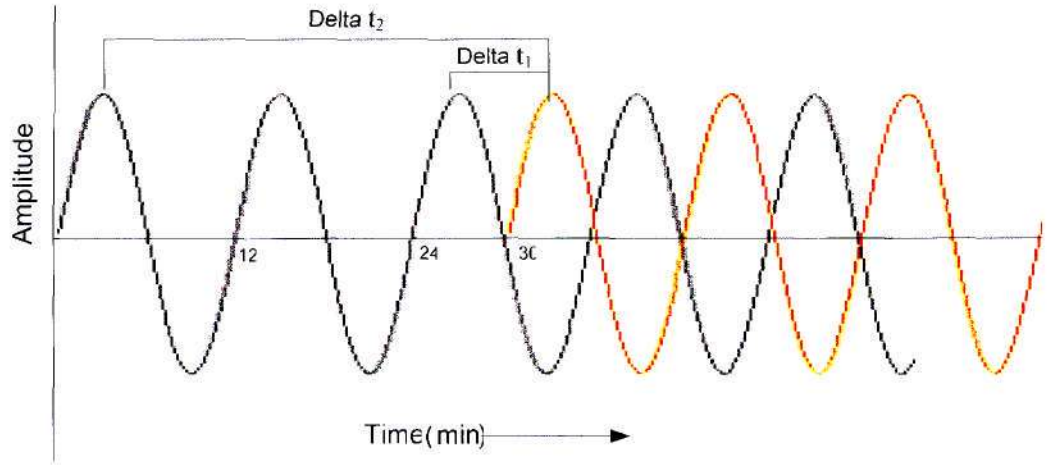

Figure 4.34: The black signal with a period of 12 min represents oscillation from solar wind and the red signal also with a period of 12 min represents the signal observed on the ground 30 min after. This figure shows the mistake in computation in the CSD method.

Figure 4.34 shows 2 oscillation both having a period of 12 min where the black sinusoid represents the oscillations observed in the solar wind and a red sinusoid represents the oscillations observed on the ground being delayed by 30 min. When computing the time delay using the CSD, the method computed the time Delay delta t_1 illustrated in Figure 4.34 which is wrong and the correct one is Delta t_2. And it is a worse case for other components because their periods are much shorter than the time delay.

The wavelet transformation is a suitable technique to use because it can minimize the resolution problem encountered using STFT due to the fact that it has a variable 'window' function as discussed in Section 2.5.3. Secondly, wavelet transform can show spectral components captured in the solar wind and those observed on the ground and deduce their time of occurrences irrespective of how long is the time delay between them. The results presented in Figures 4.30 to 4.33 show spectral components that are in the data as well as their time of occurrences. This is the superiority of wavelet transform to FT discussed in section 2.5. But just like FT, wavelet transform has some shortcomings one being that it is unable to give us the exact amplitude of the component. Thus the amplitudes in Figures 4.30 to 4.33 have arbitrary units. Nevertheless the technique still has worked well because in this section we are specifically interested in the spectral components as well as their time of occurrence and not so much on their amplitudes. Figure 4.30 shows the wavelet amplitude spectra of the velocity data from WIND satellite having 2 peaks near 1.9 mHz but at different times, one at 6.9 h and the other at 7.5 h. The peak at 7.5 h is so weak that it was considered to most probably have insignificant effect on the excitation of ULF pulsations and the peak at 6.9 h was most likely responsible. This spectral component had peak amplitude which lasted for about 48 min.

Consider making a cut in Figure 4.6 (i.e. amplitude spectra of the Goose Bay data) along the resonance latitude of 71.3° illustrated by a red line. It can be seen that the cut goes through 2 peaks, one near 0.8 mHz and another near 1.9 mHz. As such when wavelet amplitude spectra of the Goose Bay velocity data at this latitude were calculated, 2 peaks near these frequencies would be expected. Figure 4.31 shows the wavelet amplitude spectra of the Goose Bay data and indeed spectral components near 0.8 mHz (lasting ~50 min) and 1.9 mHz (lasting ~1h), consistent with the observations in Figure 4.8. Essentially Figure 4.30 shows that the WIND satellite has captured the 1.9 mHz component illustrated by red circle at about 6.9 UT illustrated by a red arrow which is believed to be the frequency of the MHD wave in the solar wind. Figure 4.31 shows the 1.9 mHz frequency component illustrated by the red circle which was captured by Goose Bay radar at about 7.4 UT as illustrated by the red arrow. The time difference of these peaks is about 30 min which is close to the travel time of 24 min of the solar wind calculated at the beginning of this section.

Figure 4.32 shows the wavelet amplitude spectra of the ACE satellite velocity data showing a broad band spectral component with maximum intensity near 1.9 mHz. This peak last for about

12 min with the peak intensity at 4.3 UT. The intensity of this peak is comparatively low and has to be treated cautiously. The spectra have been plotted from 1 mHz excluding the lower spectral components because there is no spectral component to correlate with since the 0.3 mHz component in the Syowa East data shown in Figure 4.7 did not show any FLR features.

The cut is also considered in Figure 4.7 and it goes through a very small portion of the peak near 1.5 mHz (so it is expected to have low intensity) and through peaks near 1.9, 2.3 and 2.7 mHz illustrated by a red line. As expected, wavelet amplitude spectra of the Syowa East velocity data from the resonance latitude of -72.6° shown in Figure 4.33 have peaks near these frequencies with peak intensity of component near 1.5 mHz being low. Spectral component with the peak intensity near 1.5 mHz is observed at 4.2 UT and it is not clear what its temporal extent is because it comes toward the end of the spectra. A component near 1.9 mHz is observed for 30 min with the peak amplitude at 5.1 UT. The component near 2.7 mHz last for 12 min with peak amplitude at 5.6 UT and that at 2.3 mHz last for more than 24 min with the peak amplitude at 6.8 UT. The 1.9 mHz component was captured by ACE satellite at about 4.3 UT as illustrated by the white circle and the arrow in Figure 4.32 and Syowa East radar at about 5.1 UT also illustrated by the white circle and the arrow in Figure 4.33. The time difference between these peaks is about 48 min which is close to the time delay of 53 min calculated earlier.

The results presented in Figures 4.30 to 4.33 and the above discussion add some weight to the proposal by Walker (2000) that the frequencies of the FLRs observed on the ground at least on these days, were possibly excited by the MHD waves in the solar wind. In the process energy that was carried in the solar wind was transferred into the magnetosphere. The higher frequencies observed in the radar data, for example those shown in Figure 4.32, are possibly not associated with the solar wind.

4.6 Temporal extent of ULF pulsations

In Section 4.4.2 the spatial extent of the 1.9 mHz component was investigated in all beams but for a particular point in time. Now in this section the time evolution of this component is investigated. For this purpose the instantaneous amplitude of the 1.9 mHz component was calculated and plotted in Figure 4.34 for Goose Bay data and in Figure 4.35 for Syowa East data. These figures show the snap shots of the amplitude of the 1.9 mHz component taken every 8 min from 6.8 to 7.9 UT by Goose Bay HF radar and from 4.7 to 5.8 UT by Syowa East HF radar.

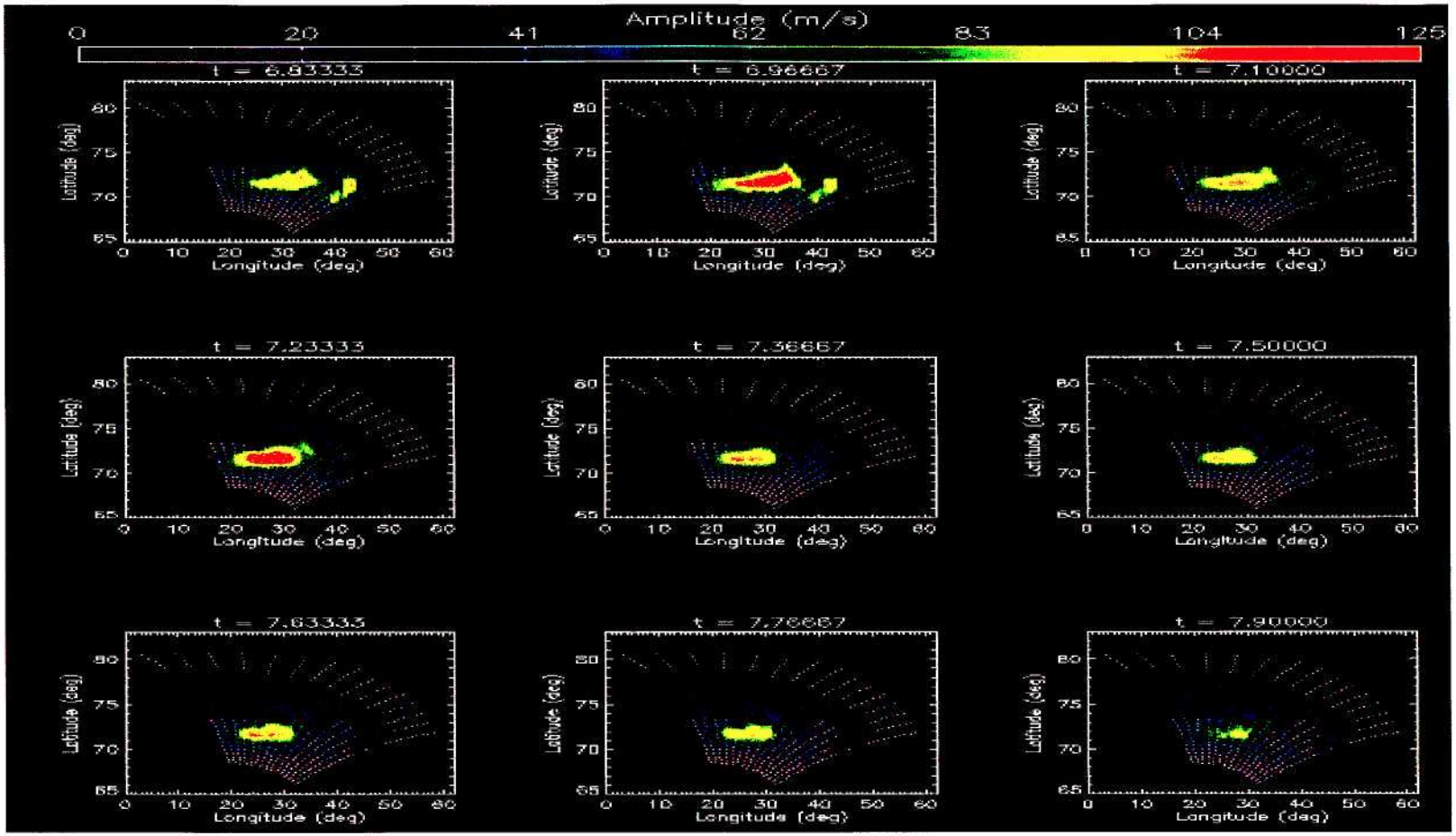

Figure 4.35: The snap shots of the instantaneous amplitude of the 1.9 spectral component taken by Goose Bay HF radar from 6.8 to 7.9 UT. The picture shows that this component was seen from 6.8 to 7.8 UT giving the temporal extent of about an hour.

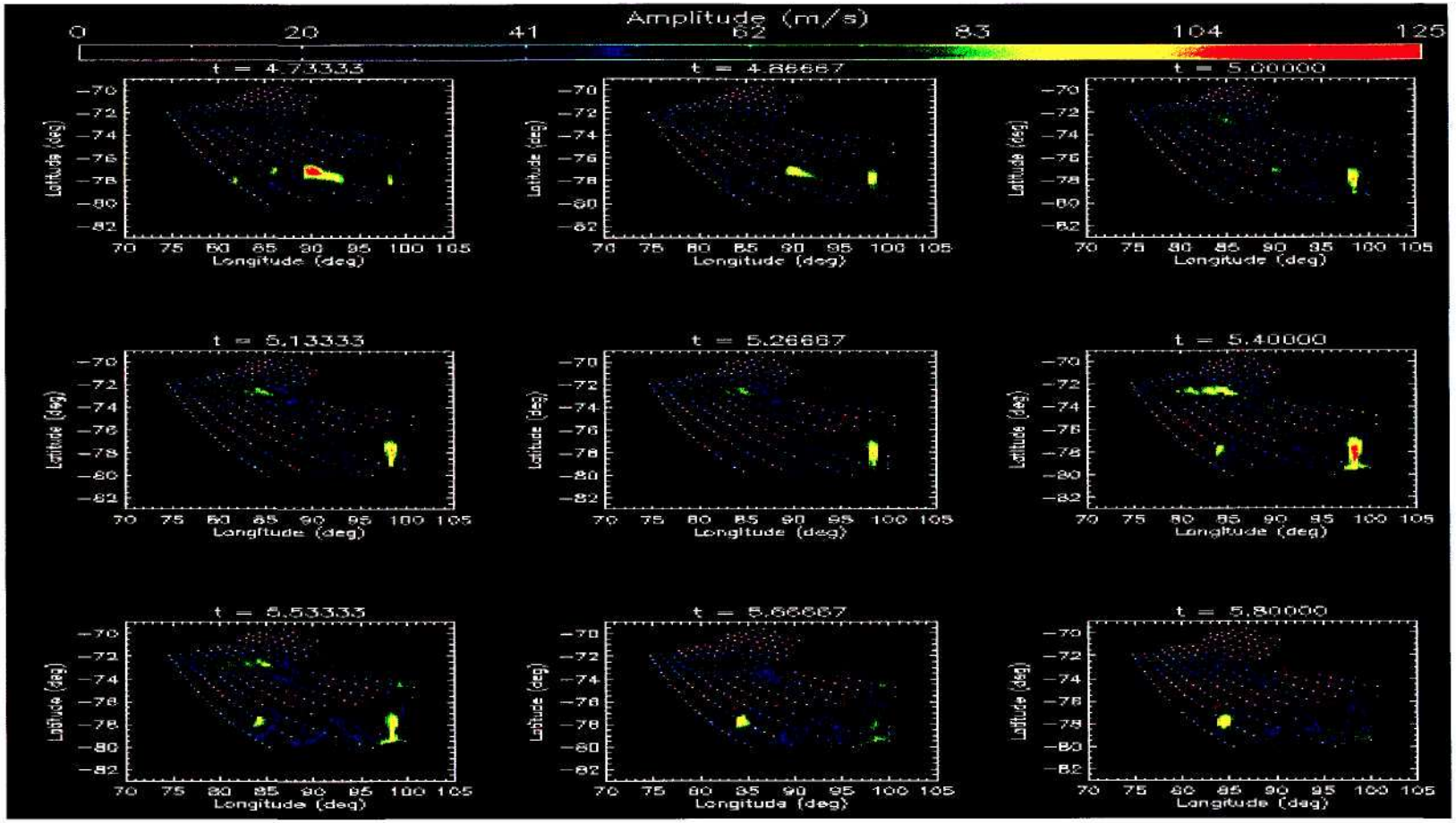

Figure 4.36: The snap shorts of the instantaneous amplitude of the 1.9 spectral component taken by Syowa East radar from 4.7 to 5.8 UT. The picture shows that the component was seen from 4.7 to 5.7 UT giving the temporal extent of about an hour.

Figure 4.35 shows that the 1.9 mHz component is seen in the data from beams 1 to 9 of Goose Bay HF radar as shown by the peak amplitude. This figure shows that this component started to be observed from about 6.8 UT having a longitudinal extent of about 25° from 20° to about 45°. This longitudinal range decreases with increasing time such that at 7.9 UT this range is about 10° from 20° to 30°. The intensity of this peak started small (~90 m/s) at 6.8 UT and increased with time and reached maximum of about 125 m/s at 7.2 UT. After this time the amplitude decreased to about 50 m/s at 7.9 UT. This peak disintegrates after 7.9 UT which gave a temporal extent of about an hour typical to that obtained by Nosé et al. (1998).

On the other hand, Figure 4.36 shows that the 1.9 mHz component is seen in the data from beams 1 to 7 of Syowa East. From this figure the 1.9 mHz component was observed from 4.7 UT having a longitudinal extent of about 20° from 75° to about 85°. This longitudinal range decreases with increasing time such that at 5.8 UT this range is about 5° from 80° to 85°. The peak amplitude is constant (70 m/s) from 4.7 UT until 5.4 UT after which it starts to decrease to about 50 m/s at 5.8 UT. The peak disappears after 5.8 UT giving the temporal extent of about an hour. The advantage of the plots in Figures 4.35 and 4.36 is that they are able show the peak amplitude, its spatial as well as its temporal extent.

Chapter 5 Discussion and conclusion

The objectives in this thesis were to use a number of signal processing techniques including Fourier analysis and wavelet analysis to study the physics of ULF pulsations and to suggest their possible sources. To achieve these objectives, HF radar data and satellite data were analysed and the results are summarized below.

The Fourier transform was used to determine the spectral content of the data sets that were analysed. Fourier transformation was the most appropriate technique to use here because in this section I was primarily interested in the accurate identification of the frequency and amplitude of the dominant spectral components. The spectral components were found to be ULF pulsations, to be more specific those that fell in the Pc5 band with the period range (150 to 600) s. In this thesis 2 data sets were used, one from Goose Bay HF radar (collected on the 11th of November 2006) and the other from Syowa East HF radar (collected on the 17th of June 2000). The length of the data from Goose Bay was 2 h sampled at 120 s and Syowa East data was 3 h long sampled at 75 s. The corresponding Nyquist frequency for the Goose Bay data is 4.15 mHz while that for the Syowa East data is 6.65 mHz which are both greater than a maximum frequency of interest (4 mHz) hence eliminating aliasing problems.

Discrete frequencies of the ULF pulsations were observed from Goose Bay data (e.g. 1.3, 1.9 mHz) and from Syowa East data (e.g. 1.3, 1.9, 2.3, 2.7 mHz) which are similar to those observed by Samson et al. (1991), Walker et al. (1992), Fenrich et al. (1995), Stephenson and Walker (2002), as well as Kepko and Spence (2003) These pulsations are assumed to be excited by magnetospheric cavity or waveguide mode. Given the length of the time series used, as specified above, the frequency resolution for each data set was about 0.1 mHz. This was particularly important to resolve the frequency components of interest given their close proximity. Another set of ULF pulsations with less common frequencies were observed, for example 1.5 mHz from Goose Bay data and 1.6 mHz from Syowa East data similar to those observed by Fenrich et al. (1995). In addition to these, spectral components with frequencies of less than 1 mHz were observed (e.g. 0.6 mHz from Goose Bay and 0.3 mHz from Syowa East data) similar to those observed by Walker et al. (1992). While the amplitudes of the various components are relatively significant, there are still unresolved issues concerning these oscillations. The first one being the observation of oscillations with frequencies of less

than 1 mHz. which do not fit with any reasonable magnetospheric model. Although source mechanism of the oscillations with frequencies greater than 1 mHz can be explained, those that are less than 1 mHz still cannot be explained. The excitation of these oscillations can possibly be attributed to other source mechanism that could be worth investigating in the future. The second aspect is the reproducibility of their frequencies, that is, why do we always observe these frequencies in spite of the continuously changing properties and conditions of the magnetospheric cavity. These issues led to the investigation of the source of ULF pulsations in the solar wind.

The analytic signal was used to establish the FLR characteristics of the spectral components of the ULF pulsations. The analytic signal was used because it was paramount to get the instantaneous amplitude and phase of a specifically identified spectral component. More specifically, the behaviour of the amplitude and phase of the spectral component needed to be investigated at the time when the amplitude was maximum. This was crucial for two reasons: (i) to increase the credibility of the deduced phases; (ii) to make sure that the latitudinal comparison of the instantaneous peak amplitude (Figure 4.35 and 4.36) was done using a common feature, in this case the instantaneous peak amplitude, given that they decay by 75 $m.s^{-1}$ (Goose Bay) and 20 $m.s^{-1}$ (Syowa East) in an hour (see later).

ULF pulsations are classified as FLRs if a particular spectral component exhibits an enhancement in amplitude with some symmetric tendency at a particular resonance latitude with an associated phase change of approximately 180° across the latitude. The instantaneous amplitude and phase of the observed spectral components were calculated as the amplitude and phase of the analytic signal. The 1.9 mHz spectral component considering the instantaneous peak amplitude from Goose Bay data was analysed and found to exhibit FLR features whereas the 0.6, 1.3 and 1.6 mHz components were not analysed because they come towards the end of the observation period. The 1.3, 1.6, 1.9, 2.3 and 2.7 mHz spectral components from Syowa East data were analysed and found to show FLR features while the 0.3 mHz component did not. This behaviour is slightly different from that observed by Walker et al. (1992) who found that a component at 0.8 mHz showed FLRs features. Detailed analysis was done on the data from beam 2 of the Goose Bay HF radar and beam 6 of the Syowa East HF radar with emphasis on the 1.9 mHz component. Amplitude and phase spectra of this component were calculated and plotted as shown in Figures 4.8 to 4.11. An

enhancement in amplitude of the 1.9 mHz component was observed over a narrow range of latitude centred on the resonance latitude of 7.13° and -73.4° in the Goose Bay and Syowa East data respectively with an associated ~180° phase change across these latitudes.

These FLR characteristics were not only limited to a few longitudes but covered a wider longitudinal range. This behaviour becomes apparent when considering the instantaneous amplitude and phase of the 1.9 mHz component for all beams on the 11th of November 2002 at 7.2 UT (Goose Bay, Figure 4.18) and on the 17th of June 2000 at 5.1 UT (Syowa East, Figure 4.20). These figures clearly show the 1.9 mHz spectral component at these times had a latitudinal peak amplitude near the resonance latitude of 71.3° (Figure 4.18) and -72.6° (Figure 4.19) in line with the results presented above. The longitudinal coverage of this component in both data sets was about 10°. Geographically the magnetic field lines can be considered to be set into oscillation by a certain driver with a well defined frequency of approximately 1.9 mHz. The field lines from latitudes near 71.3° (Goose Bay) and -72.6° (Syowa East) are considered to have a characteristic frequency matching that of the driver and thus oscillated with large resonance amplitudes. The instantaneous phase of this component was also calculated using Goose Bay and Syowa East data from all beams and the spectra was shown in Figure 4.19 and 4.21, respectively. These figures show that across the latitudes of 71.3° (Goose Bay) and of -72.6° (Syowa East) there was a phase change of about 180°. These phase changes were observed over the same longitudinal range as the peak amplitudes. The implication of this is that during the excitation, the field lines from latitudes that are lower than the resonance latitudes were oscillating at high frequency and thus were leading in phase while those from higher latitudes were oscillating at low frequencies and thus were lagging in phase and this is in line with the observations made by Walker et al. (1979), Walker at al. (1992), and Fenrich et al. (1995).

Having established that the observed oscillations were ULF pulsations and that they were classified as FLRs, their possible source was investigated. Following up on the proposition by Walker (2000) that the sources of the ULF pulsations that are seen on the ground were possibly due to the MHD waves in the solar wind, a search for the pulsations in the solar wind was undertaken. Wavelet analysis was used to do some correlation between the line-of-sight velocity data from HF radar located at Goose Bay and the x-component of the velocity data from WIND satellite collected on the 11th of November 2002. A similar correlation was also

done for Syowa East data and the ACE satellite data for 17th of June 2000. Wavelet analysis was chosen for this task because it is capable of showing the spectral components of the time series and their time of occurrence. STFT could have been used for this task, but unfortunately the duration of the time series under consideration is short hence resulting in the resolution problem discussed in Section 4.5.2. Equally problematic is using conventional cross-spectral technique because the time delay between the oscillations observed in the solar wind and those observed on the ground is much longer than the period of these oscillations. This implies that the oscillations in the solar wind would have gone through many cycles before their effect is registered on the earth making the calculation of the time delays using CSD inadequate (Section 4.5.2). The x-component of the solar wind velocity and of the position of the satellite was used to calculate the travel time of the solar wind to earth. The x-component of the velocity was chosen because the solar wind velocity is greatest in the x-direction and also much greater than the group velocity of the MHD waves in the solar wind. Therefore the total velocity in the sun-earth line is approximately in the x-direction. Therefore the solar wind data from ACE and WIND satellites were used because these satellites were close to the sun-earth line during the time of the events considered. The wavelet amplitude spectra for the above data were computed and the results are shown in Figures 4.30 to 4.33. Although other spectral components (e.g. near 1.3, 2.3, and 2.7) are observed in some of the figures, the 1.9 mHz component was observed in both the solar wind data and HF radar data. Although these frequencies do not occur precisely at f = 1.3., 1.9, 2.3 and 2.7 mHz, they are still considered as discrete frequencies similar to those observed by Samson et al. (1991). This discrepancy was also noted by Kepko and Spence (2003), Ziesolleck and Mcdiarmid (1995), and Francia and Villante (1997) as discussed in Section 4.3. The appearance of the 1.9 mHz component in the solar wind data and HF radar data gives credence to the suggestion that solar wind could be source of the pulsations.

During the events under discussion the average x-component of the velocity of the solar wind was about 458 km.s^{-1} (11th of November 2002) and 473 km.s^{-1} (17th of June 2000) whereas the x-component of the distance from the WIND satellite to the earth was 650878 km (11th of November 2002) and from the ACE satellite was 1.058×10^6 km. The resulting travel time of the solar wind to the earth was about 24 min on the 11th November 2002 and about 48 min on the 17th of June 2000. Wavelet amplitude spectra of the 1.9 mHz component from the satellite (WIND and ACE) data and the HF radar (Goose Bay and Syowa East) data were calculated respectively. From these results the time delay of the spectral component was deduced to be 30 min on the 11th of November 2002 and 53 min on the 17th of June 2000 which are close to

the travel time of the solar wind on those days. This put some weight to the proposition that at least on these dates the ULF pulsations that were observed were possibly excited by the oscillations that were carried in the solar wind and the magnetosphere was just a passive oscillator driven by some external periodic forcing. Stephenson and Walker (2002) using HF radar data and solar wind data and Kepko and Spence (2003) using solar wind data and geocynchronous magnetic field measurement , argued that the solar wind could be the source for the discrete frequencies they observed. During this process the energy from the solar wind was transferred to the magnetosphere. Although we have identified the solar wind as the possible source of the ULF pulsations, the exact source mechanism is still unknown and this can be one of the topics for further research.

The temporal as well as the spatial extent of the spectral component were investigated simultaneously as shown in Figure 4.35 from Goose Bay data and Figure 4.36 from Syowa East data. From these figures it can be seen that the 1.9 mHz component was observed for about an hour in both data sets. For Goose Bay (Figure 4.35) the onset of the spectral component was 6.8 UT with amplitude that decays from 125 $m.s^{-1}$ to 50 $m.s^{-1}$ in an hour while for Syowa East (Figure 4.36) the component started to be seen at 4.7 UT and the amplitude decays from 70 $m.s^{-1}$ to 50 $m.s^{-1}$ in 1 hour. In essence the amplitude of this spectral component decreased by ~60 % (Goose Bay) and ~29 % (Syowa East) in an hour. The typical duration of the ULF pulsations in the magnetosphere ranges from about 0.5 h to 1.5 h and the duration I got is in agreement with that obtained by Nosé et al. (1998) which is from 1.0 to 2.0 magnetic local time (MLT). The longitudinal extent of the 1.9 mHz component was found to decrease with time in such a way that in an hour the longitudinal extent decreased by 15° in both data sets. In particular it decreased from 25° to about 10° in Goose Bay and from 20° to about 5° in the Syowa East in 1 hour.

Another aspect that is worth investigating, but could not be investigated in this work, is that of conjugacy effects. This is important so as to see whether the observed ULF pulsations are global or not. Unfortunately, I could not investigate it here because of the lack of conjugate data for the days chosen for the analysis. Due to its significance such study can be worth looking at in the future.

References

Anderson, B. J., M. J. Engebretson, S. P. Rounds, L. J. Zanetti, and T. A. Potemra, A statistical study of Pc 3–5 pulsations observed by the AMPTE/CCE magnetic fields experiment: 1. Occurrence distributions, J. Geophys. Res., 95, 10,495–10,523, 1990.

Arnold, N.F., T.R. Robinson, P.B. Byrne, M. Lester, and P.J. Chapman, Super Dual Auroral Radar Network HF radar observations of fluctuations in the spectral distribution of near range meteor echoes in the upper mesosphere and lower thermosphere, Ann. Geophys., 19, 425-434, 2001.

Brook, D. and R.J. Wynne, Signal processing, Principles and Applications, Edward Arnold, London, 1998.

Bracewell, R.N., The Fourier transform and its Applications, 2nd ed., McGraw-Hill, New York, 1986.

Bristow, W. A., A. Otto, D. Lummerzheim, Substorm convection patterns observed by the Super Dual Auroral Radar Network, J. Geophys. Res., 106(A11), 24593-24610, *10.1029/2001JA000117, 2001.*

Chen, L. and A. Hasegawa, A theory of long-period magnetic pulsation, 1, Steady state excitation of field line resonance, J. Geophys. Res., 79, 1024, 1974.

Chisham, G., and M.P. Freeman, A technique for accurately determining the cusp-region polar cap boundary using SuperDARN HF radar measurements, Ann. Geophys., 21, 983-996, 2003.

Dungey, J. M., Electrodynamics of the outer atmosphere, Pa. State Ionos. Res. Lab., University Park, Sci. Rep., 69, 1954.

Dungey, J.W., Electrodynamic of the outer atmosphere, in Proc. Ionosphere Conf., pp. 229-236. Phys. Soc. of London, London, 1955.

Engebresto, M., K.H. Glassmeire, M. Stellmacher and W.J. Hughes, The dependence of high-latitude Pc5 wave power on solar wind velocity and on the phase of high speed solar wind streams, J. Geophs. Res., 103, 26,271, 1998.

Fenrich, F. R., J. C. Samson, G. Sofko, R. A. Greenwald, ULF high- and low-m field line resonances observed with the Super Dual Auroral Radar Network, J. Geophys. Res., 100(A11), 21535-21548, 10.1029/95JA02024, 1995.

Francia, P. and U. Villante, Some evidence of ground power enhancements at frequency of global magnetospheric mode at low latitudes, Ann. Geophys., 15, 12, 1997.

Greenwald, R.A., W. Weiss, E. Nielsen, N.P. Thomson. STARE: a new radar auroral backscatter experiment in northern Scandinavia, Radio Sci. 13, 1021, 1978.

Greenwald, R.A., K.B. Beker, J.R. Dudeney, M. Pinnock, T.B. Jones, E.C. Thomas, J.P. Villain, J.C. Cerisier, C. Senior, C. Hanuise, R.D. Hunsucker, G. Sofko, J. Koehler, E. Nielsen, R. Pellinen, A.D.M. Walker, N. Sato, H. Yamagishi, DARN/SUPERDARN, A global view of the dynamics of high-latitude convection, Space Science Reviews, 71, 761-796, 1995.

Hughes, W. J. Magnetospheric ULF Waves: A tutorial with a historical perspective, Geophysical Monograph, 81, 1994.

IDL's manual version 5.0, 1997

Kepko L., H. E. Spence, Observations of discrete, global magnetospheric oscillations directly driven by solar wind density variations, J. Geophys. Res., 108 (A6), 1257, doi:10.1029/2002JA009676, 2003.

Kessel, R., P. Mauricio, R. McGuire, J King at URL:

http://nssdc.gsfc.nasa.gov/nssdc_news/december95/01_king_j_1295.html, 1995.

Kivelson, M.G., and C.T. Russell, Introduction to space physics, Cambridge University press, University of California, Los Angeles, 343-350, 1995.

Kivelson, M.G., J. Etcheto, and J.G. Trotignon, Global compressional oscillations of the terrestrial magnetosphere: The evidence and a model, J. Geophys. Res., 89, 9859, 1984.

Kivelson, M.G. and Southwood D. J., Resonant ULF waves: A new interpretation, Goephs. Res. Lett., 12, 49-52, 1985.

Malinga, S.B., PhD Thesis, A comparative study of atmospheric dynamics in the mesosphere and lower thermosphere (MLT) near Grahamstown (South Africa) and Adelaide (Australia), Rhode University, 2001

Mathie, R. A., and I. R. Mann, On the solar wind control of Pc5 ULF pulsation power at mid-latitudes: Implications for MeV electron acceleration in the outer radiation belt, J. Geophys. Res., 106(A12), 29783-29796, 10.1029/2001JA000002, 2001.

McPherron, R. L., Magnetic pulsations: Their sources and relation to solar wind and geomagnetic activity, Survey in Geophysics, doi:10.1007/s10712-005-1758-7,26,545-592, 2005.

Misiti, M., Y Misiti, G. Oppenheim, J. Poggi, Wavelet Toolbox, The MathWork, 1996.

Nosé, M., T. Iyemori, S. Nakabe, T. Nagai, H. Matsumoto and T. Goka, ULF pulsations observed by the ETS-VI satellite: Substorm associated azimuthal Pc 4 pulsations on the nightside, Earth Planet Science, 50, 63-80, 1998.

Olson, J.V. and G. Rostoker, Longitudinal phase variation of the Pc 4-5 micropulsations, J. Geophs. Res., 83, 2481, 1978.

Polikar R. 'The wavelet tutorial part II ' at URL:

http://ingineering.rowan.ude/~polikar/WAVELETS/Wtpart3.html, 2002.

Provan, C., T.K. Yeoman, A comparison of field line resonances observed at the Goose Bay and Wick radars, Ann. Geophys., 15, 231-235, 1997.

Smith, J.O., Mathematics of the discrete Fourier transform (DFT)

http://ccrma.stanford.edu/~jos/ndft/, 2003.

Samson, J.C., R.A. Greenwald, J.M. Ruohoniemi, T.J. Hughes, D.D. Wallis, Magnetometer data and radar observations of magnetohydrodynamic cavity modes in the Earth's magnetosphere, Can. J. Phys., 69, 939, 1991.

Southwood, D. J., Some features of field line resonances in the magnetosphere, Planetary Space Science, 22, 483-419, 1974.

Stephenson, J.A.E. and A.D.M. Walker, HF radar observations of Pc5 pulsations drive by the solar wind, Geophys. Res. Lett., 29, No. 9, *10.1029/2001GL014291*, 2002.

Stewart, B., On the great magnetic disturbance which extended from August 2 to September 7, 1859 as recorded by photography at the kew observatory, Phil. Trans. Roy Lond., 11, 407, 1861.

Taroyan Y., R. Erdélyi, Steady state excitation of field line resonances by global waveguide modes in the magnetosphere, J. Geophys. Res., 108 (A7), 1301, doi:10.1029/2003JA009935, 2003.

Torrence, C. and G.P. Compo, A practical guide to wavelets analysis, Bulletine of the American Meteorological Society, 79, No 1, January 1998.

Walker, A.D.M., The SHARE Radar at SANAE, Antarctica, South African Journal of Science, 98, 257-268, 2002.

Walker, A.D.M., Radar studies of magnetosphere dynamics, Astrophysics and Space Science, 230, 415-430, 1995.

Walker, A. D. M., J. M. Ruohoniemi, K. B. Baker, R. A. Greenwald, J. C. Samson, Spatial and temporal behaviour of ULF pulsations observed by the Goose Bay HF radar, J. Geophys. Res., 97(A8), 12187-12202, 10.1029/92JA00329, 1992.

Walker, A.D.M., R.A. Greenwald, W.F. Stuart, and C.A. Green., STARE auroral radar observations of Pc 5 geomagnetic pulsations, J. Geophys. Res., 84, 3373, 1979.

Waters, C. L., B. G. Harrold, F. W. Menk, J. C. Samson, B. J. Fraser, Field line resonances and waveguide modes at low latitudes. 2. A model, J. Geophys. Res., 105(A4), 7763-7774, 10.1029/1999JA900267, 2000.

Yumoto, K., External and internal sources of Low-frequency MHD wave in the Magnetosphere –A Review, J. Geomag. Geoelec., 40, 293-311, 1988.

Ziesolleck, C.W.S., D.R. McDiarmid, Statistical survey of auroral latitude Pc 2 spectral and polarisation characteristics, J Geohys. Res., 100, 19,299-19,312, 1995.